MEMORANDUM
RM-4000-NASA
MARCH 1964

UNPUBLISHED PRELIMINARY DATA

GEOMETRIC AND PHOTOMETRIC PARAMETERS OF THE TERRESTRIAL PLANETS

G. de Vaucouleurs

PREPARED FOR:
NATIONAL AERONAUTICS AND SPACE ADMINISTRATION

The RAND Corporation
SANTA MONICA • CALIFORNIA

NASr-21(04)

MEMORANDUM
RM-4000-NASA
MARCH 1964

GEOMETRIC AND PHOTOMETRIC PARAMETERS OF THE TERRESTRIAL PLANETS

G. de Vaucouleurs

This research is sponsored by the National Aeronautics and Space Administration under Contract No. NASr-21. This report does not necessarily represent the views of the National Aeronautics and Space Administration.

The RAND Corporation
1700 MAIN ST. • SANTA MONICA • CALIFORNIA

PREFACE

The constitution of the surfaces and atmospheres of the terrestrial planets can be inferred in part from their diameters and albedos. The author, professor of Astronomy at the University of Texas and a consultant to RAND, has surveyed about a century of recorded observations on the diameters and albedos of the terrestrial planets, has considered the methods used and the probable errors in each series of observations, and, by the use of weighted means of the best data, has arrived at preferred values for the diameters, ellipticities and spectral albedos of Mercury, Venus and Mars.

The work was performed for the National Aeronautics and Space Administration under Contract NASr-21(04). The views and conclusions are those of the author and do not necessarily reflect those of The RAND Corporation.

ABSTRACT

A critical examination is presented of the diameters, ellipticities and spectral albedos of Mercury, Venus, and Mars derived by many observers in the course of the past 100 years. The systematic and accidental errors in the various methods are discussed, and the results are weighted accordingly to produce best estimates of the diameters, ellipticities and albedos for the three planets.

CONTENTS

LIST OF FIGURES

LIST OF TABLES

1. INTRODUCTION

The geometric and photometric parameters of the terrestrial planets are of basic importance for the planning of many experiments in the space-exploration program.

Geometric parameters to be considered here involve the equatorial diameter and ellipticity of the visible surface (be it the solid surface or some more-or-less definite cloud level). Photometric parameters involve the visual phase curve and albedo, the spectral reflectivity curve and integral (or radiometric) albedo, measuring the fraction of the solar-energy flux reflected back to space.

The diameters of the planets could, in principle, be used for terminal guidance of spacecraft (if known with sufficient accuracy); a precise value of the diameter (and ellipticity) is also required to compute the mean density, surface gravity, and atmospheric escape velocity of a planet; it may also be needed for the derivation or interpretation of atmospheric data (e.g., for Venus). The ellipticity, if known accurately, is important to test models of the density distribution in the globe and possible departures from hydrostatic equilibrium (e.g., for Mars).

The luminosity and reflectivity of the planets in ordinary visible light, i.e., near $\lambda = 0.55\ \mu$, is basic to all optical observations; the stellar magnitude of the disk at full phase determines the maximum general reflectivity or geometric albedo p of the planet and, consequently, its surface brightness (luminance) in either conventional photometric units or in absolute energy units. The phase function or law of variation of relative luminosity with phase angle (sun-planet-

observer) determines the phase integral q and, therefore, the spherical (or physical) albedo $A = pq$ measuring the fraction of the incident flux reflected in all directions of space.

The variations of p and q as a function of wavelength must be known both for the planning of observations from space probes outside the visual range and for the important information they give on the nature of the planetary surfaces and atmospheres. An integration of the spectral reflectivity function $A(\lambda)$ weighted by the solar spectral energy distribution $F(\lambda)$ gives the radiometric albedo; hence, the solar-energy flux absorbed by the planet, which is the basic element of the planetary energy balance fundamental to meteorologic theory. A more precise definition of these quantities follows.

2. GEOMETRIC PARAMETERS

2.1. Apparent diameter

The fundamental relation between the angular apparent diameter 2σ, the linear diameter $2\ r$, and the distance Δ from the observer to the center of a planet is

$$\sin \sigma = r / \Delta \quad . \tag{2.1}$$

For all planets observed from the earth, the maximum apparent diameter hardly ever exceeds 1', and the approximate relation,

$$\sigma'' = \rho''\ r / \Delta \quad , \tag{2.2}$$

where $\rho'' = 1/\sin 1'' = 206{,}264.8...$, may be used without significant error to give σ in seconds of arc. When $\Delta = \Delta_1 = 1$ astronomical unit, $\sigma = \sigma_1 = \rho''\ r / \Delta_1$ is the apparent semi-diameter at unit distance, a quantity often used in ephemerides.

2.2. Ellipticity

In general the centrifugal force of rotation causes a planet to be a spheroid of revolution flattened at the poles. If a, b are the equatorial and polar radii, the ellipticity measured by

$$f = \frac{a - b}{a} = 1 - \frac{b}{a} \tag{2.3}$$

is often expressed by its reciprocal number f^{-1}. When $f \neq 0$, the value of σ_1 given in the tables usually refers to the equatorial radius a. For Mercury and probably for Venus, the very slow rotation implies $f \simeq 0$; however, at least in Mercury, tidal action may well have induced triaxiality, as in the moon, but the possible differences between the three axes are at present undetectable.

For a planet in hydrostatic equilibrium, the polar flattening f depends on the ratio I/Mr^2, the ratio of the moment of inertia I of the planet about its polar axis to its mass M times its squared radius r. The relation is expressed by the Radau--Darwin formula (Darwin, 1876):

$$\frac{I}{Mr^2} = \frac{2}{3}\left[1 - \frac{2}{5}\sqrt{1+\eta}\right], \tag{2.4}$$

where

$$\eta = \frac{5m}{2f} - 2, \tag{2.5}$$

if

$$m = \frac{3\pi}{G\rho T^2} \tag{2.6}$$

is the ratio of centrifugal force to gravity at the equator (G = the gravitational constant, ρ = the mean density, and T = the period of rotation of the planet). The two extreme theoretical cases are a planet whose mass is concentrated in a small central nucleus and for which f = 0.50 m, and a homogeneous planet for which f = 1.25 m. A value f > 1.25 m would require a decrease of density with increasing depth in the planet, which is, of course, impossible for a planet in hydrostatic equilibrium, but may not be impossible -- within limits -- if there are significant departures from such equilibrium, i.e., where uncompensated stresses are present in the crust or mantle. This case may be realized in Mars, whose observed optical value of f exceeds 1.25 m (Subsection 8.3).

2.3. Refraction correction

On an airless planet, such as the moon and Mercury, the apparent limb is determined by the overlapping profiles of the highlands and mountains and not by a geometric reference surface, such as the geoid. By analogy with the earth and the moon, the observed planetary diameter may, therefore, be larger than that of the reference spheroid by some 5 to 10 km. The relative difference is $\approx$ 0.1 to 0.2 per cent for Mercury, and $\approx$ 0.1 per cent for Mars.

On a planet surrounded by a transparent atmosphere, the apparent limb is defined by the refracted image of points of the surface slightly beyond the geometric edge (Fig. 1); the difference $2\,\Delta\sigma = 2\,(\sigma - \sigma_0)$ between apparent and true diameter is given by the theory of astronomical refraction (Danjon, 1959)

$$r = n_0\, r_0 \quad , \tag{2.7}$$

or

$$\frac{\Delta\sigma}{\sigma} = (n_0 - 1) \quad , \tag{2.8}$$

where n_0 is the refractive index at the visible surface. For Earth $n_0 = 1.0003$ (0° C, 1 atm.) and by Eq. (2.7) $r - r_0 = 1.9$ km. The relative enlargement of the diameter is equal to the refractivity of the atmospheric gas at the surface (Eq. 2.8). Remembering that

$$\frac{n - 1}{n_0 - 1} = \frac{p}{p_0}\,\frac{T_0}{T} = \frac{273}{T}\,p \quad , \tag{2.9}$$

if p is measured in atmospheres, the probable value of the enlarging factor for Mars and Venus, assuming $p \approx 0.1$ atm. and $T \approx 230^\circ$ K near

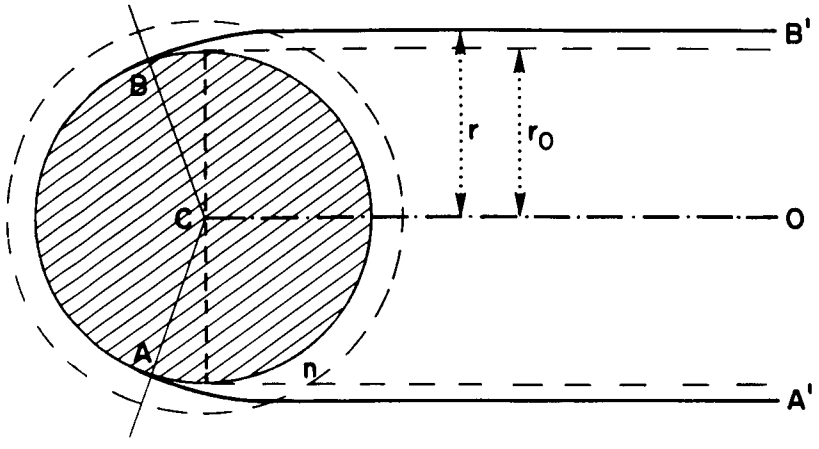

Fig. 1 Enlargement of planetary disk by atmospheric refraction

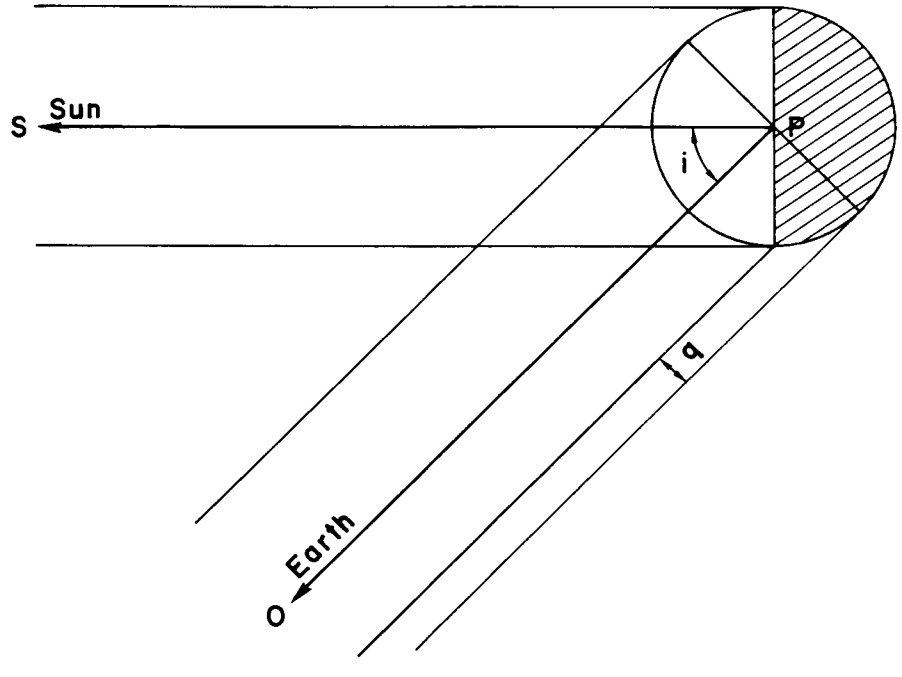

Fig. 2 Phase angle and phase defect

cross section of the spheroid whose plane makes an angle i with the tangent plane.

Both angles can be readily computed when the heliocentric rectangular coordinates of the planet and of the observer are known. For Mercury and Venus the latitude of the center is irrelevant since the ellipticity is presumed negligible; for Mars, the celestial coordinates of the pole are known with sufficient accuracy (de Vaucouleurs, 1964), but the ellipticity is uncertain (Subsection 8.3).

Except at exact opposition, the equatorial diameter of Mars is not directly observable, and the polar diameter is the quantity most frequently measured. The relation between the true polar diameter and the pseudo polar diameter measured along the line of cusps is readily derived in terms of f, φ_0 and of the angle between the projected polar axis and the line of cusps (Trumpler, 1927).

2.6. Conversion factors

Astronomical observations of the planets give directly the apparent diameter $2\sigma''_1$ at unit astronomical distance Δ_1; the linear diameter 2r in kilometers follows through Eq. (2.2) when the value of Δ_1 in physical units is known. Conversely, the geodetically measured equatorial radius r_1 of the earth subtends at unit astronomical distance an angle $\pi_\odot$, the mean horizontal equatorial parallax of the sun.

From recent determinations (Pettengill, et al., 1962; Muhleman, et al., 1962) the following values will be used here:

$$\Delta_1 = 149{,}598{,}000 \pm 500\text{: (m.e.) km},$$

the visible surfaces (and a mixing ratio $CO_2/N_2 \approx 1/20$ by volume), is $\Delta\sigma/\sigma \approx 0.35 \times 10^{-4}$, or $(r - r_0) \approx 0.2$ km (Venus), and 0.1 km (Mars) which is negligible for most applications.

2.4. Atmospheric layers

On a planet with a cloudy or hazy atmosphere, such as Venus, the apparent limb may not refer to the surface of the solid globe, but to the "top" of an atmospheric layer whose altitude above the solid surface may vary with latitude and wavelength. Rough estimates of this altitude for Venus and Mars (Section 7, 8) are of the order of 20 to 40 km, or about 0.5 per cent.

2.5. Phase defect

When the planet is not in exact opposition with the sun, the diameter in the plane of sun-planet-observer (or illumination equator) is reduced by the geometric phase defect q (Fig. 2) given by

$$q/r = 1 - \cos i \quad , \tag{2.10}$$

where i is the phase angle S-P-O. The fraction of the disk illuminated is

$$k = \frac{1}{2} (1 + \cos i) \quad . \tag{2.11}$$

The line of cusps or line perpendicular to the direction of maximum phase defect does not generally coincide with the projection of the rotation axis. The apparent outline of the planet is then composed of two half ellipses (L,T): the limb (L) is the intersection of the tangent plane (to the celestial sphere) with the spheroid corresponding to some latitude φ_0 of the center of the disk (where the observer is at the zenith); the terminator (T) is the projection of a central

r_1 = 6,378.16 ± 0.03: (m.e.) km, and

$\pi_\odot$ = 8 " 794 17 ± 0"000 05 (m.e.).

The conversion factor from apparent angular diameter at unit astronomical distance to linear diameter is

1" = 725.272 ± 0.002 (m.e.) km

3. PHOTOMETRIC UNITS

3.1. Visual units

The surface density of luminous flux or illumination E is expressed in luces (1 lux = 1 lumen m^{-2}); a lux is the illumination produced at normal incidence by one unit of luminous intensity or "candela" at a distance of one meter. Other units: 1 phot = 10^4 lux (1 cd at 1 cm); 1 foot-candle = 1 lumen per square foot = 10.764 lux.

The "surface brightness" or luminance L is expressed in candelas per square centimeter; it is the luminous intensity per unit area of the emitting surface normal to the direction of observation. The luminance of a Lambert disk receiving an illumination of 1 phot is $L_1 = 1/\pi = 0.318$ cd cm^{-2} = 1 Lambert. Other unit: 1 foot-Lambert = 1.076×10^{-3} Lambert.

A source of average luminance L and area dS (as projected on the plane normal to the direction of observation) has, by definition, an intensity dI = L dS and produces at a distance Δ an illumination $dE = dI/\Delta^2 = L\ dS/\Delta^2$; but $dS/\Delta^2 = d\omega$ is the solid angle subtended by dS at distance Δ; hence, the luminance can be expressed either as the intensity of the (projected) unit area of the source or as the illumination produced by the unit solid angle of the source. The second definition is especially useful when considering a luminous volume whose emitting surface is indefinite (e.g., the sky).

3.2. Energy units

The surface density of radiant-energy flux or irradiance E_e is expressed in ergs per square centimeter per second (and per Angström

if it is in a specified narrow spectral range). Other units: 1 watt cm^{-2} = 10^7 erg cm^{-2} sec^{-1}; 1 cal cm^{-2} min^{-1} = $\frac{1}{60}$ x 4.185 x 10^7 = 6.98 x 10^5 erg cm^{-2} sec^{-1}.

The radiance L_e of an emitting surface is the radiant intensity per unit area of the surface normal to the direction of observation; it is expressed in erg cm^{-2} sec^{-1} per steradian (and per Angström where required). The radiance of a perfect radiator (black body) in thermal equilibrium with an irradiance of 1 watt cm^{-2} is $L_e = 1/\pi$ = 0.318 w cm^{-2} per steradian.

3.3 Magnitude systems

The traditional system of visual stellar magnitudes m_v measures the illumination E which determines the luminous flux $\Phi = E\,S$ entering a given optical system having an entrance pupil of area S. By definition,

$$m_v = \mu_1 - 2.5 \log E \quad . \qquad (3.1)$$

The constant μ_1, the "stellar magnitude" of 1 lux, is not precisely known and its definition as the magnitude of a star observed "at sea level in the zenith on a very clear day" (Fabry, 1924) was rather unsatisfactory on account of the fluctuations of atmospheric transmission. If it is defined in agreement with the more logical modern convention by the illumination at the limit of the atmosphere, an earlier discussion of a variety of determinations (de Vaucouleurs, 1954, pp. 328-331) may be revised as follows:

comparison with sun: $m_v = -26.81$, $E = 1.40 \times 10^5$,

$\Delta m = 12.86$, $\mu_1 = -13.95$

comparison with moon: $m_v = -12.74 + 0.24 = -12.50$, $E = 0.25$,

$\Delta m = -1.51$, $\mu_1 = -14.01$

comparison with Vega: $m_v = +0.04 + 0.24 = +0.28$,

$\Delta m = -14.46$, $\mu_1 = -14.18$.

The revision takes into account changes from the old international photovisual magnitude system to the V system (see below), from the old international candle to the candela, and makes allowance for an average sea level atmospheric absorption of 0.24 mag. The adopted value

$$\mu_1 = -14.05 \pm 0.05: \qquad \text{(p.e.)}$$

is still subject to a rather large margin of error.

The uncertainty is of little consequence, since only magnitude differences are measured in practice, and absolute determinations require only a knowledge of the photometric constants for the sun (Subsection 3.5 below). In practice, the zero point of the V system is defined by the mean magnitude of 10 primary standard stars (Johnson, 1954). This system replaces the earlier "international photovisual system" IP_v defined by stars of $m_v = 8$ to 13 in the North Polar sequence; in the mean $V = IP_v - 0.02$.

The luminance may be expressed in (visual) magnitudes per square second of arc (or square degree, or steradian), since stellar magnitude is a measure of illumination. (See Subsection 3.1) Since 1 cm subtends 1" at a distance $\rho'' = 206{,}264.8$ cm $= 2{,}062.648$ m, 1 cd cm^{-2} corresponds to $m''_v = \mu_1 + 5 \log \rho'' \approx -14.15 + 16.57 \approx +2.4$ mag sec^{-2}.

3.4. Color indices and effective wavelengths

When detailed spectrophotometric data are not available, a rough indication of energy distribution is given by color indices -- the difference between magnitudes measured through two or more broad-band filters. By definition,

$$C_{1,2} = m_1 - m_2 = -2.5 \log \frac{\int_0^\infty E(\lambda)\, \tau_1(\lambda)\, Q_1(\lambda)\, d\lambda}{\int_0^\infty E(\lambda)\, \tau_2(\lambda)\, Q_2(\lambda)\, d\lambda}, \quad (3.2)$$

where $\tau(\lambda)\, Q(\lambda)$ is the product of the spectral transmission function of the filter-and-optical system and the quantum efficiency function of the receiver defining the spectral region of the magnitude m. For the standard photometric systems U, B, V, the magnitudes refer to broad bands in the ultraviolet, blue, and visual (yellow) ranges defined by specified filter + photocathode combinations (Johnson, 1954; Harris, 1961).

The center of gravity of the area under the curve $E(\lambda)\, \tau(\lambda)\, Q(\lambda)$ defines the effective (or more precisely the isophotic) wavelength λ_e of a given source--filter--receiver combination; the effective wavelengths of a number of common photometric systems for the solar radiation function $E_s(\lambda)$ are listed in Table 1 (de Vaucouleurs, 1960; Harris, 1961).

A "gray" or neutral scatterer would have the same color indices as the source of illumination; intrinsic color, i.e., selective reflectivity, is indicated by the positive or negative "color excess" of the body with respect to the color index of the sun over the same spectral range. Most planets have positive color excesses, i.e., are "redder" than the sun. Earth and Venus at large phase angles (when in crescent phases) have small negative color excesses, i.e., are bluer than the sun, mainly because of Rayleigh scattering in their atmospheres.

If $E_s(\lambda)/E_s(V)$ is the relative spectral energy distribution function of the sun, normalized to $\lambda = \lambda_v$, and $\delta C(\lambda) = C(\lambda) - C_s(\lambda)$ is the color excess of a planet, the relative spectral-energy distribution function of the planet is given, in first approximation, by

$$\log \frac{E(\lambda)}{E(V)} = \log \frac{E_s(\lambda)}{E_s(V)} - 0.4\, \delta C(\lambda) \quad . \qquad (3.3)$$

It would be necessary in a second approximation to allow for the change of effective wavelength of the filter + receiver combination depending on the source function. For instance, λ_e for the B system varies from approximately 0.44 μ for white stars ($B - V \approx 0$) to 0.46 μ for red stars ($B - V \approx + 1.5$); the range is smaller in the U and V systems with their smaller bandwidths. The error is often small enough to be neglected and decreases rapidly with bandwidth $\Delta\lambda$; it is completely negligible for the narrow bandwidths ($\Delta\lambda < 0.01\ \mu$) used in "monochromatic" magnitude systems and in spectrophotometry. In the latter case, precise allowance must be made for the effect of even slight differences between

the absorption spectra of the sun reflected by a planet and those of the comparison stars since such differences may cause apparent fluctuations in the derived spectral energy curve of the planet (Guérin, 1962).

Except perhaps for the moon and Mercury, the spectral energy distribution of sunlight selectively reflected by a planet varies with phase angle because of the varying contributions of the surface and of the atmosphere. This is measured by a phase dependence of the color indices; data on this subject are still scanty and limited mainly to the U - B and the B - V indices.

3.5. Solar units

The illumination produced by the sun at unit distance, sometimes called the "luminous solar constant" (Sharonov, 1936; de Vaucouleurs, 1954, p. 329) is, approximately

$$E_s = 1.40 \times 10^5 \text{ lux } (= 1.3 \times 10^4 \text{ foot-candle}) \quad ,$$

and the corresponding luminance of a Lambert disk exposed to it is

$$L_1 = 4.5 \text{ cd cm}^{-2} \ (= 14 \text{ Lamberts}) \quad .$$

The energy flux received from the sun at unit distance, or "solar constant" (Allen, 1958), is very nearly

$$E_s^* = 2.00 \text{ cal cm}^{-2} \text{ min}^{-1}$$

or

$$\int_0^\infty E_s \ (\lambda) \ d\lambda = 1.40 \times 10^6 \text{ erg cm}^{-2} \text{ sec}^{-1} = 0.14 \text{ w cm}^{-2} \quad ,$$

and the corresponding radiance of a black disk in radiative equilibrium with it is

$$\int_0^\infty L_0 (\lambda)\, d\lambda = 34 \text{ erg cm}^{-2} \text{ sec}^{-1} \text{ deg}^{-2} \quad .$$

The visual magnitude of the sun (at unit distance) is still uncertain, perhaps by as much as 10 per cent (or 0.1 mag.), and this uncertainty will be reflected in the albedo values. From several discussions of classical and modern determinations (de Vaucouleurs, 1954, p. 329; Harris, 1961, p. 275),

$$m_s (V) = - 26.81 \quad ,$$

with an estimated probable error of 0.02 to 0.03 mag.

The color indices of a star having the same spectral type G2 V as the sun, are as follows (de Vaucouleurs, 1960; Harris, 1961):

$$U' - V = +0.63,\ U - B = + 0.14,\ B - V = + 0.63,\ V - R = + 0.45,$$

$$R - I = + 0.29.$$

The spectral-energy distribution function of integrated solar radiation is known with sufficient accuracy for the problems of broad-band multicolor photometry of the planets. The values in Table 2, adapted from Allen (1955), are normalized to a solar constant of 2.00 cal cm^{-2} min^{-1}. Here and in Fig. 3, the absorption spectrum of the sun is smoothed over an effective bandwidth of 0.01 μ. The normalization factor corresponds very nearly to a spectral irradiance

$$E_s (V) = 200 \text{ erg cm}^{-2} \text{ sec}^{-1} \text{ per Angstrom}$$

at the effective wavelength $\lambda_v \simeq 0.555\ \mu$.

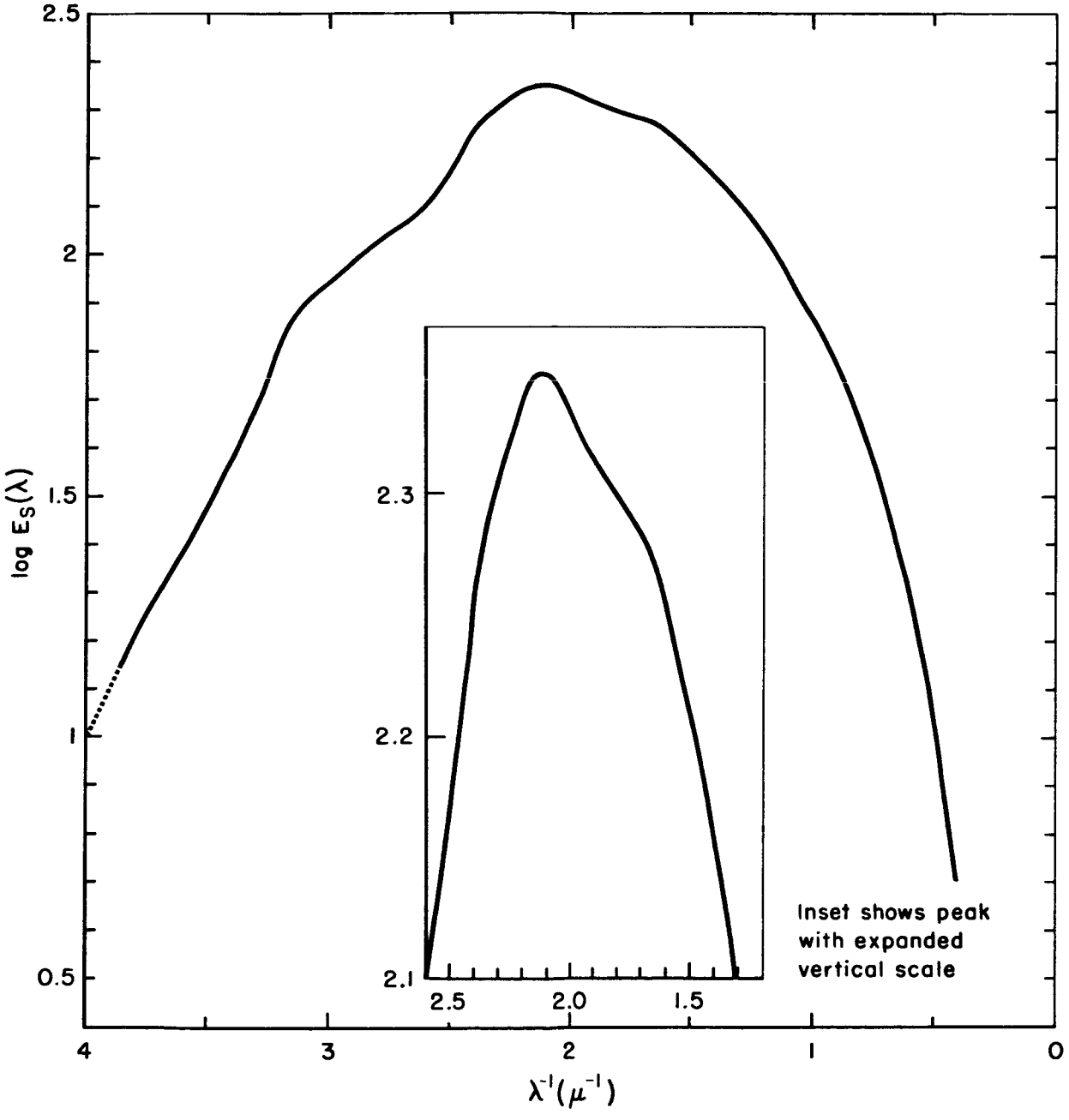

Fig. 3 Smoothed spectral energy distribution of solar radiation

By integration of $E_s(\lambda)$, the fraction

$$k_s(\lambda) = \frac{\int_0^{\lambda} E_s(\lambda)\, d\lambda}{\int_0^{\infty} E_s(\lambda)\, d\lambda} \tag{3.4}$$

of the energy radiated at wavelengths less than λ can be computed (Fig. 4); in particular, $k_s = 1/2$ for $\lambda = \lambda_s(1/2) = 0.715\ \mu$; i.e., half the solar energy is in the infrared radiations of $\lambda > \lambda_s(1/2)$. Because the infrared albedos of the planets are still poorly known -- or unknown -- the computation of the radiometric (or integral) albedos are accordingly uncertain (Subsection 12.3).

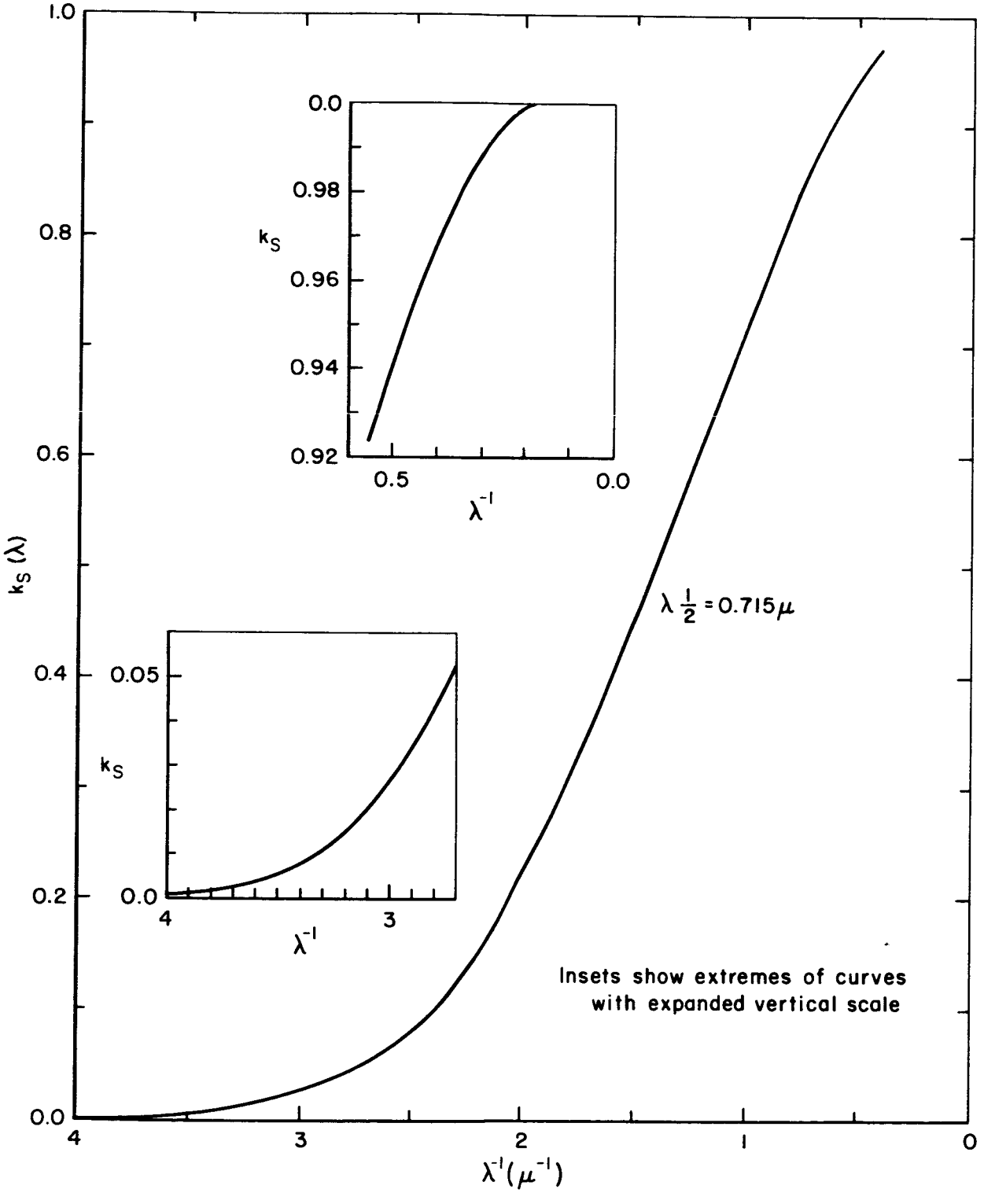

Fig. 4 Fraction of integrated solar radiation emitted between 0 and λ

4. PHOTOMETRIC PARAMETERS

4.1. Reduced magnitudes

Let E_s be the flux density (or "illumination") received (in a given spectral range) from the sun at unit astronomical distance, E(i) the flux density received from the planet when it is at distance R from the sun and Δ from the earth, and i the phase angle sun-planet-station. By definition, the relation between the corresponding apparent magnitudes m_s and m is

$$\log \frac{E(i)}{E_s} = 0.4\ (m_s - m) \quad . \tag{4.1}$$

In astronomical practice, the observed magnitudes are reduced to some standard values of R and Δ, usually $R\,\Delta = 1$, through the inverse-square law

$$E\ (R,\Delta,i) = \frac{E(1,1,i)}{R^2\ \Delta^2} \tag{4.2}$$

and

$$m_1\ (i) = m\ (i) - 5 \log R\,\Delta \quad . \tag{4.3}$$

In particular, when $i = 0$ (full phase),

$$m_1\ (0) = m\ (0) - 5 \log R(0)\ \Delta\ (0) \quad . \tag{4.4}$$

This situation $R\,\Delta = 1$ with $i = 0$ is a mathematical fiction; some astronomers prefer to reduce the data to the planetary mean distance at opposition, $R_0\Delta_0 = R_0\ (R_0 - 1)$, if R_0 is the semimajor axis of the orbit, which is physically observable for an exterior planet such as

Mars. For interior planets the data are reduced to R_0 and $\Delta_0 = 1$, again a fictitious situation for i = 0. The usual convention, $R\,\Delta = 1$, will be adopted here. The reduction constants in the relation

$$m_1\,(R\,\Delta = 1) = m\,(R_0\,\Delta_0) - 5 \log R_0\,\Delta_0 \qquad (4.5)$$

are as follows:

	Mercury	Venus	Mars
R_0	0.3871	0.7233	1.5237
$R_0\,\Delta_0$	0.3871	0.7233	0.7980
$-5 \log R_0\,\Delta_0$	2.061	0.703	0.490

4.2. Phase functions

The phase function is defined by

$$\Phi\,(i) = \frac{E\,(i)}{E\,(0)} \qquad (4.6)$$

and given by

$$\log \Phi\,(i) = 0.4\,[m_1\,(0) - m_1\,(i)] \quad . \qquad (4.7)$$

It measures the relative luminous intensity of the planet as a function of phase angle normalized to unity at full phase (for the same $R\,\Delta$). The phase function may be represented by a plot of the reduced magnitude $m_1\,(i)$ in rectangular coordinates or better by the diffusion indicatrix, a plot of $\Phi\,(i)$ in polar coordinates (Fig. 5).

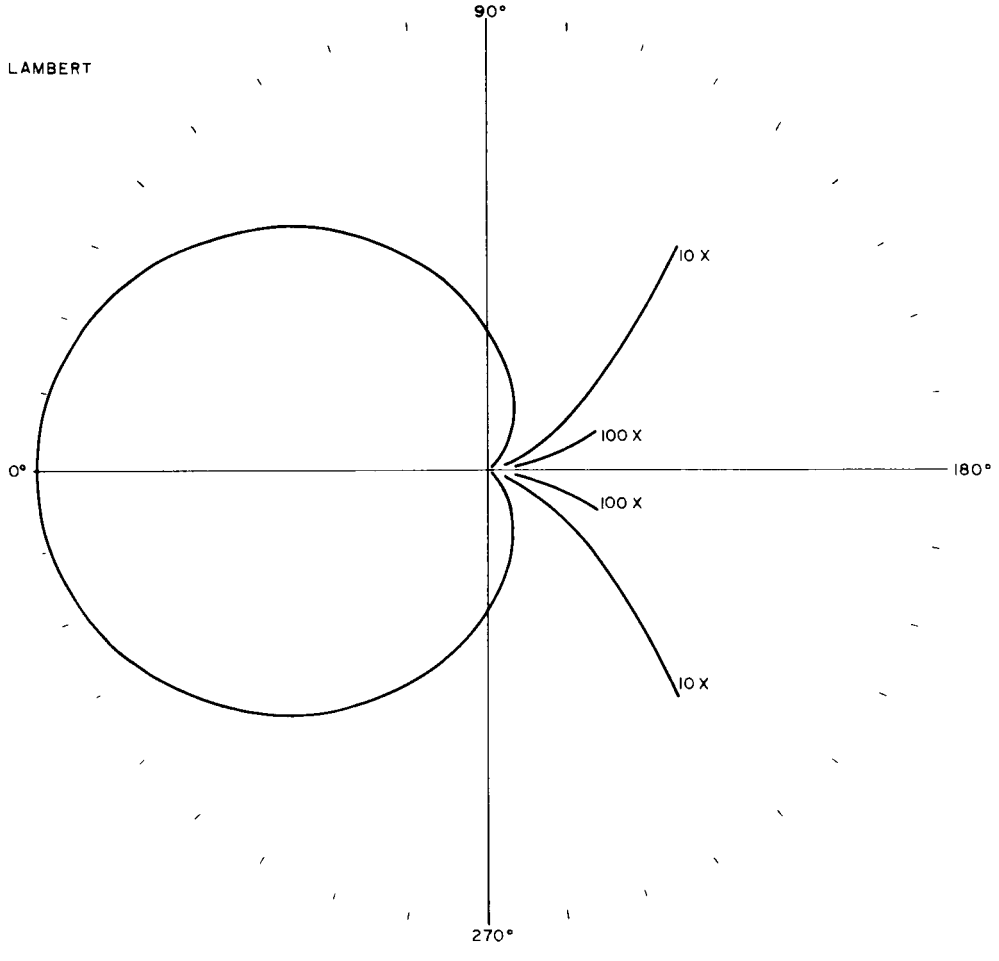

Fig. 5 Phase curve of Lambert sphere
$\Phi_0(i)$ in polar coordinates

The mean relative luminance of the planet at phase i is

$$\beta\ (i) = \frac{L\ (i)}{L\ (0)} = \frac{\Phi\ (i)}{k} = \frac{2\ \Phi\ (i)}{1 + \cos\ i} \quad , \qquad (4.8)$$

where the illuminated fraction of the disk k is given by Eq. (2.11). Here the average luminance of the disk at full phase L (0) is taken as unity.

4.3. Geometric albedo

The geometric albedo p is the ratio of the average luminance of the planet at full phase (i = 0) to that of a perfectly diffusing surface (Lambert surface) at the same distance from the sun and normal to the incident radiation. It is also equal to the ratio of the luminous intensity of the planet at full phase to that of a Lambert disk of equal diameter normally illuminated and at the same distances R (to the sun) and Δ (to the observer). If r is the linear radius and σ the angular semi-diameter of the planet at distance Δ,

$$p = \frac{E\ (0)}{E_s}\ \frac{R^2\ \Delta^2}{r^2} = \frac{E\ (0)}{E_s}\ \frac{R^2}{\sin^2\ \sigma} \quad . \qquad (4.9)$$

If σ_1 is the apparent semi-diameter at unit distance, and if we write $m_0 = m_1\ (0)$, then Eqs. (4.1), (4.2), and (4.9) give

$$\log_{10}\ p = 0.4\ (m_s - m_0) - 2\ \log_{10}\ \sin\ \sigma_1' \quad . \qquad (4.10)$$

Here, σ_1' is the radius of a circle having the same projected area as the planet's disk; for an observer in the equatorial plane of a planet of ellipticity f,

$$\sigma_1' = \sigma_1 \sqrt{1 - f} \simeq \sigma_1\ (1 - \frac{f}{2}) \quad . \qquad (4.11)$$

For all terrestrial planets, σ_1' differs from σ_1 by less than 0.5 per cent. By substituting Eqs. (2.1) and (2.2) in Eq. (4.10),

$$\log p = 0.4\ (m_s - m_0) - 2 \log \frac{\sigma_1''}{\rho''} \quad , \tag{4.12}$$

where σ_1'' is in seconds of arc and $\log \rho'' = 5.314\ 425$.

The luminance of a Lambert disk illuminated by the sun at normal incidence and at unit astronomical distance is, by definition,

$$L_1 = \frac{E_s}{\pi} \quad . \tag{4.13}$$

The average luminance of a planet at full phase and distance R to the sun is, by Eqs. (4.9) and (4.13),

$$L\ (0) = p\ \frac{L_1}{R^2} = \frac{E\ (0)}{\pi \sin^2 \sigma} \quad . \tag{4.14}$$

4.4. Phase integral and spherical albedo

The spherical albedo (or Bond Albedo) $A = p \cdot q$ is the ratio of the total luminous flux (or quantity of light per unit time) reflected by a sphere in all directions to the total flux intercepted by it in a beam of parallel light. The phase integral q is, by definition,

$$q = \int_0^{2\pi} \Phi\ (i) \sin i\ di \quad . \tag{4.15}$$

If the phase law Φ (i) is symmetrical with respect to the direction of incidence,

$$q = 2 \int_0^{\pi} \Phi\ (i) \sin i\ di \quad . \tag{4.16}$$

This assumption can always be made for purposes of computation, even if the actual phase law is asymmetrical (the moon and Mercury), by considering a mean phase law

$$\overline{\Phi\ (i)} = \frac{1}{2}\ [\Phi\ (i) + \Phi\ (2\pi - i)] \quad . \tag{4.17}$$

The phase integral q is equal to the volume inside the surface generated by rotation about the polar axis of the phase curve Φ (i) plotted in polar coordinates (Fig. 5).

For an ideal sphere following Lambert's law of scattering

$$L = L_1 \cos \theta \quad , \tag{4.18}$$

where θ is the angle of incidence, the phase function is

$$\Phi_0\ (i) = \frac{1}{\pi}\ [\sin i + (\pi - i)\cos i] \tag{4.19}$$

and

$$q_0 = \frac{3}{2} \quad . \tag{4.20}$$

Since the albedo of a perfectly scattering sphere is, by definition, $A_0 = 1$, it follows that $p_0 = A_0/q_0 = 2/3$; hence, the average luminance of a Lambert sphere at full phase and unit astronomical distance from the sun is

$$L_0 = \frac{2}{3}\ L_1 = \frac{2}{3}\ \frac{E_s}{\pi} = 0.2122\ E_s \quad . \tag{4.21}$$

No real planet obeys Lambert's law, and departures are often large; in general, Φ (i) decreases more rapidly than Φ_0 (i) away from full phase. This is especially true of planets without an atmosphere

(the moon and Mercury), for which $q \simeq 0.5$ to 0.6; planets with atmospheres (Mars, Earth, and Venus) have $q \simeq 0.9$ to 1.1; and the major planets (Jupiter, Saturn, etc.) may have $q \simeq 1.5$ to 1.7. For the moon, Mercury, and Venus (and also for Earth through observations of the earth-shine on the moon), Φ (i) can be determined directly; for Mars and all exterior planets, only a small range of phase angles can be directly observed, and q must be estimated by extrapolation of the phase curve.

4.5. Russell rule

As noted by Russell (1916), if p (i) is the value of p computed from E (i) instead of E (0) in Eq. (4.9), the albedo may also be written

$$A = p\ (i)\ \frac{q}{\Phi\ (i)} \quad . \tag{4.22}$$

According to Russell, the second factor is very nearly a constant $q/\Phi\ (i) \simeq 2.20$ (to about ± 5 per cent) when $i = 50^{\circ}$ for all observed phase functions. (It is 2.12 for Lambert's.) Hence, the empirical formula

$$A \simeq 2.20\ p\ (50^{\circ}) = 2.20\ \frac{E\ (50^{\circ})}{E_s}\ \frac{R^2\ \Delta^2}{r^2} \tag{4.23}$$

may be used to give the Russell-Bond albedo when the complete phase curve is not known. More recently, Harris (1961) found $q = 2.17\ \Phi\ (50^{\circ})$ from modern phase curves for Mercury, Venus, Earth, and the moon.

Since no theoretical expression is available to represent the observed phase laws, it is customary to use empirical interpolation formulae of the form

$$m = m_0 + 5 \log R\ \Delta + a\ i + b\ i^2 + c\ i^3 \tag{4.24}$$

where $m_0 \equiv m_1$ (0). For Mars, the range of phase angles observable from Earth is $0 \leq i < 48^{\circ}$; the coefficients b, c cannot be derived, and a is often called the phase coefficient (expressed in magnitude per degree); then, by Russell's rule,

$$q = 2.20 \cdot 10^{-0.4 \cdot 50\, a} , \tag{4.25}$$

or

$$\log q = 0.34242 - 20\, a . \tag{4.26}$$

4.6. Radiometric albedo

Monochromatic observations of m (λ) and m_s (λ) give the spectral reflectivity function p (λ) and the spectral variation of the phase integral q (λ); hence, the spectral albedo A (λ) = p(λ) q(λ). If E_s (λ) is the spectral energy distribution function of solar radiation, the integral geometric albedo for the total solar radiation is defined by

$$p^* = \frac{\int_0^\infty p(\lambda)\, E_s\, (\lambda)\, d\lambda}{\int_0^\infty E_s\, (\lambda)\, d\lambda} \tag{4.27}$$

and

$$q^* = \frac{\int_0^\infty q(\lambda)\, E_s\, (\lambda)\, d\lambda}{\int_0^\infty E_s(\lambda)\, d\lambda} . \tag{4.28}$$

The radiometric or integral spherical albedo,

$$A^* = p^* \cdot q^* , \tag{4.29}$$

is the fundamental quantity of theoretical meteorology; it determines

the fraction $(1 - A^*)$ of the incident solar energy absorbed by the planet (surface and atmosphere). The total solar energy flux absorbed by the planet is

$$F^* = (1 - A^*)\, \pi\, r^2\, \frac{E_s^*}{R^2} \quad , \tag{4.30}$$

where E_s^* is the terrestrial solar constant (in erg cm^{-2} sec^{-1}), r the planetary radius (in cm), and R the distance to the sun (in astronomical units). Computation of the integrals in Eqs. (4.27) and (4.28) requires the values of $p(\lambda)$ and $q(\lambda)$; these are still often unknown, especially in the infrared which contributes about half the solar radiant energy (Subsection 3.5). The assumption, often made in the past, that $p^* \simeq p_v$, where V refers to the visual effective wavelength $\lambda_v \simeq 0.555\mu$, is correct only for a "gray" planet (i.e., one having the same color as the sun); it is incorrect for all real planets, and the error is especially large (almost 100 per cent) for a strongly colored planet such as Mars (Subsection 12.3)

4.7. Spectral irradiance

The monochromatic energy flux density or spectral irradiance received <u>from</u> a planet at unit distance ($R\,\Delta = 1$) and full phase ($i = 0^\circ$) is given by

$$\log E_0(\lambda) = \log E_s(\lambda) + 0.4\,[m_s(\lambda) - m_0(\lambda)] = \log E_s(\lambda)\, K(\lambda) \quad . \tag{4.31}$$

It is convenient to normalize this quantity to the visual effective wavelength, $\lambda_v = 0.555\ \mu$.

$$E_0(V) = E_s(V)\, K(V) \quad , \tag{4.32}$$

where $E_s(V) = 200$ erg cm^{-2} sec^{-1} A^{-1} (cf. Subsection 3.5), and as above $E_0 \equiv E$ ($i = 0$, $R\,\Delta = 1$). Then, at any other wavelength

$$E_0(\lambda) = E_0(V)\,\frac{E_s(\lambda)\,K(\lambda)}{E_s(V)\,K(V)} = E_0(V)\,\frac{E_s(\lambda)p(\lambda)}{E_s(V)p(V)} \quad . \qquad (4.33)$$

At other phases and distances, the spectral irradiance at λ_v is

$$E_v(i,R\,\Delta) = \frac{E_v(0,1)\cdot\Phi_v(i)}{R^2\,\Delta^2} \quad , \qquad (4.34$$

and at other wavelengths

$$E_\lambda\,(i,\,R\,\Delta) = E_v(i,\,r\,\Delta)\,\frac{\Phi_\lambda(i)}{\Phi_v(i)}\,\frac{E_s(\lambda)}{E_s(V)} \quad . \qquad (4.35)$$

If a planet is observed through an optical system of aperture area S, focal length F, and transmission factor $T(\lambda)$, the energy flux incident in the image is

$$e_\lambda(i,R\Delta) = \frac{S}{R^2\Delta^2}\,E_0(V)\,\Phi_i(V)\int_0^\infty \frac{\Phi_i(\lambda)}{\Phi_i(V)}\,\frac{E_s(\lambda)}{E_s(V)}\,\frac{p(\lambda)}{p(V)}\,T(\lambda)\,d\lambda \quad , \qquad (4.36)$$

and the average energy flux per unit area of the image (irradiance) is

$$\frac{e_\lambda}{S} = \frac{e_\lambda}{\pi(\sigma F)^2\,k(i)} = \frac{S}{\pi F^2\sigma_1^2}\,\frac{\Phi_i(V)}{k(i)}\,\frac{E_0(V)}{R^2}\int_0^\infty \frac{\Phi_i(\lambda)}{\Phi_i(V)}\,\frac{E_s(\lambda)}{E_s(V)}\,\frac{p(\lambda)}{p(V)}\,T(\lambda)\,d\lambda \quad , \qquad (4.37)$$

where k (i), the illuminated fraction of the disk, is given by Eq. (2.11). It is assumed that σ is small enough to use the approximation (2.1). The energy available to a receiver of quantum efficiency $Q(\lambda)$ follows by multiplication of the integrands through $Q(\lambda)$ in Eqs. (4.36) and (4.37).

5. APPARENT DIAMETER MEASUREMENTS

The apparent diameters of planets are notoriously difficult to measure; published values for the apparent diameters at unit distance vary from less than 6" to more than 7" for Mercury; from 16"6 or less to 17"6 or more for Venus; from under 9"0 to over 9"6 for Mars. A correct interpretation of such measurements requires some understanding of the methods used, observational difficulties and systematic errors.

5.1. Filar micrometer

Two fine wires can be moved by a precision screw in the focal plane of a telescope until they appear tangent to the opposite limbs of the planet's disk or are judged by the eye to be spaced by a distance equal to the planet's diameter. Because of the unsteadiness of telescopic images due to atmospheric turbulence ("seeing"), irregular refractions, erratic telescope drive and other causes of instability (e.g., wind), taking filar micrometer measurements has been aptly compared to shooting at an eggshell floating on a water jet. Even under the best circumstances, it is very difficult to define what it is that the observer measures; wires can be set tangent internally or externally to the disk and a correction applied for the thickness of the wires (often ranging from 0"1 to 1"), or the wires may be set to bisect the edge, an operation that requires considerable judgment.

(a) Bright disk. The observer never sees a perfectly sharp image of the object but a kind of optical "ghost," which always significantly suffers from such distortions as diffraction, chromatic aberration, and aberrations of the eye, notably irradiation and astigmation. All these effects combine to replace the "rectangular"

photometric profile of even an ideal flat disk of uniform luminance by a smoothed distribution with indefinite edges such as in Fig. 6. There is no way of knowing exactly where the observer's eye--brain system will set the apparent edge of this continuous distribution, whether near AA', or BB', or CC'. It is often assumed, with some support from laboratory experiments, that the apparent edge is at or near the point of maximum slope, which for a large enough disk is close to the geometric edge, but this is not necessarily so in all circumstances. The position of the apparent edge depends very much on the brightness of the surrounding field; in the case of a dark field around a bright planet observed at night, the edge is likely to be near AA', as light will be seen spilling over the geometric edge under such circumstances, and the brighter the planet the greater this "irradiation" effect. For instance, observations of Venus by Barnard (1902) with the Yerkes 40-inch refractor gave for the reduced diameter 17"39 (5 nights, no filter) and 17"14 (8 days, amber filter), or a differential irradiation error $\delta\sigma$ (night minus day) = + 0"25. For a planet of such high luminance as Venus, which is some 10 to 50 times brighter than the daytime sky, the residual daytime irradiation may be easily of the same order of magnitude. For a planet of lower surface brightness such as Mercury and, especially, Mars the apparent edge of the image is more likely to be near CC' for daytime observations, and the measured apparent diameter will be too small. For example, Campbell (1895), observing Mars through a yellow filter with the Lick 36-inch refractor (aperture stopped to about 15 in. by a diaphragm), noted that measures made at night are 0"3 to 0"6 greater than measures made after sunrise; likewise, Lowell (1895, 1896)

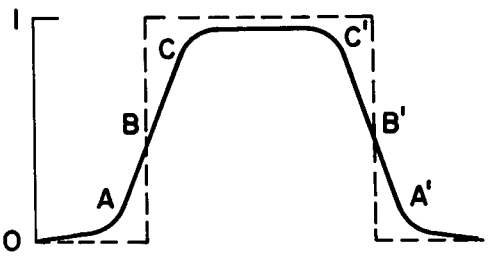

Fig. 6 Photometric profile of diffraction image of uniform bright disk

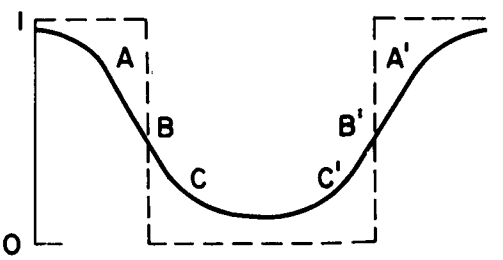

Fig. 7 Photometric profile of diffraction image of dark disk

estimated irradiation at 0"3 for the equatorial diameter of Mars, and 0"6 for the polar diameter when the bright polar caps are present. Other estimates are 0"53 (Kaiser, 1872) and 0"76 (See, 1901).

(b) Black disk. If the planet appears as a black disk on a bright background, as Mercury and Venus in transit, the photometric profile is reversed as in Fig. 7; the planet appears as a black core surrounded by a fuzzy penumbra, and whether the apparent edge will be in AA', or BB', or CC', depends, in an unpredictable manner, on the particular combination of observing circumstances -- atmospheric seeing, telescopic aperture, magnification, observer, etc. Experience, however, generally shows that the apparent edge is likely to be nearer CC', since the observer apparently notices more readily the positive effect of sunlight encroaching on the dark spot than the negative effect of light depletion around the dark spot. The effect is especially large during solar transits, because bad seeing is prevalent in daytime, particularly as the telescope is pointing straight at the sun and the telescope aperture is often strongly diaphragmed to prevent excessive heating, which causes diffraction effects to be correspondingly increased. For instance, Campbell (1895) took 32 filar micrometer measurements of Mercury with the Lick 36-inch refractor, stopped to 8 inches, during the transit of 1894. He derived a mean diameter of 8"468 ± 0"012, corresponding to 5"726 ± 0"008 at unit distance, which is probably as much as 1" too small (i.e., the apparent diameter was measured as much as 1"5 too small, an error of 18 per cent). Similarly Barnard (1895) derived a reduced diameter of 6"04 from micrometer measures with the Lick 12-inch refractor, diaphragmed to 4 inches, during the transit of 1891 when

the seeing was poor. From measures with the same instrument, stopped to 5 and 6 inches, during the transit of 1894 when the seeing was good, he derived a reduced diameter of 6"22, which is still about 0"5 too small, an error of 9 per cent. It is clear that in such cases the observer measures the dark core CC' of the image (Fig. 7). The apparent edge of this core is itself poorly defined and depends among other things on magnifying power; for instance a new reduction of Barnard's observations of 1891 and 1894 discloses a systematic difference between apparent diameters measured with high magnification (x 500) and low magnifications (x 150, x 175), $2\,\delta\sigma$ (H - L) = + 0"355 (1891) and + 0"405 (1894) or nearly 4 per cent; the total range of the reduced diameter $2\,\sigma_1$ is from 5"98 ± 0"04: p.e. (1891, low power, poor seeing) to 6"29 ± 0"03 p.e. (1894, high power, good seeing).

There are also considerable systematic differences (or "personal equation") between observers in locating the edge of the image; for instance during the transit of Mercury of 1914 (Jonckheere, 1914) numerous filar micrometer measurements of the apparent diameter by several observers with the Greenwich Observatory 28-inch refractor, stopped to 15 and 20 inches, under good seeing conditions, vary systematically from 9"38 ± 0"03 m.e. (154 meas.) to 9"74 ± 0"04 m.e. (132 meas.), a 3.8 per cent change. Although all observing conditions were the same, the reduced diameters vary from 6"33 to 6"56.

(c) Contacts. A similar effect applies to diameters derived from timing the apparent contacts of the sun's edge with the limbs of Mercury or Venus. The geometric profile is replaced by the smoothed photometric profile AB....G, which becomes A'B' ....G' when the planet

approaches the sun's limb $\alpha\beta$. In the region of depressed luminosity near G', where images of the sun and the planet limbs overlap, the "black drop" effect is observed (Fig. 8). The apparent contact is the progressive and indefinite merging of two penumbral zones whose timing becomes subject to much arbitrariness. For instance, Innes (1925), discussing all observations of transits of Mercury from 1677 to 1924, found a slow secular increase in the derived apparent diameter at unit distance:

Epoch	1677--1756	1769--1802	1822--1848	1861--1881	1891--1924
$2\sigma_1$	6"02	6"06	6"10	6"14	6"16

There was a simultaneous <u>decrease</u> of the sun's diameter derived from the same data. These variations are clearly an effect of the slow decrease of instrumental aberrations as telescopic equipment improved, but even modern data are far from free of aberration and a "present" value of 6"2 extrapolation from Innes' data is still certainly too small. For instance, Williams (1939) derived a diameter of 6"30 from an analysis of 16 transits between 1799 and 1927, while Clemence and Whittaker (1942) deduced a diameter of 6"41 from 32 observations of the transit of 1940.

5.2. Irradiation correction

The classical approach to the correction of measures for "irradiation" is not satisfactory and occasionally leads to values even more grossly in error than the uncorrected data. The assumption is that the irradiation error is a constant c and that the observed value can be expressed by

$$\sigma = \frac{\sigma_1}{\Delta} + c \quad . \tag{5.1}$$

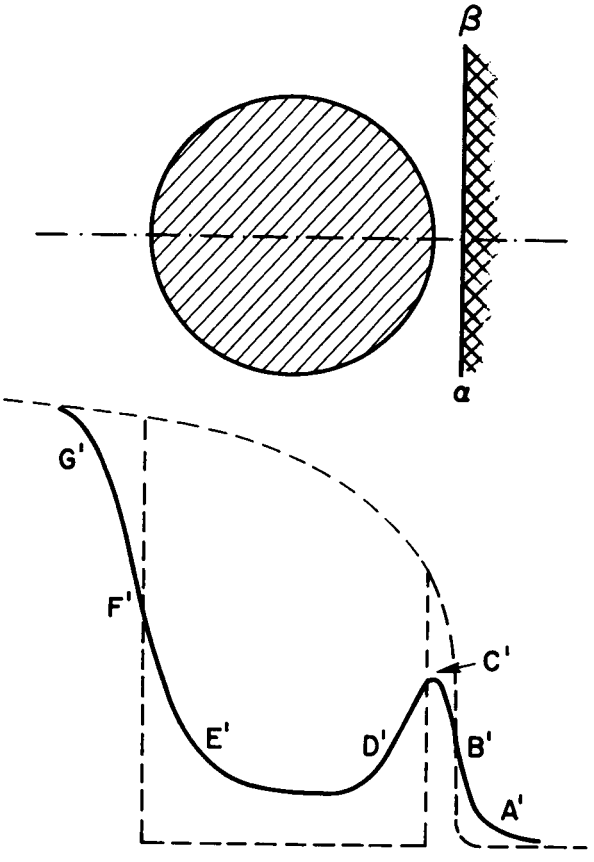

Fig. 8 Photometric profile of Mercury or Venus near contact during transits

This error model fails because the systematic errors are not constant and vary not only with the changing luminance of the sky background with phase angle, but also (for the interior planets) with the variable size and shape of the planetary disk. Thus, for Mars, which is observed at night near opposition, in the twilight near quadratures and in daytime at smaller elongations, not only do nighttime observations uncorrected for irradiation give reduced equatorial diameters in the range 9"6 to 9"7 which are clearly too large (Campbell, 1892, 1895; Barnard, 1897), but a treatment of both daytime and nighttime observations through Eq. (5.1) leads to values of the polar diameter in the range 9"4 to 9"6 which are still too large (Wirtz, 1912; Rabe, 1928).

Similarly a plot (Fig. 9) of the measured apparent diameter of Venus reduced to unit distance by simple distance scaling, i.e., $2\sigma_1 = 2\sigma\Delta = d_1$, shows a systematic trend which clearly does not obey Eq. (5.1). For most observers the reduced value d_1 of $2\sigma_1$ increases from $d_1 \approx 16"6$ when $d \approx 10"$ near full phase to a maximum of $d_1 \approx 17"1$ when $d \approx 35"$ near quarter phases; then it often decreases to $d_1 \approx 16"9$ when $d \approx 50"$ to $60"$ in the narrow ring phases. This trend is present in measurements made with both filar micrometers (Drew, Rabe, Danjon) and double-image micrometers (Kaiser, Muller). It is clear that if observations with $d < 30"$ to $40"$ only are fitted by Eq. (5.1), the result will be a grossly over-corrected reduced diameter in excess of 17"0 and often in the range 17"2 to 17"6. Occasionally d_1 is more nearly constant and it may even show an opposite trend (see Fig. 9, Wirtz). The oversimplified error model expressed by Eq. (5.1) is, therefore, not applicable.

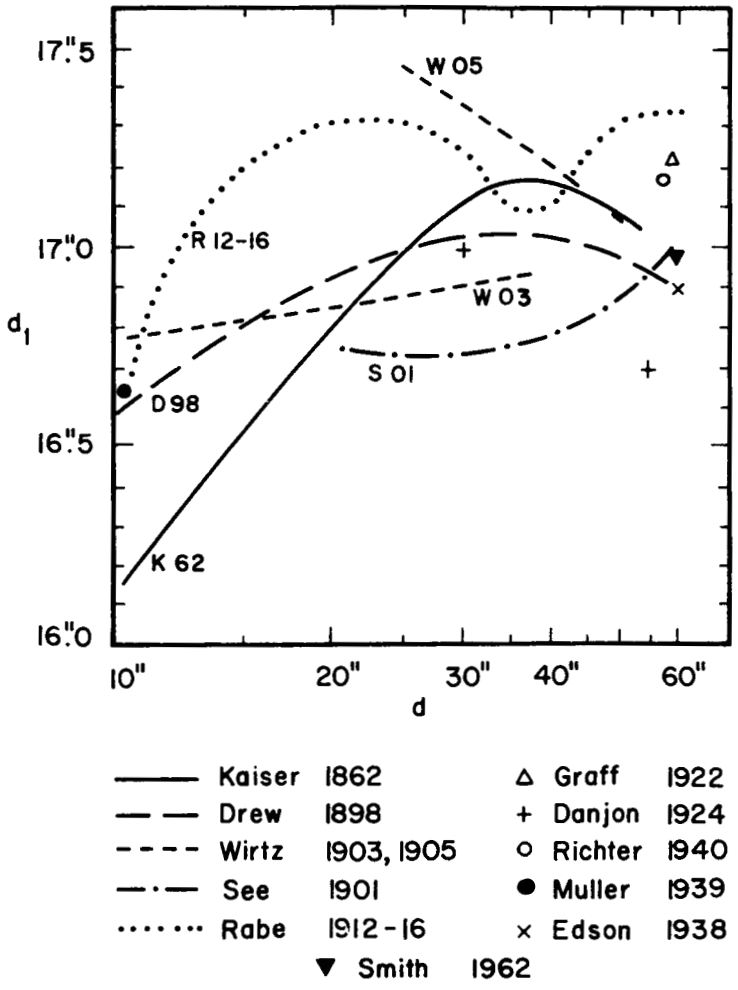

Fig. 9 Systematic errors in micrometer measurements of Venus

5.3. Limb darkening

Apart from irregular surface or atmospheric markings, the luminance of planetary disks is not uniform. The limb may be either brighter or darker than the center of the disk. Planets with a scattering and absorbing atmosphere, such as Venus and Mars, show limb darkening at the longer wavelengths ($\lambda > 0.5\ \mu$) and, at least for Mars, limb brightening at the shorter wavelengths ($\lambda < 0.5\ \mu$). Planets without an atmosphere such as the moon and Mercury may be more or less uniform up to the limb. Limb darkening has a serious effect on diameter measurements with both filar and double-image micrometers. The photometric profile along a diameter affected by both limb darkening and optical aberrations is as in Fig. 10. Even for a large disk, the half intensity points BB' are now inside the geometric edge and the diameter BB' measured with a double image micrometer will be smaller than the geometric diameter DD'. This effect together with bad seeing is probably responsible for the usually small diameter values of Venus and Mars measured with double-image micrometers in daytime near superior conjunction; for example, Kaiser (1872) observing with an 8-inch refractor at Leiden under bad seeing conditions derived for Venus a mean reduced diameter of 16"20 from 10 days of double-image measurements near the superior conjunction of 1862, when the apparent diameter of Venus was about 10"5, and of 16"31 from 11 days in 1865 when the apparent diameter was about 13"5 (Fig. 9). These values are about 0"5 to 0"6 or 3.0 to 3.5 per cent too small. The error is smaller when the seeing conditions are better. In filar micrometer measurements where irradiation compensates in part for the effect of the limb darkening the error is also smaller; for example, other measurements of Venus near superior conjunction,

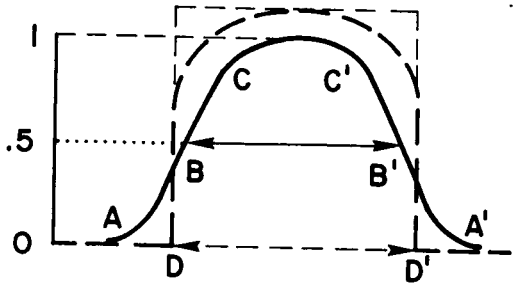

Fig. 10 Photometric profile of bright disk affected by limb darkening and optical aberrations

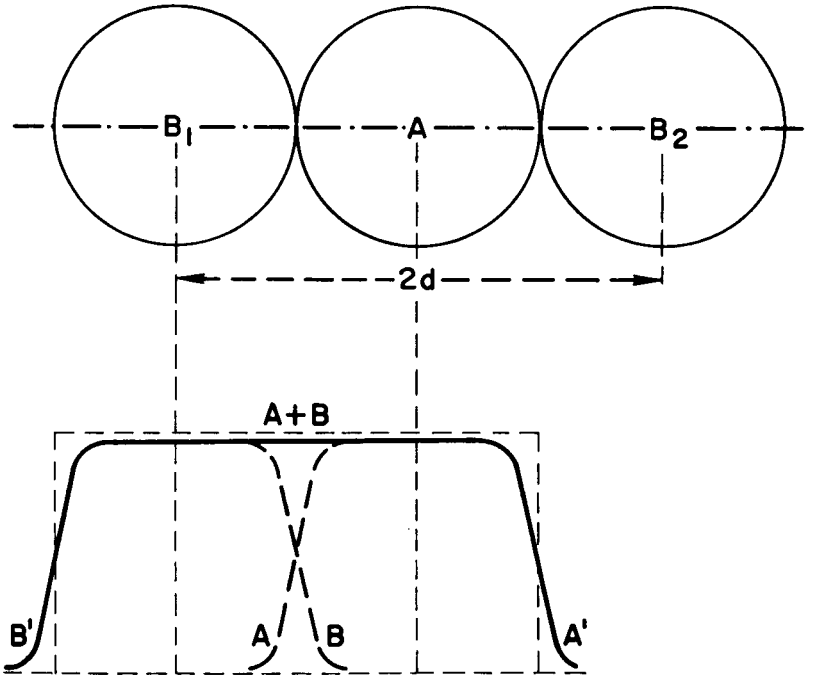

Fig. 11 Geometric and photometric principle of double-image measurements of diameter of planetary disk

when the apparent diameter was about 11", gave values for the reduced diameter ranging from 16"6 to 16"8 (Table 3) and averaging 16"66, which is still about 0"2 or 1.2 per cent too small.

Similarly, measurements of the polar diameter of the faint disk of Mars observed in daytime near superior conjunction result in values ranging from 9"00 (Muller, double image, 6-inch Strasbourg in 1937--38, $d \approx 4"$ to 6"5) to 9"22 (See, filar micrometer, 26-inch Washington in 1901, $d \approx 6"$), which are from 0"1 to 0"3 too small, or from 1.0 to 3.5 per cent.

5.4. Double-image micrometer

Two identical images, A and B, are produced in the focal plane of the telescope; they can be moved with respect to each other by a precision screw until their opposite limbs appear to be in contact first in position 1, then in position 2 (Fig. 11). The displacement is equal to twice the common diameter of the images. The image may be split by means of a heliometer, in which the two halves of an objective slide against each other, or by a variety of birefringent prism systems sliding either along the optic axis or across it. The observer judges that contact is established when neither a dark space, nor a brighter overlap region exists between the two images; at this moment the sum of the complementary photometric profiles of the opposite limbs is equal to the constant luminance of each image assumed uniform. This is a sensitive criterion because the region of greatest slope of the photometric profile occurs near the half-intensity points B, B' (Fig. 12). However, the simple assumption that these points coincide with the geometric edge of the image is true only for very large zones or disks. For small disks, whose radii are but a few times

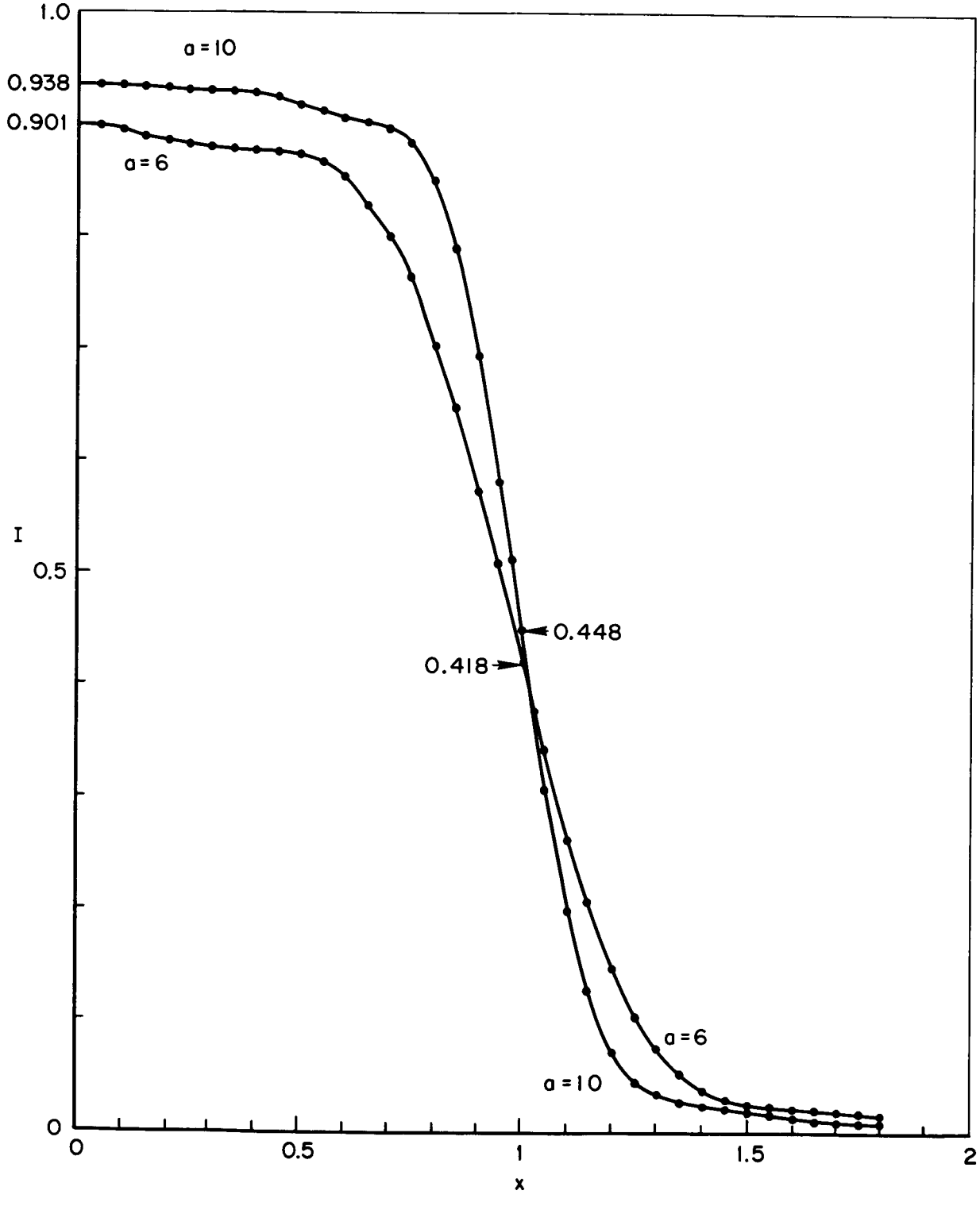

Fig. 12 Theoretical diffraction profiles of small disks (Camichel 1958)

the width of the transition zone, a complete calculation of the intensity distribution in the image is necessary. Camichel (1958) shows that the maximum luminance in the center of the image -- or contrast in the case of a black disk on a luminous background -- is reduced compared with its geometric value because of the redistribution of energy by diffraction (or other aberrations). Fig. 12 shows, for example, the theoretical brightness distribution along a diameter in the diffraction image of a small disk having a relative diameter $a = 6$ or 10 times that of the diffraction disk $\delta = 1.22\ \lambda/R$ (R = radius of objective), i.e., $a = 1.22\ \pi\epsilon/\delta$, if ϵ is the apparent diameter. The brightness distribution along the common axis of the overlapping images produced by a double-image micrometer is shown in Fig. 13; it is very nearly constant, i.e., the images appear just in contact, when the separation of the centers of the images is 2 per cent for $a = 6$, and 1 per cent for $a = 10$ <u>smaller</u> than the geometric diameter of the object. Experimental observations of test disks indicate that the actual error may be about twice as large as the theoretical values for pure diffraction, perhaps because of residual aberrations (Fig. 14). For very small diameter values ($a < 1.5$) the error changes sign as the measured diameter tends toward the constant value $\approx 0.85\ \delta$ when $\epsilon \to 0$ (this is the resolution limit for a double star with equal components). In practice, δ is often increased by residual optical aberrations and atmospheric turbulence. The following tabulation, based on Fig. 14, gives the corrections applicable to double-image measurements of Mercury in transit when $\epsilon \approx 10''$, for apertures $2R = 4$ to 12 inches.

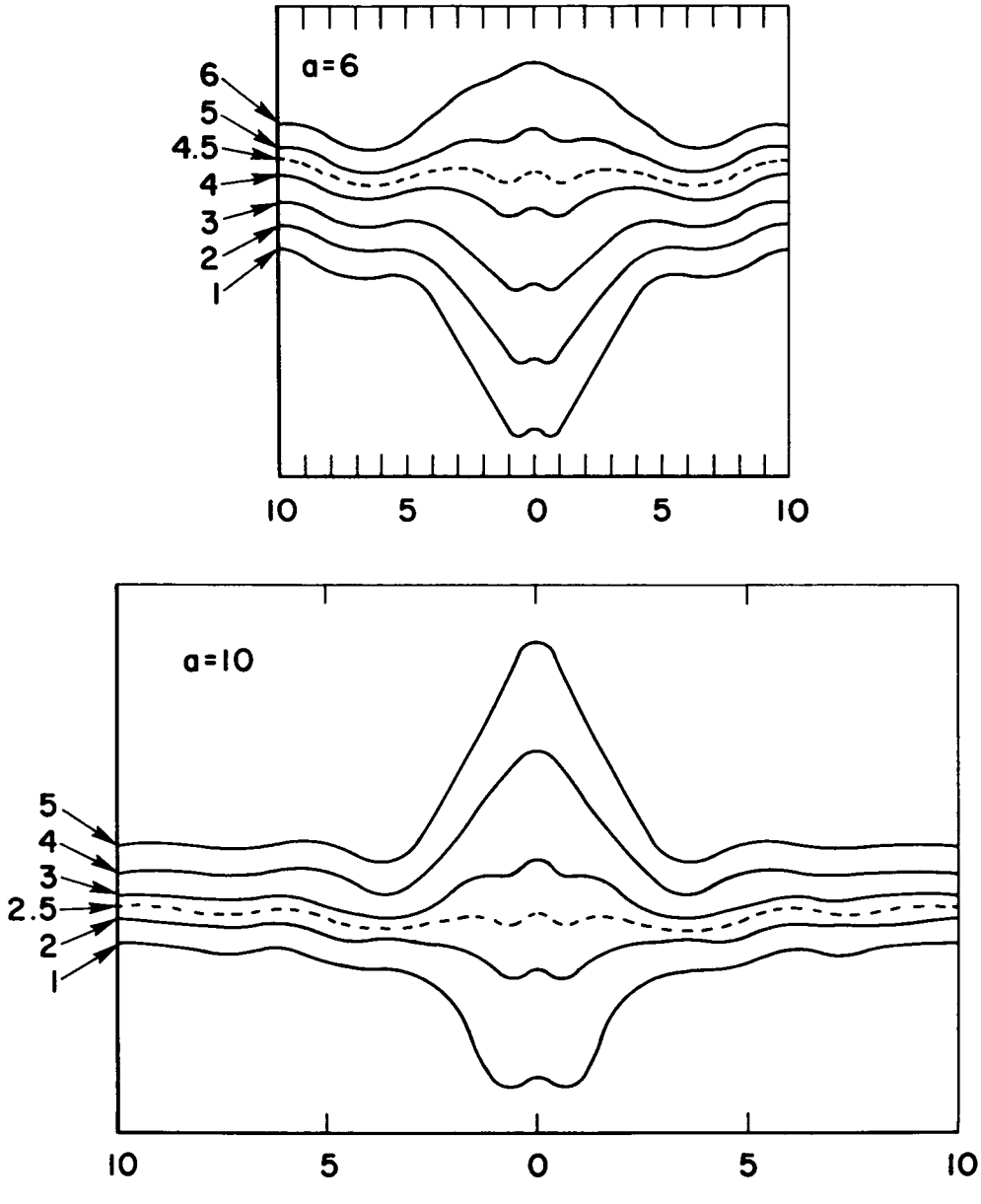

Fig. 13 Photometric profiles near apparent contact of small disks in double-image micrometer (Camichel 1958)

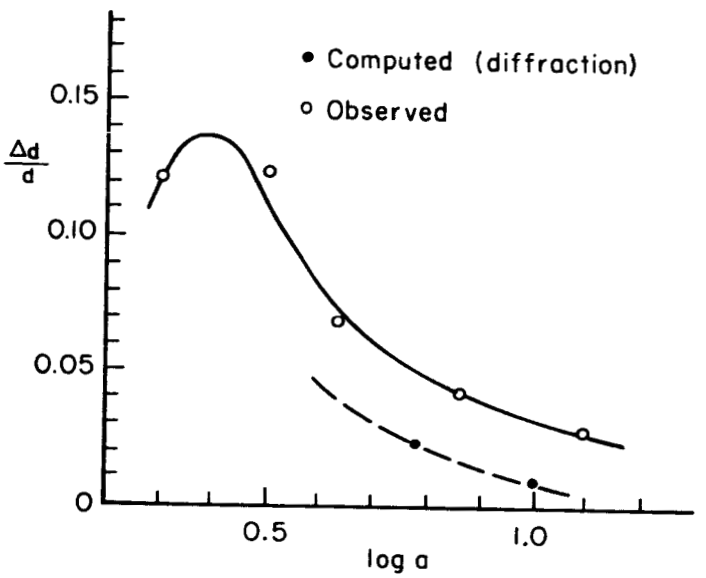

Fig. 14 Computed and observed systematic errors in double-image measurements of small disks (Camichel 1958)

2 R (in.)	4	6	8	12
δ (λ = 0.56 μ)	2".8	2".1	1".4	1".0$_5$
a (ϵ = 10")	13.7	18.2	27.3	36.5
corr. $\delta\,\sigma/\sigma$	+ 0.025	+ 0.020	+ 0.015	+ 0.010
$2\,\delta\,\sigma_1$	+ 0".17	+ 0".13	+ 0".10	+ 0"07

Heliometer or birefringent micrometer measurements of Mercury in transit (Table 3) with 6- to 7-inch telescope apertures give a mean reduced diameter $\approx$ 6"5, which, according to the above tabulation, requires a minimum correction of 2 per cent or about 0"13 on $2\sigma_1$; allowance for seeing and aberrations may raise this value to 0"2 and $2\sigma_1 \approx$ 6"7.

Similarly birefringent micrometer measurements of Mars in daytime near superior conjunction in 1937--38 with a 6-inch refractor (Muller, 1949) give a reduced polar diameter $\approx$ 9"00, which, with $\epsilon \approx$ 5" (a $\approx$ 9) requires a correction $\delta\,\sigma/\sigma \approx +0.035$ or $2\,\delta\sigma_1$ = + 0"32, and $2\sigma_1 \approx$ 9"32.

5.5. Photoelectric method

A photometric method, first suggested by E. Hertzsprung, is applicable to Mercury and Venus during transits. The flux passing through a circular aperture placed in the focal plane of the telescope is measured by means of a photoelectric photometer, (1) with the planet centered in the aperture, and (2) in nearby regions of the photosphere, or preferably at the same point after the planet has moved a small distance from it. In principle, the ratio of the fluxes in (1) and (2) gives the fractional area blocked off by the planet,

$$\varphi_1/\varphi_2 = (D - d)^2 \,/\, D^2 \quad , \qquad (5.2)$$

if D is the diameter of the aperture, d that of the planet's disk in the same units. The angular value of D is $D'' = \rho'' D/F$, where F is the focal length; if $F \simeq 10$ meters, $D > 0.5$ mm for $D'' > d'' = 10''$ (Mercury), and $D > 3$ mm for $D'' > d'' \approx 60''$ (Venus). If the full potential accuracy of the method is to be realized, precise measurements of D and F, or of D'' are essential. This is not as simple as one may think when a precision of the order of 10^{-3} is required, although a combination of geometric and photometric techniques leads to the desired accuracy.

In addition to possible calibration errors, more important sources of systematic errors include (a) variations of atmospheric transparency during the observations, (b) uneveness of the photosphere, and especially (c) differences in the distribution of scattered light in positions (1) and (2), in particular due to variable atmospheric turbulence. The first two effects can be reduced by suitable precautions during the observations; the third requires a semi-empirical correction. The method was first applied at the Pic du Midi Observatory during the transit of Mercury of November 1961 (Camichel and Rösch, 1962); the sun was at a low elevation during the transit, and fluctuations of the order of 5 per cent were recorded in the flux φ_1 transmitted by a 17'' aperture due to seeing effects on the 10'' disk of Mercury (while φ_2 was essentially constant).

6. DIAMETER OF MERCURY

The apparent diameter of Mercury has been derived from

(a) filar or birefringent micrometer or heliometer measurements of the small bright disk (in gibbous or crescent phases) in daytime or at twilight, near the times of maximum elongations, when the apparent diameter is in the range of 6" to 8",

(b) micrometer or heliometer measurements of the larger, black disk during the transits of the planet in front of the sun, when its apparent diameter is at maximum, varying from 10" to 13" because of the eccentricity of the orbit,

(c) timings of intervals between internal and external contacts of the disk with the sun's limbs during transits,

(d) photometric measurements of the fraction of the photospheric flux passing through a small aperture and blocked off by the planet's disk during the solar transit of November 7, 1960.

The measurements of the 19th century have been collected by Kaiser (1872), Ambronn (1891), and See (1901). The main measurements made during transits or in daytime between 1832 and 1878, separated according to method of measurement, lead to the following mean values (p.e. are listed):

19	values obtained by filar micrometer measurements during transits of 1832, 1845, 1861, 1868, 1878, and ranging from 5"65 to 6"94...	6"25 ± 0"06
4	values obtained by timing the duration of passage of the disk behind fixed wires during the transits of 1845, 1861, 1878, and ranging from 5"92 to 7"03.....	6"43 ± 0"21
7	values obtained by heliometer or double-image micrometer measurements during the transits of 1832, 1868, 1878, and ranging from 6"07 to 6"98	6"56 ± 0"07
2	values obtained with double-image micrometer in daytime between 1841 and 1865	6"64

The unweighted mean of the four methods $2\sigma_1 = 6"47 \pm 0"06$ (p.e.) is probably too small (Section 5); the mean of the heliometer or double-image micrometer measurements $2\sigma_1 = 6"60$ is probably nearer the truth, though probably still too small (Subsection 5.4).

The main results since 1880, collected in Table 3, show again a large range of variation from less than 6" to over 7" and attributable to the difficulties attending the measurement of a small planetary disk as discussed in Section 5. These are diffraction and poor daytime seeing in method (a), excessive turbulence and irradiation in method (b), the same aggravated by the sun's limb darkening and other effects (black drop) in method (c). Although it is not entirely free of such errors, method (d) appears <u>a priori</u> to be the most reliable of all methods but has been applied only once since 1880.

Micrometer measurements in daytime (1,2) range from 6"42 to 6"78 (excluding aberrant values), with a mean about 6"6; micrometer measurements and timings in transits (3,5) range from 6"21 to 6"83, with about the same mean; measurements during the 1960 transit, including photoelectric photometry (6), and ranging from 6"54 to 6"83

are in better agreement, with a mean about 6"7. Double-image methods (2,5) average 6"56; according to Subsection 5.4 a correction of + 0"10 to + 0"13 may be required, for a corrected diameter $2\sigma_1 \approx 6"67$. Filar-micrometer methods (1,3) are probably more subject to systematic errors, and the average 6"5 is too small. The timing of contacts leads to still smaller diameters except for the Austin observations of the 1960 transit, when the quantity estimated was the rate of change of distance between the limbs of the sun and planet rather than the times of apparent contact.

Considering only the 1960 transit, and correcting method (5) by + 0"10, the straight mean,

$$2\sigma_1 = 6"73 \pm 0"02 \text{ (p.e.)} \quad ,$$

is probably as good an estimate of the diameter of Mercury as may be made at present. The corresponding linear diameter is

$$2R = 4{,}880 \pm 15 \text{ km} \quad .$$

7. DIAMETER OF VENUS

The apparent diameter of Venus has been derived from

(a) filar or birefringent micrometer or heliometer measurements of the bright disk in daytime or twilight,

(b) filar micrometer or photographic measurements of the narrow crescent phases near inferior conjunction when the horns of the crescent are extended by atmospheric scattering and, occasionally, form a continuous bright ring around the dark hemisphere,

(c) filar micrometer and heliometer measurements of the dark disk during transits of the sun,

(d) timing of the external and internal contacts between the limbs of Venus and of the sun during transits,

(e) timing of the occultation of Regulus by Venus on July 7, 1959,

(f) an analysis of radar-range determinations during the inferior conjunction of 1960.

Filar-micrometer measurements of the bright disk are affected by little understood systematic errors. As noted in Subsection 5.2 the classical correction for "irradiation" is erroneous, and all corrected values so derived must be rejected.

That values greater than 17"0 are certainly too large is indicated by the accurate value of the diameter derived from

observations of the times of immersion and emersion of Regulus during its occultation by Venus on July 7, 1959 (de Vaucouleurs and Menzel, 1960; Menzel and de Vaucouleurs, 1961; Taylor, 1963); the diameter so derived,

$$2\,\sigma_1\,(z_0) = 17''012 \pm 0''006 \text{ (p.e.)} \quad ,$$

refers to a low-density layer of the upper atmosphere, well above the top of the opaque cloud-layer which defines the optical diameter of Venus.

This result is confirmed by all micrometer measurements taken during transits or on the narrow-crescent phases when systematic errors are minimized. Table 4 lists the more reliable modern determinations.

The low diameter values derived from measurements of the small, round disk in daytime near superior conjunction may be explained by the effect of limb darkening, and in the case of double-image measurements by the effect discussed in Subsection 5.4; according to the table at the end of Subsection 5.4, a correction of +1 to +2 per cent or +0''2 to +0''3 on $2\,\sigma_1$ may be expected. The large diameter values observed near quadrature are probably due to the effect of irradiation at the bright cusps. The diameter values derived from measurements of the large, narrow crescent near inferior conjunction may be nearer the correct value. However, if the micrometer settings are made at the outer edge of the bright crescent, the reduced diameter d_1 is probably still too large; if, on the other hand, the settings are made on the tips of the crescent (or on the thin ring of

light scattered by the haze and cloud cover at grazing incidence), the reduced diameter d_1 should be very close to the true value of $2\sigma_1$ which must be less than 17"0. The means of the values less than 17"0 in Table 4 are 16"88 ± 0"06 for 3 values near quadrature ranging from 16"72 to 16"97, and 16"88 ± 0"04 for 5 values near inferior conjunction ranging from 16"69 to 16"97. The corresponding means of values greater than 17"0 are 17"16 ± 0"03 (4 values) and 17"18 ± 0"04 (5 values), in agreement with Barnard's daytime value of 17"14 (cf, Subsection 5.1).

Diameters derived from transit observations should give a close lower limit; the values assembled in Table 5 range from about 16"65 to 16"95 with a weighted mean d_1 = 16"83 ± 0"03, in good agreement with the best daytime determinations. It seems safe to conclude that the optical diameter of Venus at the altitude z_c of the top of the cloud layer (observed tangentially) is greater than 16"7 or 16"8 and smaller than 17"0. The adopted mean is

$$2\sigma_1 (z_c) = 16"88 \pm 0"02 \text{ (p.e.)} \quad .$$

The corresponding linear diameter is

$$2R_c = 12{,}240 \pm 15 \text{ km} \quad .$$

The diameter of the solid globe $2R_0$ must depend at present on an atmospheric model; most current models (Kellogg and Sagan, 1961) suggest that $z_c \approx 30$ to 40 km; if so, $2R_0$ = 12,170 ± 20 km. This value agrees well with the preliminary estimate from radar observations (Muhleman, et al., 1962) which suggest $2R_0$ = 12,200 ± 100 km.

8. DIAMETER AND ELLIPTICITY OF MARS

The apparent diameter of Mars has been derived from

(a) filar micrometer, birefringent micrometer and heliometer measurements of the large bright disk observed at night near opposition,

(b) filar micrometer, birefringent micrometer and heliometer measurements of the small disk observed in daytime near superior conjunction,

(c) micrometer and microphotometer measurements of large-scale photographs taken at various phases, mainly at night between quadrature and opposition,

(d) micrometer measurements of the apparent angular distance of surface markings of known areographic coordinates,

(e) micrometer determinations on large-scale photographs taken near opposition of the apparent dimensions of the elliptical paths of surface details as they are carried across the disk by the rotation of the planet.

8.1. Visual diameter

Visual micrometer measurements of the bright disk near opposition are affected by the same errors due to diffraction, irradiation, and turbulence discussed in Section 5. Nighttime observations uncorrected for irradiation give reduced equatorial diameters d_1' in the range 9"6 to 9"7 (Campbell, 1892, 1895; Barnard, 1897), which are clearly too large. Attempts to correct for an assumed constant error c by

Eq. (5.1) are not completely successful because of the changing sky background from night near opposition to twilight near quadratures and daytime at smaller elongations. This indiscriminate treatment of both day and night observations leads to values of the polar diameter d_1'' in the range 9"4 to 9"6 (Wirtz, 1912; Rabe, 1928), which are still too large.

Daytime observations of the very small round disk near superior conjunction (See, 1901; Muller, 1949) give reduced polar diameters d_1'' in the range 9"0 to 9"2, which are too small because of diffraction and limb darkening effects (cf. Subsection 5.3).

The 19th century determinations of the (visual) diameters and ellipticity of Mars have been collected by Hartwig (1879) and See (1901). From the latter compilation the mean <u>equatorial</u> diameter derived from 22 determinations (most of them uncorrected for irradiation) with filar and double-image micrometers between 1784 and 1896 is $d_1' = 9''678 \pm 0''025$ (p.e.), and from 13 determinations (most of them corrected for an assumed constant error) with heliometers between 1852 and 1896 it is $d_1' = 9''338 \pm 0''023$ (p.e.). The mean diameter adopted in the ephemeris, after Hartwig (1911), is $d_1 = 9''36$ ($d_1' = 9''41$, $d_1'' = 9''32$).

The more reliable 19th century determinations of the <u>polar</u> diameter d_1'', corrected for an assumed constant error (Hartwig, 1879, 1911; Campbell, 1895; Wirtz, 1912; Rabe, 1928), are collected in Table 6. Their unweighted mean is $d_1'' = 9''34 \pm 0''02$; however, as shown by the plot of these corrected values against c (Fig. 15), the error model (5.1) is faulty, and the interpolated value for $c = 0$, $d_1'' = 9''305 \pm 0''02$, may be preferred.

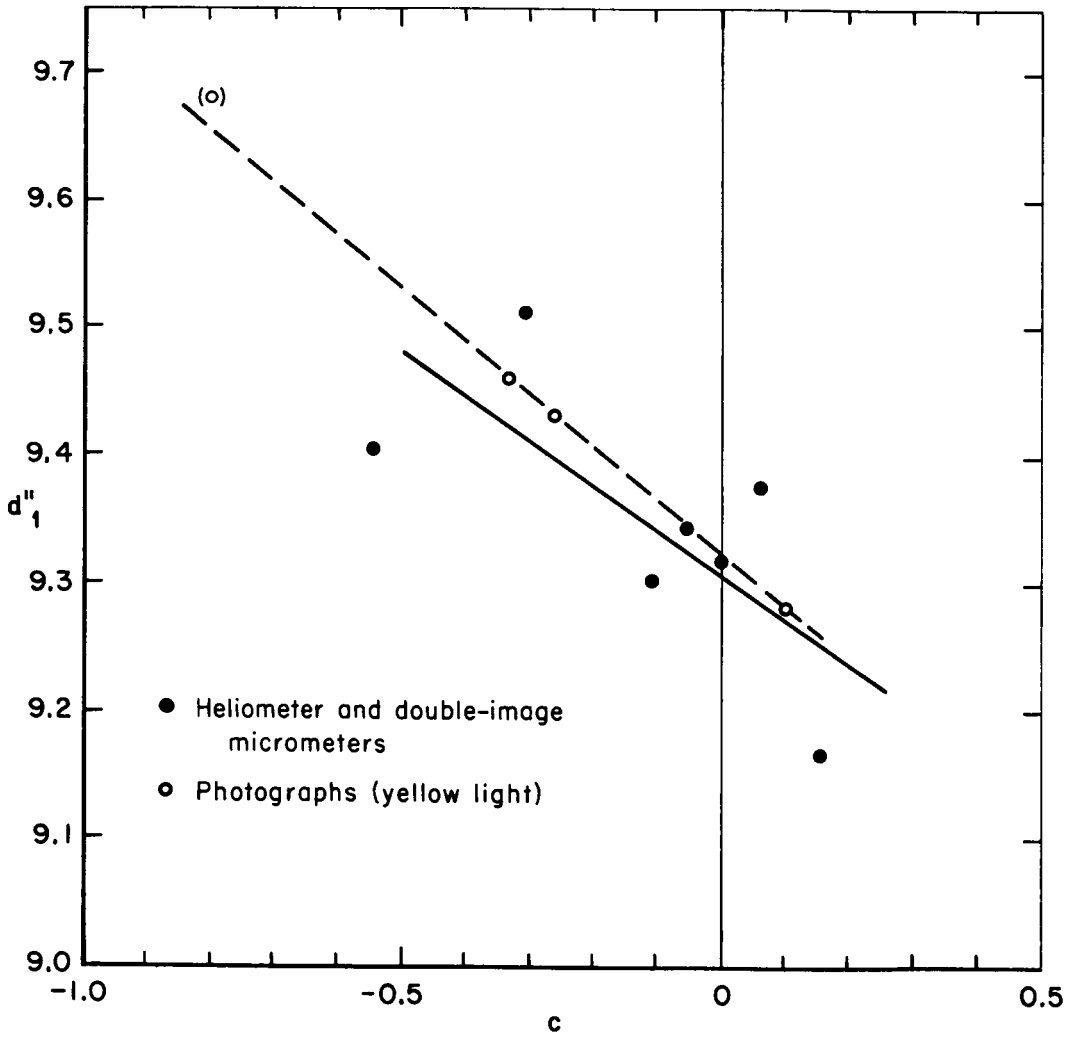

Fig. 15 Apparent polar diameter of Mars corrected for assumed constant error c as a function of c

The best recent visual determinations with a birefringent micrometer on the Pic du Midi 24-inch refractor by Dollfus, et al. (1962) near the perihelic oppositions of 1954, 1956, and 1958 -- listed in Table 7 -- give $d_1'' = 9''31$ in both red and blue light with an estimated error $\pm$ 0"03 or less. If, however, the results for 1956 which may have been affected by excessive atmospheric haziness are rejected, the mean value is reduced to $d_1'' = 9''29$. The ellipticity is $f = 0.0117$ in either case.

8.2. Photographic diameter

Micrometric measurements of photographs (Van de Kamp, 1925, 1928; Trumpler, 1927; Reuyl, 1941) are subject to large systematic errors depending on image density, seeing, and other parameters; in general, the measured diameter increases with density (photographic "irradiation") and this the more rapidly the poorer the seeing (Reuyl, 1941). Diameters reduced to some constant density representing "well-exposed" images are then assumed to be affected by constant errors as in Eq. (5.1). Modern determinations of the mean diameter (actually the diameter perpendicular to the maximum phase defect, which averages 0"01 greater than the polar diameter) so derived are in the range 9"4 to 9"5, when measures refer to the outer edge of images, and near 9"2 (Wright, 1925) when measures refer to the zone of maximum contrast.

The best photographic determination by micrometer measurements of photographs is that of Trumpler (1927) during the perihelic opposition of 1924; the equatorial and polar diameters from the yellow images reduced to a standard density, but uncorrected for constant

error are $d_1' = 9''413 \pm 0''02$, $d_1'' = 9''32 \pm 0''02$. An attempt to include a constant error term gives $d_1' = 9''37 \pm 0''06$, with $c = +\ 0''10 \pm 0''16$. However, the error model is not adequate, and a plot of photographic diameters against c (Fig. 15) gives for c = 0 the interpolated value $d_1'' = 9''32 \pm 0''02$, in good agreement with the heliometer and double-image results.

The photographic diameter can be derived also from microphotometer tracings of plates taken at or near opposition; diameters defined by the points of maximum slope on tracings taken every 30° of position angle have been measured by Camichel (1954, 1956) on photographs in yellow light with the 15-inch and 24-inch refractors of the Pic du Midi Observatory within 2 or 3 days of the oppositions of 1941 to 1954. The equatorial diameter is $d_1' = 9''33 \pm 0''012$ and the mean ellipticity $f = 0.012 \pm 0.002$ ($d_1'' = 9''22 \pm 0''012$). No correction for density or irradiation was applied; however, reduced diameters d_1 vary with apparent diameter d in a way suggesting a systematic effect of the form (5.1); a plot of d_1' versus 1/d suggests $d_1' \approx 9''8$, $c \approx -\ 0''8$ ($d_1'' = 9''68$). (See Fig. 15.)

To summarize, the apparent <u>polar</u> diameter of Mars at unit distance is certainly greater than 9"2 and smaller than 9"4. The best determinations, listed in Table 8a, indicate a mean value $d_1'' = 9''315 \pm 0''010$ (p.e.).

Direct determinations of the apparent <u>equatorial</u> diameter suggest a lower limit of 9"3 and an upper limit of 9"5. The best determinations, listed in Table 8b, indicate a mean value $d_1' = 9''415 \pm 0''02$ the mean values agree closely with Trumpler's determinations. However, the direct determination of the equatorial diameter has lower weight than

the polar value because of the larger phase corrections; it may be strengthened by a consideration of the ellipticity of the disk measured directly near opposition.

8.3. Ellipticity

The apparent ellipticity f_0 of Mars has been much discussed ever since Darwin (1876) noticed that it is greater than the classical limiting value for a homogenous planet in hydrostatic equilibrium (cf. de Vaucouleurs, 1954: Lamar, 1962). The latter is close to the observed dynamical ellipticity derived from the motion of the line of apsides and nodes of the orbits of the satellites $f_c = 0.00525$ (Woollard, 1944, corrected to $2\,\sigma_1 = 9''30$).

The 19th century determinations of the optical ellipticity were discussed by Hartwig (1879), who derived a mean value $f_0 = 0.0104$ from measurements made with heliometer or double-image micrometers.

A summary of the best modern determinations is given in Table 9. The range is from 0.002 (Campbell, 1892; Young, 1894) to 0.020 (Schur, 1896, 1899), suggesting a mean $f_0 \approx 0.011$. Excluding these extreme values, the unweighted mean of n = 15 values is $f_0 = 0.0106 \pm 0.0005$; the mean weighted by number of nights is $f_0 = 0.0095$ (n = 103 nights). Taking into account the 19th century results, the adopted value is

$$f_0 = 0.0105 \pm 0.0005 \text{ (p.e.)} \quad ,$$

which corresponds to a diameter difference at unit distance $d_1' - d_1'' = +\,0''100 \pm 0''005$.

The adopted values of the equatorial and polar diameters of the disk in yellow light then are

$$2\,\sigma_1' = 9''415 \pm 0''010,$$

$$2\,\sigma_1'' = 9''315 \pm 0''010,$$

corresponding to the linear diameters

$$2\,R_1' = 6{,}828 \pm 7 \text{ km},$$

$$2\,R_1'' = 6{,}756 \pm 7 \text{ km},$$

$$R_1' - R_1'' = 36 \pm 2 \text{ km}.$$

The dynamical ellipticity accounts for $R_c' - R_c'' = 18$ km, only half the observed value.

8.4. Atmospheric layers

The greater oblateness of the visible disk might be explained by assuming that the apparent limb of the planet in yellow light is defined by the top of a dust-laden convective layer in the lower atmosphere, and that this layer has greater height in the equatorial regions. Thus, on Earth the mean altitude of the tropopause increases from 7 km at the poles to 17 km near the equator (Goody, 1949). Considering that the value of the scale height in the lower atmosphere of Mars is over twice the value of Earth (de Vaucouleurs, 1954, p. 125), a change of 18 km in the altitude of the tropopause appears plausible.

The suspicion that the diameter observed in yellow light refers to an atmospheric layer rather than the solid surface is supported by visual and photographic determinations of the diameter of the globe, from measurements of surface details (Wirtz, 1912;

Trumpler, 1927; Camichel, 1954, 1956), and by diameters derived from photographs in red light which may also refer to the surface (however, limb darkening may affect these results). The values listed in Table 10 range from 9"12 to 9"48 for the equatorial diameter, and from 9"00 to 9"30 for the polar diameter; the means of all values are $d_1' = 9"28 \pm 0"03$ (n = 8), $d_1'' = 9"19 \pm 0"03$ (n = 6), or $d_1' - d_1'' = + 0"09 \pm 0"04$; (three pairs (d', d") in common give $d_1' - d_1'' = +0"041 \pm 0"045$. Within the uncertainties of the data, the following values, which are consistent with the dynamical ellipticity, might be provisionally adopted:

$$d_1' = 9"27 \pm 0"03, \qquad d_1' - d_1'' = + 0"05,$$

corresponding to a linear diameter: $2 R_s' = 6,723 \pm 22$ km.

In support of this interpretation, we note that the polar diameter $d_1'' = 9"22$ agrees well with values derived from micrometer measurements in daytime, when the Martian atmosphere may become invisible through the brighter terrestrial atmospheric light; the weighted mean of three such values in Table 10 (Muller: 9"00, See: 9"222, Campbell: 9"254) is $d_1'' = 9"225 \pm 0"02$.

If this interpretation is accepted, the height of the atmospheric layer visible in yellow light at the limb is:

$z' = 1/2\ (9"415 - 9"27) = 0"072 \pm 0"016 = 52 \pm 12$ km at the equator;

$z'' = 1/2\ (9"315 - 9"22) = 0"048 \pm 0"011 = 35 \pm 8$ km at the poles.

If the top of this layer marks the Martian tropopause, the average altitude of 40 to 50 km is perhaps an overestimate but not altogether implausible, considering that measured elevations of clouds on Mars occasionally exceed 20 and even 30 km (de Vaucouleurs, 1954). Dollfus

(1962) has also estimated that in the case of observations with double-image micrometers the apparent thickness of the atmospheric layer visible at the limb is about 30 km (at the half-brightness level as smoothed by diffraction).

Against this interpretation we note that the ellipticity of the disk derived by Trumpler (1927) from 40 plates in red light is $f = 0.0098 \pm 0.0011$, in substantial agreement with the value observed in yellow light. More to the point is the value of the ellipticity of the globe itself, also derived by Trumpler from the paths of surface details on the disk, $f_s = 0.0113 \pm 0.0048$, i.e., again close to f_0. Nevertheless, the size of the probable error is such that the possibility that $f_s = f_c$ is not excluded by the data either.

It must be conceded that the evidence is not conclusive and that the true diameter and the ellipticity of the solid surface of Mars remain uncertain. The diameter and the ellipticity of the visible disk in yellow light are observationally well-determined, but this diameter refers to an atmospheric layer whose altitude is poorly known; a range of 20 to 50 km at the equator, and possibly 10 to 30 km at the poles is indicated. With these values the diameter of the solid surface is in the range

$$6{,}723 \pm 22 \leq 2\,R_s' < 6{,}828 \pm 7, \text{ with } 18 \pm 2 \leq R_s' - R_s'' \leq 36 \pm 2 \ .$$

For definiteness

$$2\,R_s' = 6{,}750 \pm 20 \text{ km}, \quad \text{and } 2\,R_s'' = 6{,}700 \pm 20 \text{ km}$$

may be provisionally adopted.

9. VISUAL PHASE CURVE, ALBEDO AND COLOR INDEX OF MERCURY

The visual magnitude and phase curve of Mercury rest mainly on observations by G. Muller (1893) and by A. Danjon (1949, 1954). The phase law is rather uncertain because the planet is difficult to observe outside the phase angle interval $35^{\circ} < i < 125^{\circ}$, and when it is visible, it is almost always at rather low elevations in the sky where absorption corrections are less certain.

Muller represented his observations of 1878--1888 by the phase function

$$m = - 0.901 + 2.838 \cdot 10^{-4} (i - 50^{\circ}) + 1.023 \cdot 10^{-4} (i - 50^{\circ})^2 \quad . \qquad (9.1)$$

The constant term is for $i = 50^{\circ}$ and $R_0 \Delta_0$ (cf. Subsection 4.1); the corresponding value at full phase is $m(0) = - 2.06$; the reduction to $R \Delta = 1$ is + 2.06 (Section 4), hence $m_1(0) = 0.00$. A plot of the magnitudes of Muller's comparison stars in the Potsdam system versus modern magnitudes and colors in the B, V system gives the relation $V - m = - 0.19 + 0.04 (B - V)$. For the approximate color of Mercury (see below), namely $(B - V) = + 1.12$, $V - m = - 0.15$ and $V_1(0) = - 0.15$. Through the Russell rule (Subsection 4.5) the magnitude at phase angle 50° is of special interest: $V_1(50) = - 0.90 + 2.06 - 0.15 = + 1.01$.

Danjon represented his observations by the phase law:

$$m = - 0.21 + 3.80 \cdot 10^{-2} i - 2.73 \cdot 10^{-4} i^2 + 2.00 \cdot 10^{-6} i^3 \quad . \qquad (9.2)$$

The constant term is for $i = 0^{\circ}$ and $R \Delta = 1$. A plot of the magnitudes of the comparison stars versus V, B - V gives $V - m = - 0.13$ for $B - V \leq + 1.0$, and $V - m \approx + 0.20$ for $B - V \geq + 1.2$. For the color of Mercury, $V - m = - 0.17$, and $V_1(0) = - 0.38$. Also $m (50^{\circ}) = + 1.26$, and $V_1 (50^{\circ}) = + 1.09$.

Danjon has given reasons why his phase law should be preferred to Muller's (essentially because it represents better an eclipse observation at $i = 3^{\circ}$); if Muller's constant term m (50) = -0.90 is reduced with Danjon's formula then $m_1(0) = -0.90 - 1.47 + 2.06 = -0.36$, and $V_1(0) = -0.46$, or 0.08 mag. brighter than Danjon's zero point. The unweighted mean,

$$V_1 (0) = -0.42,$$

may be adopted. The uncertainty is difficult to estimate because of the extrapolation involved. For $i = 50^{\circ}$, however, the corresponding value is $V_1(50) = +1.05$ with an estimated probable error of 0.02 or 0.03 mag.

Numerical integration of the phase law (9.2) gives for the phase integral (Subsection 4.4) q = 0.560 (Danjon's value 0.563), while Russell's rule (Subsection 4.5) leads to $q = 2.20\ \Phi\ (50^{\circ}) = 2.20 \cdot 0.258 = 0.568$, or with Harris' coefficient 2.17, q = 0.560. The large departure from a Lambert sphere, for which $q_0 = 1.50$, is also indicated by the values of $\Phi\ (i)/\Phi_0(i)$ listed in Table 11 and by the polar plot of the phase function in Fig. 16. Note that the extrapolated values in the unobserved range $i > 130^{\circ}$ are increasingly uncertain and probably meaningless for $i > 160^{\circ}$. However, as the column $\Phi(i) \sin i$ shows, their contribution to the phase integral is negligible.

With the adopted magnitude of the sun and the apparent radius of Mercury at unit distance, the geometric and physical albedos computed by means of Eq. (4.12) are (Table 12):

$$p\ (V) = 0.104, \qquad A\ (V) = 0.058 \quad .$$

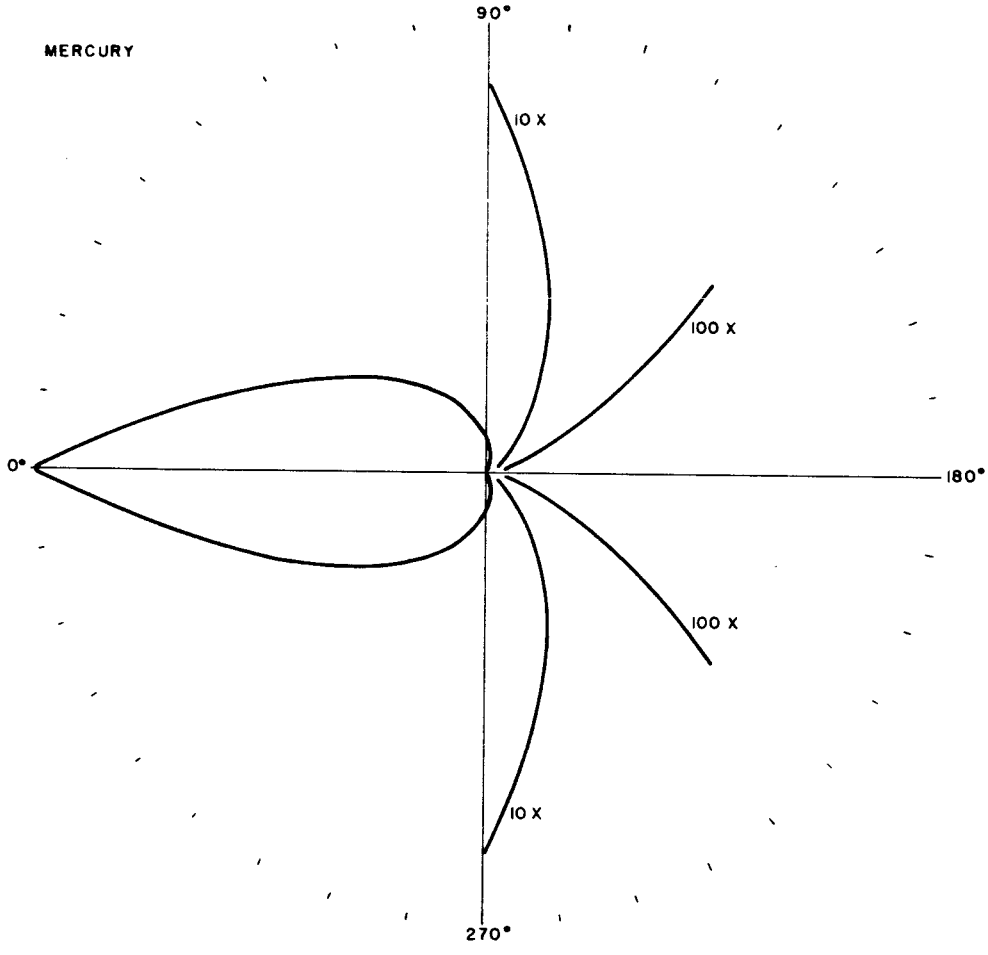

Fig. 16 Visual phase function of Mercury in polar coordinates

The estimated probable errors from all sources are about 4 or 5 per cent. These values are very close to the corresponding figures for the moon (also listed in Table 11 for comparison).

The color index of Mercury can be derived from Danjon's color measure D, being the difference between green and red filter magnitudes; the comparison stars give the relation B - V = 2.38(D + 0.465) and for the mean color measure of Mercury D = +0.008; B - V = +1.12.

From unpublished measurements at McDonald and Lowell observatories, Harris (1961) quotes a "rather uncertain" value B - V = +0.83. By comparison with the color index of the sun (Subsection 3.5), the color excess of Mercury is E (B - V) = +0.34 for the adopted mean value B - V = +0.97. Harris (1961) quotes also color index values V - R = +0.85, R - I = +0.52, and I (2μ)/I(1μ) = 3.5 ($\odot$ = 1.00); the large value of this ratio is due mainly to planetary thermal emission and is no longer a measure of surface reflectivity.

These scanty data on the spectral reflectivity of Mercury are collected in Table 13 where the quantity E($\mathbb{Q}$ - $\odot$) is the color excess of Mercury relative to the sun normalized to the V band; assuming that this quantity is independent of phase angle, the corresponding spectral albedo is given by

$$\log p_\lambda/p_V = -0.4\ E\ (\mathbb{Q} - \odot) \quad . \qquad (9.3)$$

The same data for the moon are listed for comparison; in the mean E($\mathbb{Q}$ - $\odot$) = 1.18 E($\mathbb{C}$ - $\odot$). If the relation holds in the near ultraviolet, p_λ(U) $\approx$ 0.053. The tentative spectral reflectivity curve (geometric albedo) is illustrated in Fig. 17. As long as the ultraviolet or infrared phase curves are unknown, the phase integrals, spectral spherical albedo, and radiometric albedo cannot be computed.

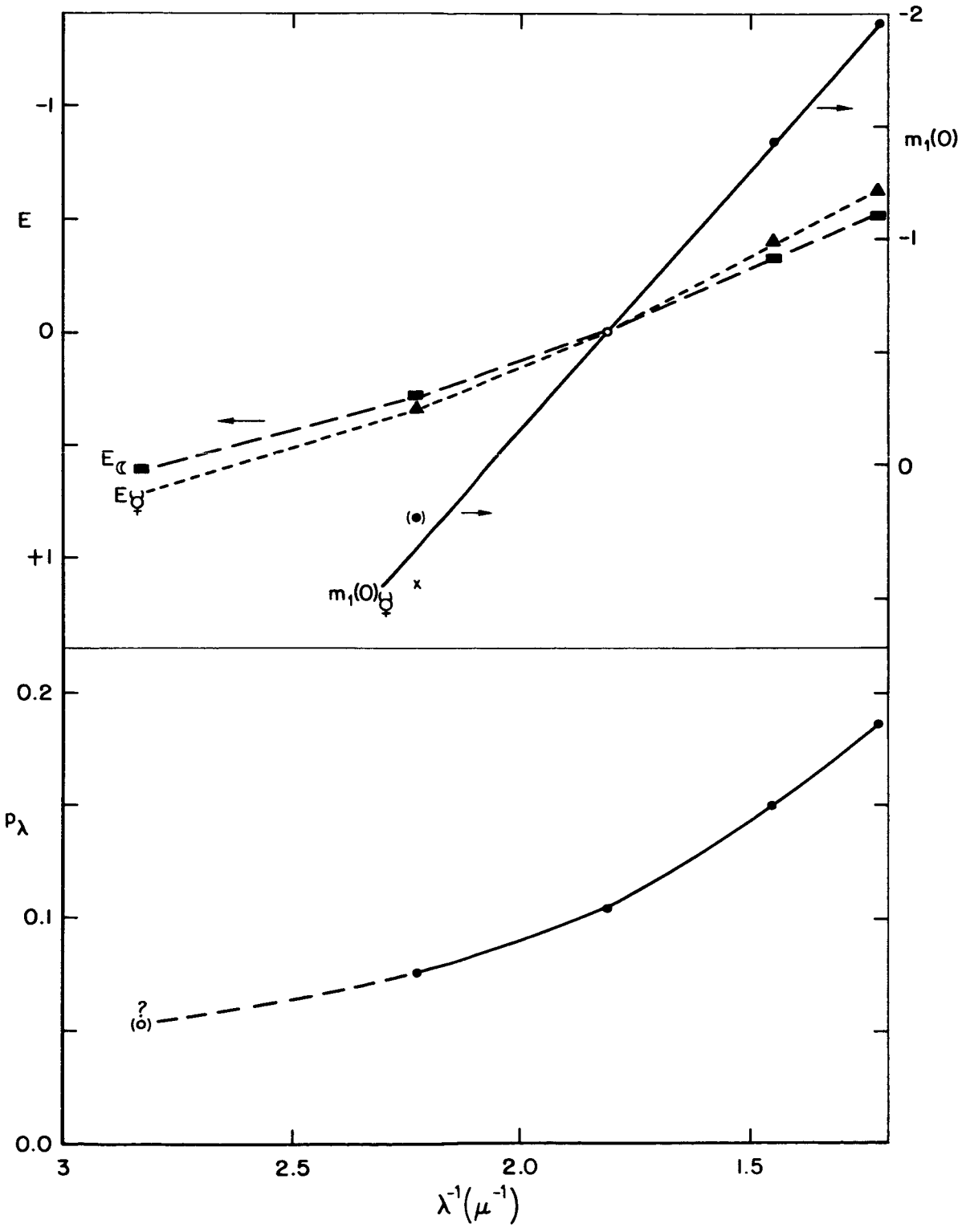

Fig. 17 Tentative spectral reflectivity curve of Mercury

10. VISUAL PHASE CURVE, ALBEDO AND COLOR INDEX OF VENUS

10.1. Visual phase curve and albedo

The main determinations of the visual phase curve of Venus are by Muller (1893, 1926), Danjon (1949) and Knuckles, Sinton and Sinton (1961). The first two are from visual observations, the third from photoelectric observations. There are striking differences between the three phase functions illustrated in Fig. 18.

Muller's original phase function (1893),

$$m = -4.707 + 1.322 \cdot 10^{-2}\, i + 0.4247 \cdot 10^{-6}\, i^3 \quad , \qquad (10.1)$$

gave for the phase integral $q = 1.194$ (Russell, 1916). An integration of his revised phase function (1926) given in tabular form only, leads to $q = 1.078$.

The constant in Eq. (10.1) is for $R_0\Delta_0$; the reduction to $R\,\Delta = 1$ is +0.705. The reduction to the V system (see Section 9) for an average color index $B - V = +0.8$ (see below) is $V - m = -0.16$; hence, $V_1(0) = -4.707 + 0.705 - 0.16 = -4.16$. At $i = 50^\circ$, $V_1(50^\circ) = -3.99 + 0.705 - 0.16 = -3.44$.

Danjon's phase function (1949),

$$m = -4.14 + 0.09 \cdot 10^{-2}\, i + 2.39 \cdot 10^{-4}\, i^2 - 0.65 \cdot 10^{-6}\, i^3 \quad , \qquad (10.2)$$

gives the high value $q = 1.296$. However, these observations are probably affected by systematic errors due to the variations of apparent diameter and shape of the nonstellar image of the planet as seen through the photometer.

The constant in Eq. (10.2) refers to $R\,\Delta = 1$; reduction to the V system (cf. Section 9) is $V - m = -0.13$ for the color range of Venus; hence, $V_1(0) = -4.14 - 0.13 = -4.27$, and $V_1(0) = -4.14 + 0.56 - 0.13 = -3.71$.

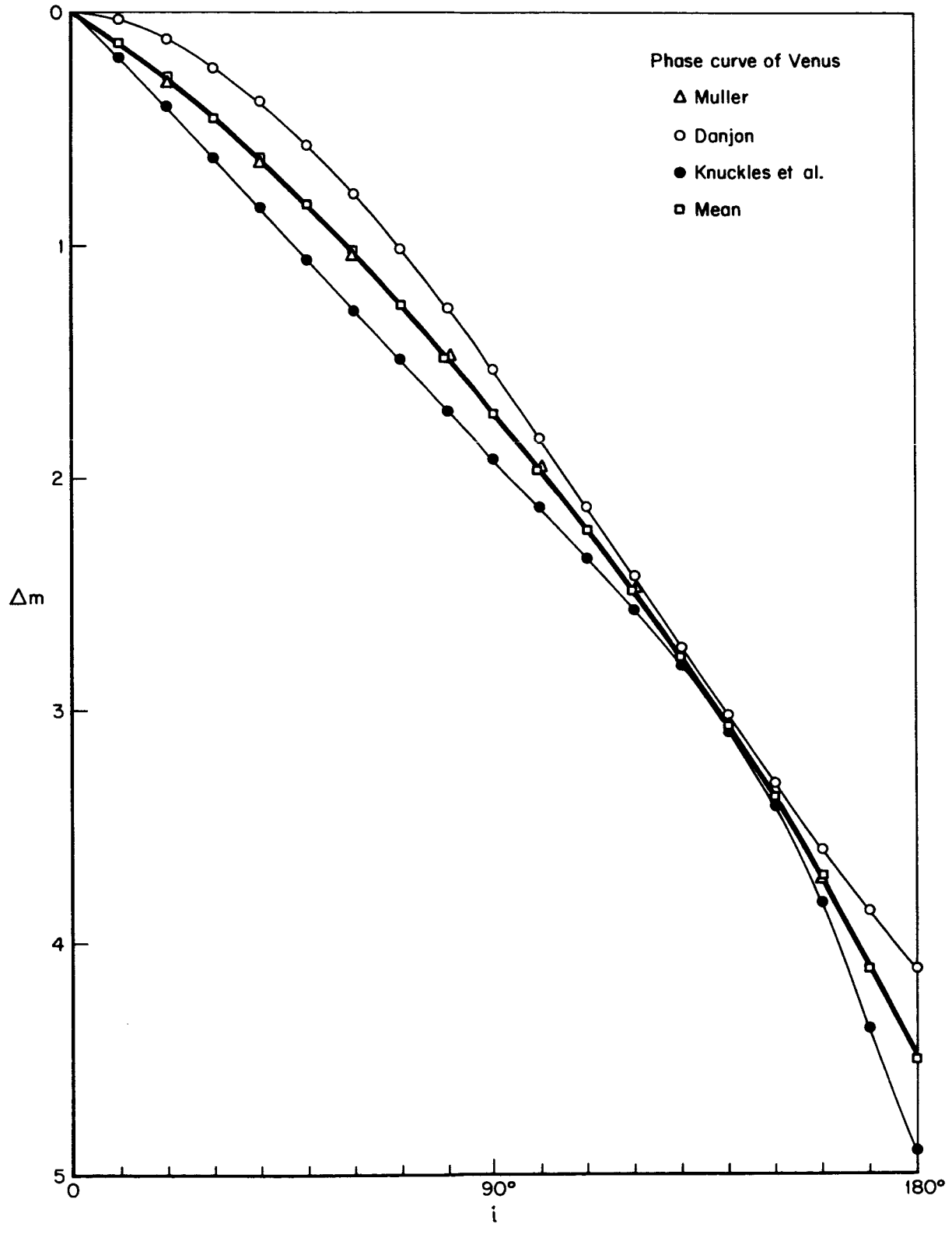

Fig. 18 Data on visual phase curve of Venus

The phase function of Knuckles, et al. (1961) is given in tabular form only and $q(V) = 0.888$; thus $V_1(0) = -5.47 + 0.705 = -4.765$, and $V_1(50^\circ) = -4.40 + 0.705 = -3.695$. However, the data show a large scatter in the 9 observations at phase angles $i < 30^\circ$, and no observations were made at $i < 15^\circ$; the extrapolation to $i = 0^\circ$ is obviously subject to great uncertainty. A comparison of the observed values at $i = 50^\circ$ will help.

The photovisual observations of King (1919) were all taken in the interval $52^\circ < i < 69^\circ$ and can be reduced to $i = 50^\circ$ without appreciable error through any one of the phase functions; in this range the phase coefficient is $dm/di = +0.021$ mag. per degree; the average of 8 observations is $P_v(50^\circ) = -4.09$ for $R_0\triangle_0$, and the comparison stars give $V - P_v = -0.11$; hence $V_1(50^\circ) = -4.09 + 0.705 - 0.11 = -3.50$.

The data are collected in Table 14. For the present the straight mean of the phase functions plotted in Fig. 18 may be adopted as the most plausible solution. The adopted phase function is tabulated in Table 15 and shown by the solid line in Fig. 18; it is very close to Muller's curve. The phase integral is $q = 1.087$, and $V_1(0) = V_1(50) - 0.83 = -4.41$. With these figures the geometric and physical albedos (Table 12) are

$$p = 0.65 \qquad \text{and} \qquad A_v = 0.70_5 \quad .$$

The systematic errors in the component data prevent a formal computation of probable errors, but a plausible estimate of the "uncertainty" is about 5 per cent or 0.05 mag.

10.2. Color index and spectral reflectivity

The color index of Venus near quadrature (King, 1923; Link, 1956) is several tenths of a magnitude greater (i.e. redder) than the sun's (B - V = +0.63). Danjon's observations through green and red filters give a mean color measure D = +0.005 corresponding to B - V = +1.11 (cf. Section 9); no indication is given of possible variations with phase angle.

In the same range of phase angles the photoelectric data of Knuckles, et al. (1961) give a nearly constant value B - V = +0.80, but a rapid decrease at phase angles $i < 40^{\circ}$ and $i > 120^{\circ}$ is in evidence (Fig. 19). The drop near $i \approx 40^{\circ}$ looks suspect, especially in U - B (note that observations are by different observers and for different years); the V data also seem to be subject to systematic errors (see above) in this range, although differential color measurements should be less subject to such errors. The data are certainly reliable at larger phase angles and up to $i \approx 160^{\circ}$. The rapid decrease of the color index at $i > 120^{\circ}$ is confirmed by scattered earlier data (Link, 1956). This blueing is evidently due to increased atmospheric scattering (by small particles and molecules) of the light reflected by the planet as $i \rightarrow 180^{\circ}$ (forward scattering) in the crescent phases. The blueing near full phase ($i \rightarrow 0^{\circ}$), if it is not due to systematic errors, may be due also -- at least in part -- to increased molecular scattering in the direction of propagation (backward scattering). The detailed theoretical interpretation of the luminosity and color phase curves of Venus is still a challenge to the theorists of atmospheric scattering (Horak, 1950).

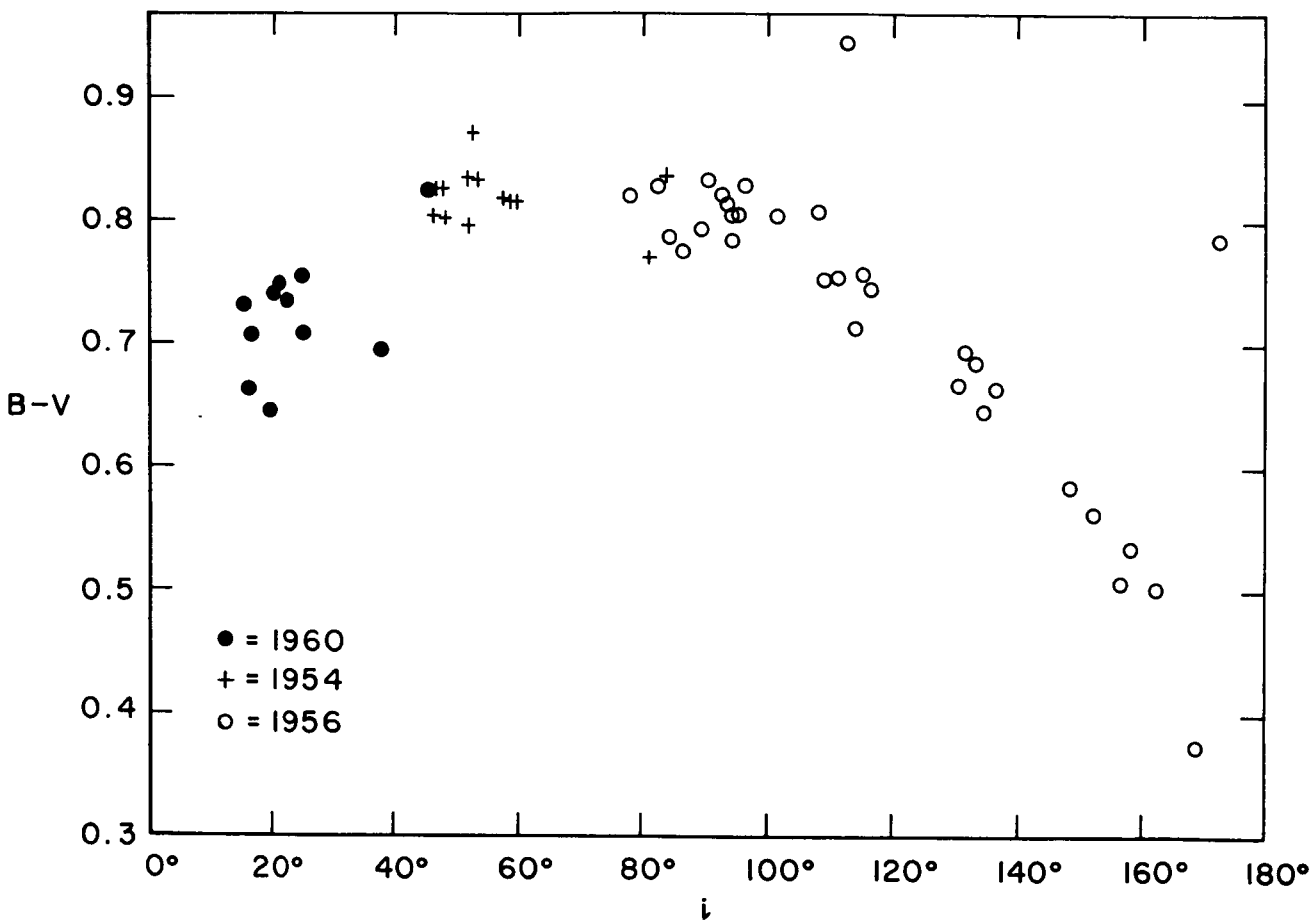

Fig. 19a Phase dependence of color indices B - V of Venus
(after Knuckles, Sinton and Sinton, 1961)

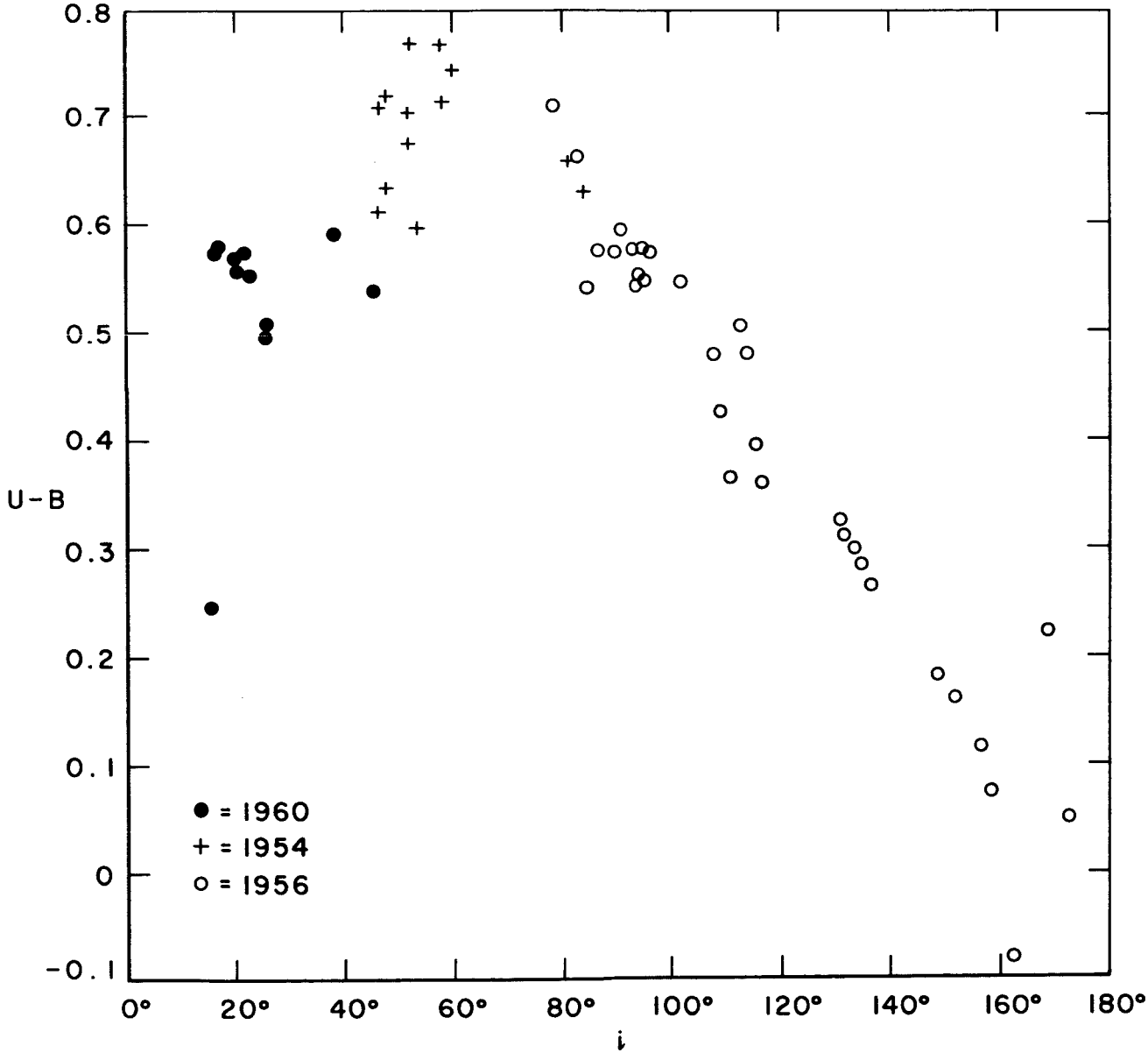

Fig. 19b Phase dependence of color indices U - B of Venus (after Knuckles, Sinton, and Sinton, 1961)

Because of this variation of color with phase, the values of p and q will depend on color; however, as is apparent from Fig. 19 a, b, extrapolation to $i = 0^{\circ}$ (to derive p) is subject to a large uncertainty. In addition, the phase integrals q in U and B may share the systematic errors of the V data (see above); differential variations, $\Delta q = q(B) - q(V) = -0.125$, $\Delta q = q(U) - q(B) = -0.114$ should be more reliable; if so $q(B) = 1.078 - 0.125 = 0.953$, and $q(U) = 0.839$. The data do not seem to be good enough yet to warrant an independent derivation of $A = pq$ in color bands other than V.

The relative spectral reflectivity in the range 0.38 to 0.65μ is shown in Fig. 20 (dotted line) from measurements made by Kozyrev (1954) at phase angle $i = 43^{\circ}$. The break near 0.45μ is in qualitative agreement with some data (Evershed, 1919), but the quantitative agreement with others is poor, e.g., center and limb spectral data in the range 0.38 to 0.48μ by Polozhenzeva (1962). There is no agreement either with the broad-band data discussed above; thus from Kozyrev's curve read at the effective wavelengths of the B and V bands, a color excess with respect to the sun $E(B - V) = +0.47$, or $B - V = +1.20$ is predicted, as against $B - V = +0.80$, observed near the same phase by Knuckles, et al. (1961). The value $B - V = +1.11$ from Danjon's data agrees better, but strictly speaking measures only the red--green gradient. For comparison, Harris (1961) quotes from unpublished data at unspecified phase angles $U - B = +0.50$, $B - V = +0.82$, and also $I(2\mu) / I(1\mu) = 1.61$ (sun = 1).

These various data are compared in Fig. 20. It is clear that neither the spectral reflectivity nor the radiometric albedo of Venus can be derived with any degree of confidence.

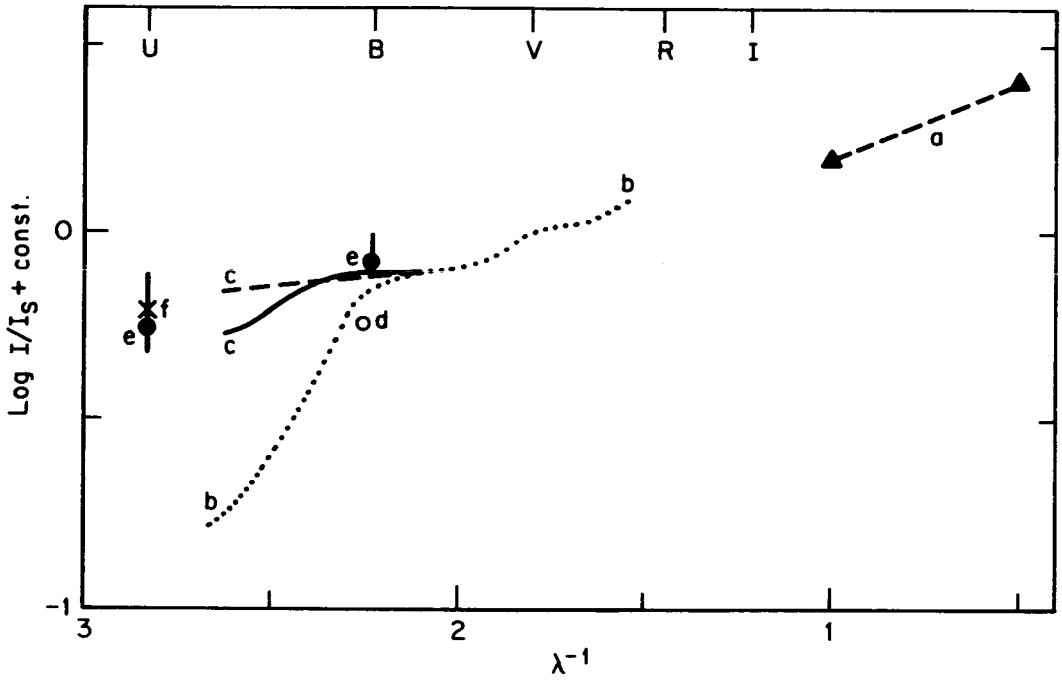

a - Harris, after Kuiper (1961), arbitrary zero point
b - Kozyrev (1954), smoothed
c - Polozhenzeva (1962), center (continuous), limb (dashed), arbitrary zero point
d - Danjon (1949), from red-green gradient
e - Knuckles et al. (1961), U-B, B-V and range
f - Harris (1961), U-B

Fig. 20 Relative spectral reflectivity data for Venus

11. VISUAL PHASE CURVE AND ALBEDO OF MARS

11.1. Average phase curve

Direct observations of the phase curve of Mars are limited to $i < 48^{\circ}$; in this range, departures from a linear phase law are negligible, and the phase curve is defined by the reduced magnitude $m_0 \equiv m_1(0)$ and the phase coefficient $\underline{a}$ (cf. Eq. 4.24). The visual magnitudes and phase coefficient of Mars were determined visually by Zöllner (1865), Muller (1893) and Radlova (1940), photographically by King (1923) and Livlander (1933), and photoelectrically by Johnson and Gardiner (1955), de Vaucouleurs (1960) and Harris (1961).

Muller's extensive observations from 1877 to 1889 give probably the best determination of the phase coefficient, $\underline{a} = +0.01486$ mag./deg (Fig. 21). Muller derived also $m_0 = -1.787$ for the magnitude at mean opposition in the Potsdam system. A reduction of Muller's data to the V system by Harris (1961) gives $V_1(0) = -1.51$, in agreement with the modern data (Table 16).

Becker (1933) has reduced to the Harvard system many series of observations from 1843 to 1931. The data seemed to indicate that the visual magnitude of Mars at mean opposition varies as much as 0.48 mag., but an independent reduction of the older observations by Harris (1961) does not confirm the large amplitude (maximum range: 0.13 mag.). Seasonal and longitudinal effects are of the same order of magnitude or larger (see below).

The photovisual observations by King (1923) during the oppositions of 1916 to 1922 gave a mean magnitude $m_0 = -2.00$ or -2.04, depending on the method of reduction, and $\underline{a} = +0.0152$ or $+0.0167$ mag./deg.;

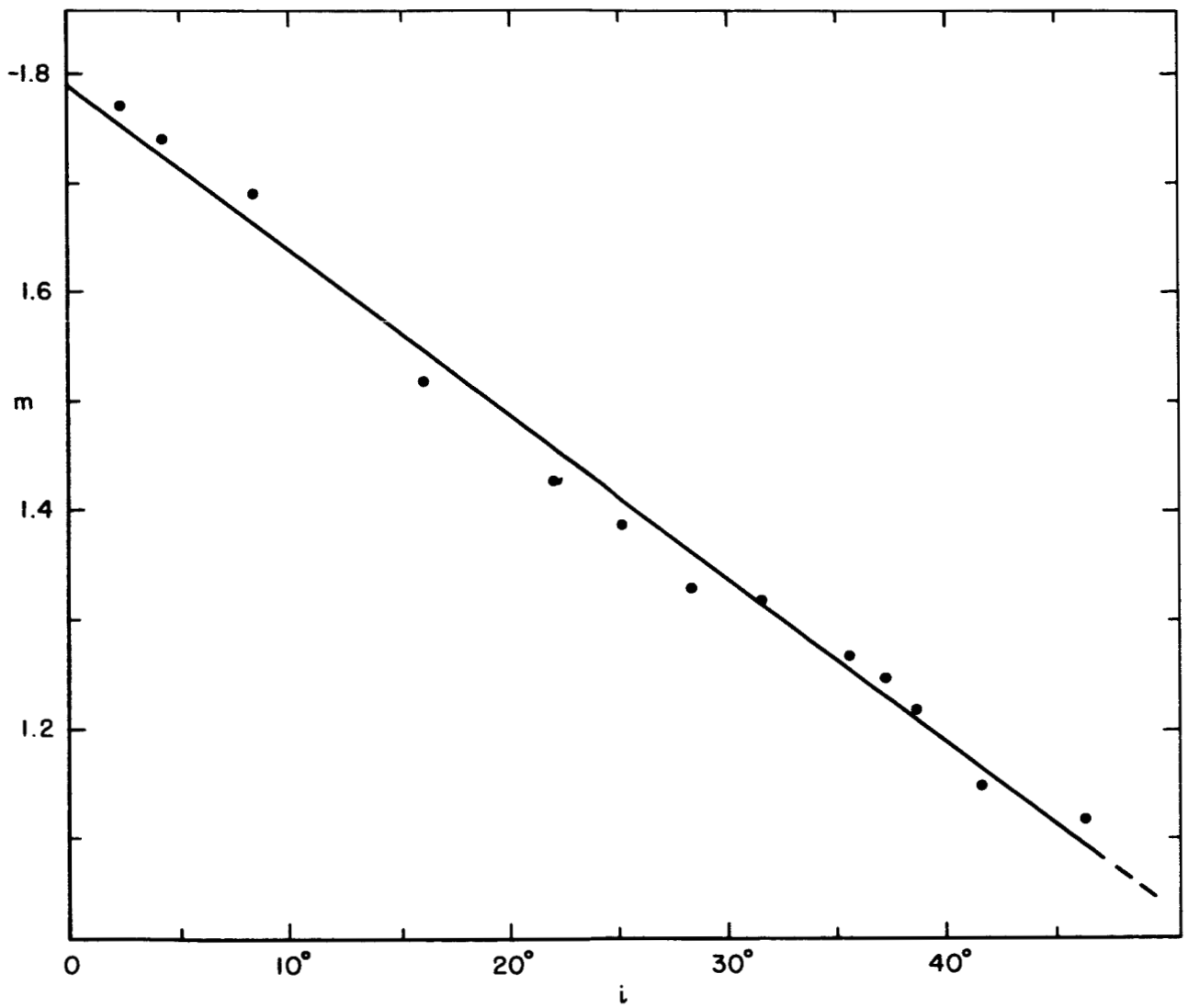

Fig. 21 Mean visual phase curve of Mars, 1877--1889 (after Muller 1893)

this corresponds to $V_1(0) = -1.50$ or -1.54 in agreement with the detailed reduction to the V system by Harris (Table 16).

The visual observations of Radlova (1940) during the opposition of 1939 give $m_0 = -1.84$ at mean opposition, or by the comparison stars, $V_1(0) = -1.38$ -- with some uncertainty.

From numerous photovisual observations in 1926--27, 1928 and 1930--31 Livländer (1933) derived $m_0 = -2.22$, corresponding roughly to $V_1(0) = -1.7$, but the phase coefficient $\underline{a} = +0.019$ mag./deg. seems too high.

The modern photographic and photoelectric data (Tables 16 and 18) give $V_1(0) = -1.52 \pm 0.01$ and $a(V) = +0.015$ mag./deg.

Since the phase angle does not exceed 48°, the phase function must be extrapolated, for instance by analogy with Earth. The values in Table 17, derived for Earth by Danjon (1936) from observations of the earthshine on the moon give a phase integral $q(E) = 1.10$, while the Russell rule gives $2.20\ \Phi\ (50^\circ) = 1.09$ in good agreement. For Mars the visual phase function computed with the phase coefficient $\underline{a} = 0.015$ mag./deg. gives $\overline{\Phi\ (i)_{\sigma}} / \Phi\ (i)_{\delta} = 0.98$ in the range $10^\circ \leq i \leq 40^\circ$; the phase function of Mars given in Table 17 was derived from that of Earth by assuming that this ratio drops to 0.97 and remains constant for $i > 40^\circ$.

Numerical integration of this phase function leads to $q(M) = 1.076$, while the Russell rule gives $2.00\ \Phi\ (50^\circ) = 1.060$. The mean value $q = 1.07$ was used to compute the albedo in Table 19 and with the adopted constants

$$p = 0.149 \text{ and } A_v = 0.159$$

with estimated mean errors of 3 and 5 per cent respectively.

11.2. Longitudinal variations

The visual brightness of Mars varies slightly with the longitude ω of the central meridian and the changing presentation of its surface markings. This effect was first observed by Lau (1914), who recorded visually an amplitude of 0.17 mag. between a maximum near $\omega = 120^{\circ}$ and a minimum near $\omega = 300^{\circ}$ (Fig. 22), and by Guthnick and Prager (1914, 1918), who compared Mars photoelectrically with β Gem through a red filter in 1914 and 1916; similar variations are shown by the photoelectric observations of Johnson and Gardiner (1955) and of de Vaucouleurs (1960). The fact that the variations are caused by the unequal distribution of bright and dark areas on the surface of the planet can be demonstrated by direct integration of the areas and relative luminances of the surface markings (de Vaucouleurs, 1942). Some variability in the longitudinal effect from year to year is observed, as could be expected from the variable areocentric declination of Earth (northern at aphelic oppositions, southern at perihelic oppositions), from occasional changes in the surface markings, and from erratic atmospheric phenomena. The latter dominate in the shorter wavelengths, and no significant longitudinal effect is expected nor observed at $\lambda < 0.50\mu$ (Fig. 23).

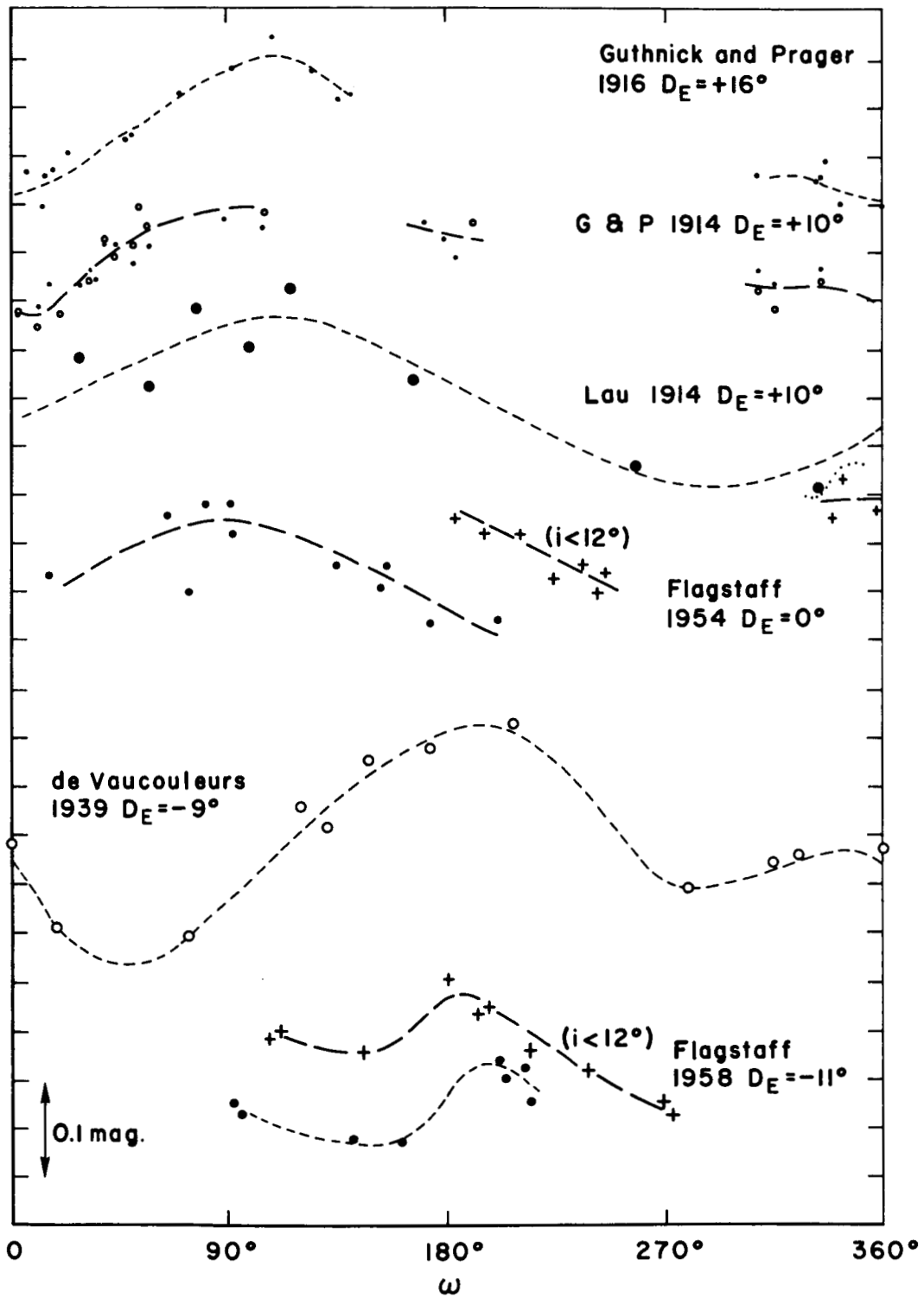

Fig. 22 Longitudinal variations of magnitude of Mars at wavelengths $\lambda > 0.5\mu$

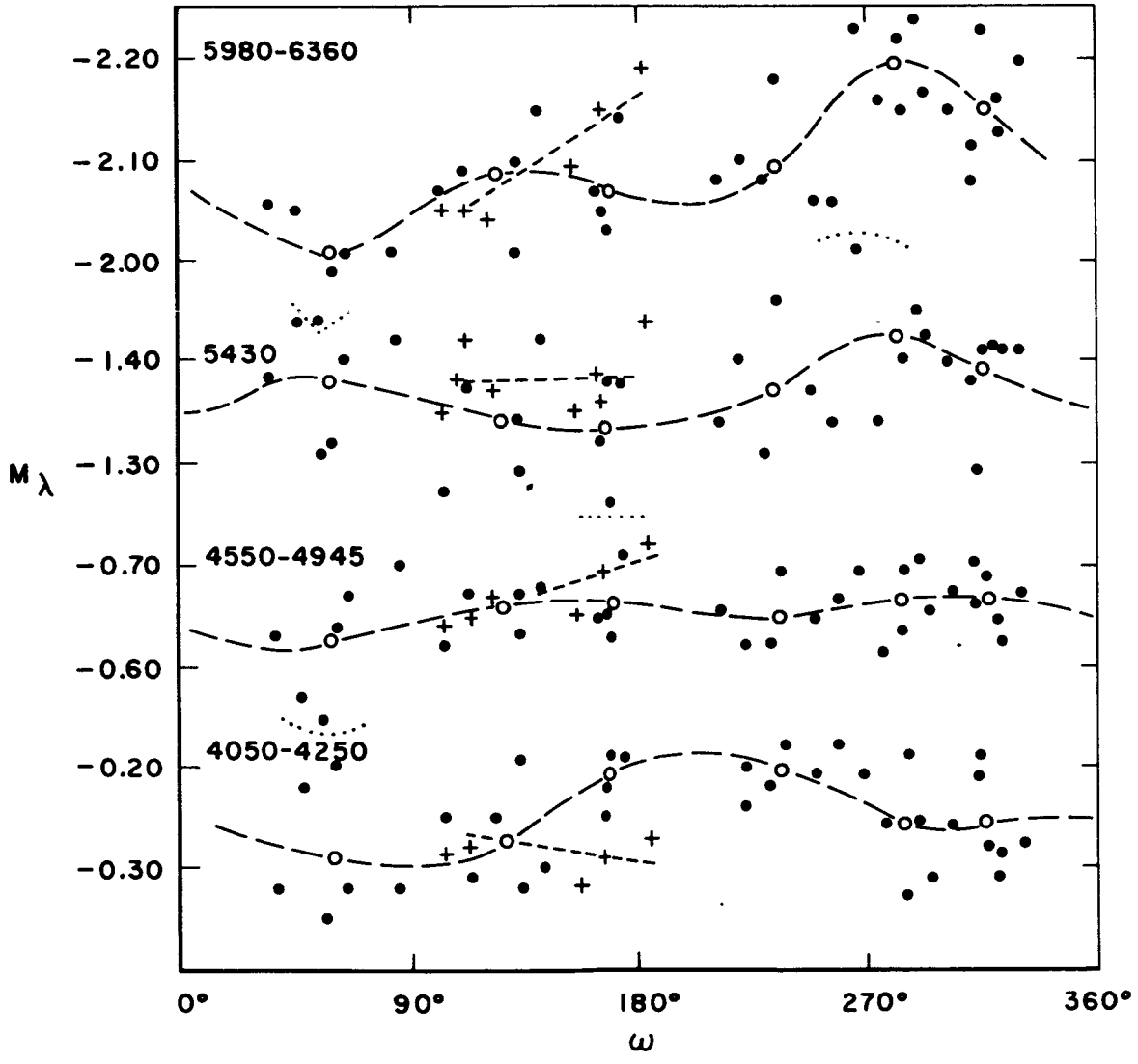

Fig. 23 Independence of longitudinal variations of spectral magnitudes of Mars at short and long wavelengths (Mount Stromlo 1954). Vertical crosses denote $i < 10^{\circ}$; open circles denote mean points

12. COLOR INDEX, SPECTRAL REFLECTIVITY AND RADIOMETRIC ALBEDO OF MARS

12.1. Color index

The old visual and photographic data on the color index of Mars, discussed in Physics of the Planet Mars (de Vaucouleurs, 1954), are of relatively little interest now that more precise photoelectric data on the spectral reflectivity are available for a longer interval of wavelengths than the original photographic--photovisual range. The values of the magnitude at opposition in Table 18 are taken from a recent re-discussion of modern photographic and photoelectric data supplemented by new observations (de Vaucouleurs, 1960). Both m_0 and the phase coefficient $\underline{a}$ are strongly wavelength-dependent. Figure 24 shows the spectral variation of the phase coefficient from the Mount Stromlo photographic spectral photometry (Woolley, et al., 1953, 1955) and the Flagstaff photoelectric photometry (Johnson and Gardiner, 1955). At $\lambda > 0.6\mu$, light is reflected mainly by surface, the phase coefficient is $\underline{a}$ = 0.012 mag./deg., and by the Russell rule q = 1.3 (suggesting a fairly smooth surface). At $\lambda < 0.5\mu$, light is reflected mainly by the atmosphere, $\underline{a}$ = 0.018 mag./deg., and q = 0.94 (indicating strong departures from both isotropic and Rayleigh scattering, for which q = 1.50 and 1.67). At the effective visual wavelength, $\lambda = 0.55\mu$, both components contribute, $\underline{a}$ = 0.015 mag./deg., q = 1.07 (Section 11).

Because of the greater value of the phase coefficient at $\lambda < 0.5\mu$, Mars is redder at large phase angles; the reddening coefficient in B - V is about 0.03 mag./deg., and the color index

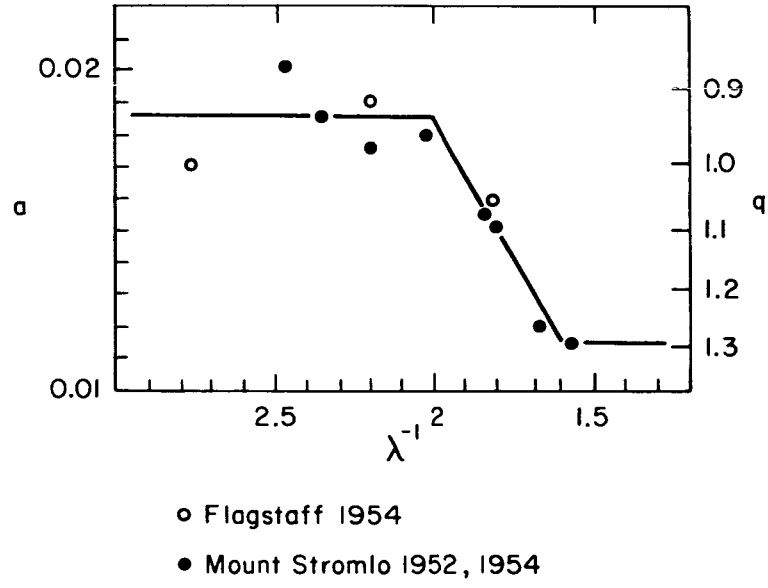

Fig. 24 Spectral variation of phase coefficient (a in mag./deg.) and phase integral q of Mars

increases by Δ (B - V) = 0.15 mag. between opposition and quadrature. At large phase angles, say i > 130° to 140°, Mars may be expected to become bluer because of increasing atmospheric scattering. There is also some evidence for a color variation depending on season or hemisphere presentation or both; an earlier discussion (de Vaucouleurs, 1954) suggested the following values in the IPg, IPv system.

	At opposition	At quadrature
Near aphelion	+ 1.30	+ 1.50
Near Perihelion	+ 1.45	+ 1.65

12.2. Spectral reflectivity curve

The spectral reflectivity curve of Mars can be derived from the Mount Stromlo spectrophotometric data of 1952, 1954 (Woolley, et al., 1953, 1955) and the Flagstaff photoelectric data of 1945, 1958 (Johnson and Gardiner, 1955; de Vaucouleurs, 1960), supplemented for the infrared by unpublished data of Hardie (quoted by Harris, 1961), which refer to an unspecified phase angle. The spectral magnitudes are listed in Table 18 and are plotted in Fig. 25; within the uncertainties of the data the $m_1(\lambda^{-1})$ curve can be represented by two straight segments:

$$m_1(\lambda^{-1}) = -1.50 + 2.80(\lambda^{-1} - 1.80) \quad \text{for } 0.4 < \lambda < 0.8\mu (1.2 < \lambda^{-1} < 2.5),$$

and

$$m_1(\lambda^{-1}) = +0.40 \quad \text{for } \lambda < 0.4\mu (2.5 < \lambda^{-1} < 3.0).$$

The values of the spectral albedo listed in Table 19 were computed from the observed values rather than the interpolated ones; some allowance was made for the probable variation with wavelength of the

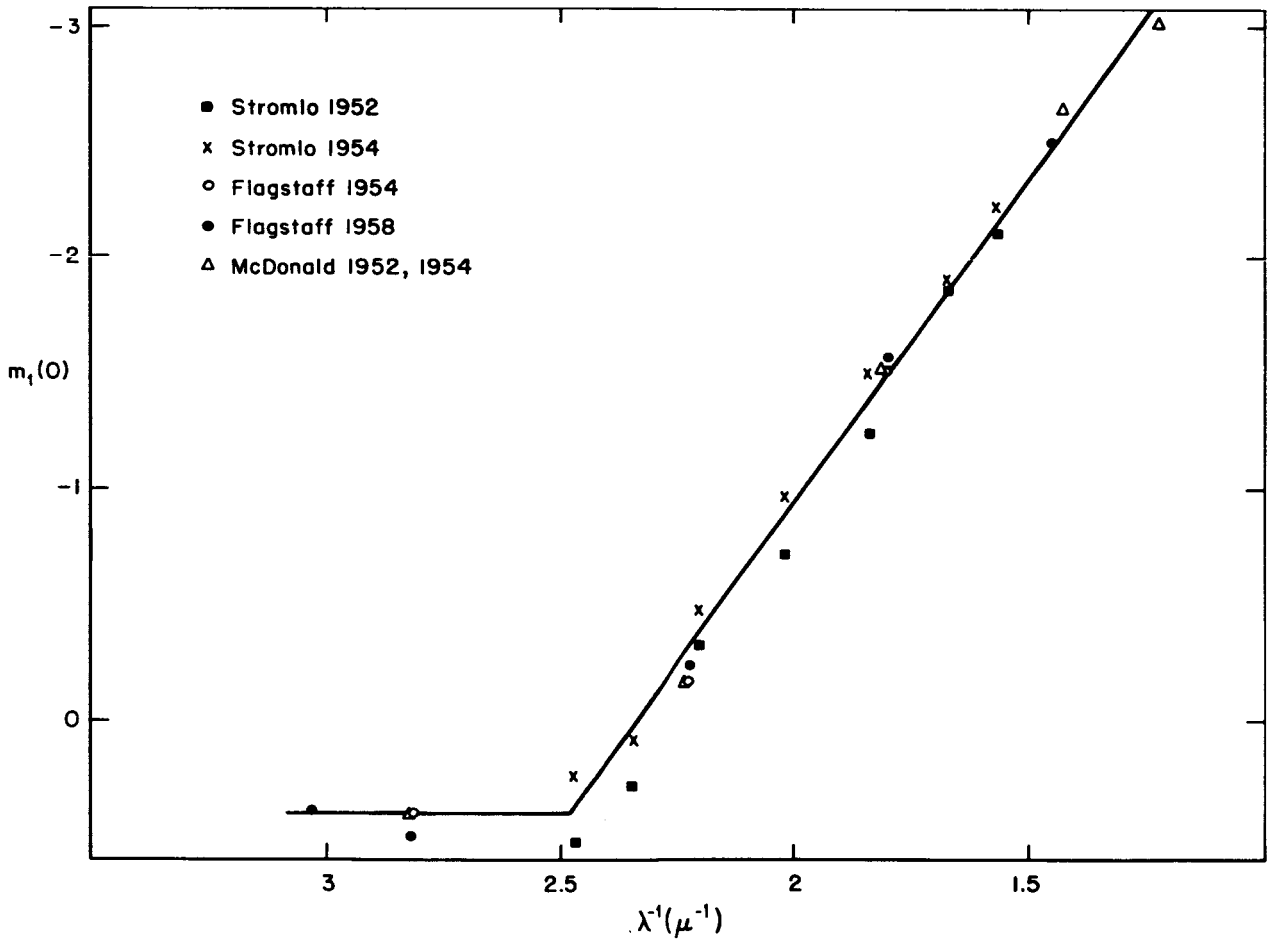

Fig. 25 Monochromatic magnitudes $m_1(0)$ of Mars, 1952, -54, -58

apparent diameter of the effective reflecting surface (Subsection 8.4) and for the phase integral, the latter being quite uncertain for $\lambda < 0.4\mu$ and $\lambda > 0.7\mu$. The spectral reflectivity curve plotted in Fig. 26 shows that Mars is red and bright in the visible and near infrared, but "gray" and very dark in the near ultraviolet. This result suggests that either the scattering particles strongly absorb (like carbon smoke) or the atmospheric molecular component includes a strongly absorbing gas in this spectral region. A marginal rocket observation at $\lambda = 0.274\mu$ (Bogess and Dunkelman, 1959), indicating an albedo of 0.24, suggests that atmospheric scattering or fluorescence or both become significant at shorter wavelengths, but this result requires confirmation.

Very little information is available on the reflectivity of Mars beyond 1μ; according to Kuiper (quoted by Harris, 1961), the intensity ratio $I(2\mu)/I(1\mu)$ is the same for the sun and for Mars (at an unspecified phase angle); this suggests that the infrared albedo does not much exceed its value $p = 0.3$ at 0.8μ. In the far infrared ($\lambda > 3$ to 5μ), a reasonable expectation is that the reflectivity decreases to a small value ($p \approx 0.1$?) consistent with the black-body approximation used in the reduction of radiometric observations in the 8- to 14-μ band. A plausible extrapolation is illustrated by curve no. 4 in Fig. 27.

It is clear that, although Mars has been more consistently observed than other planets, much remains to be done to define its photometric parameters better, especially in the ultraviolet and in the infrared.

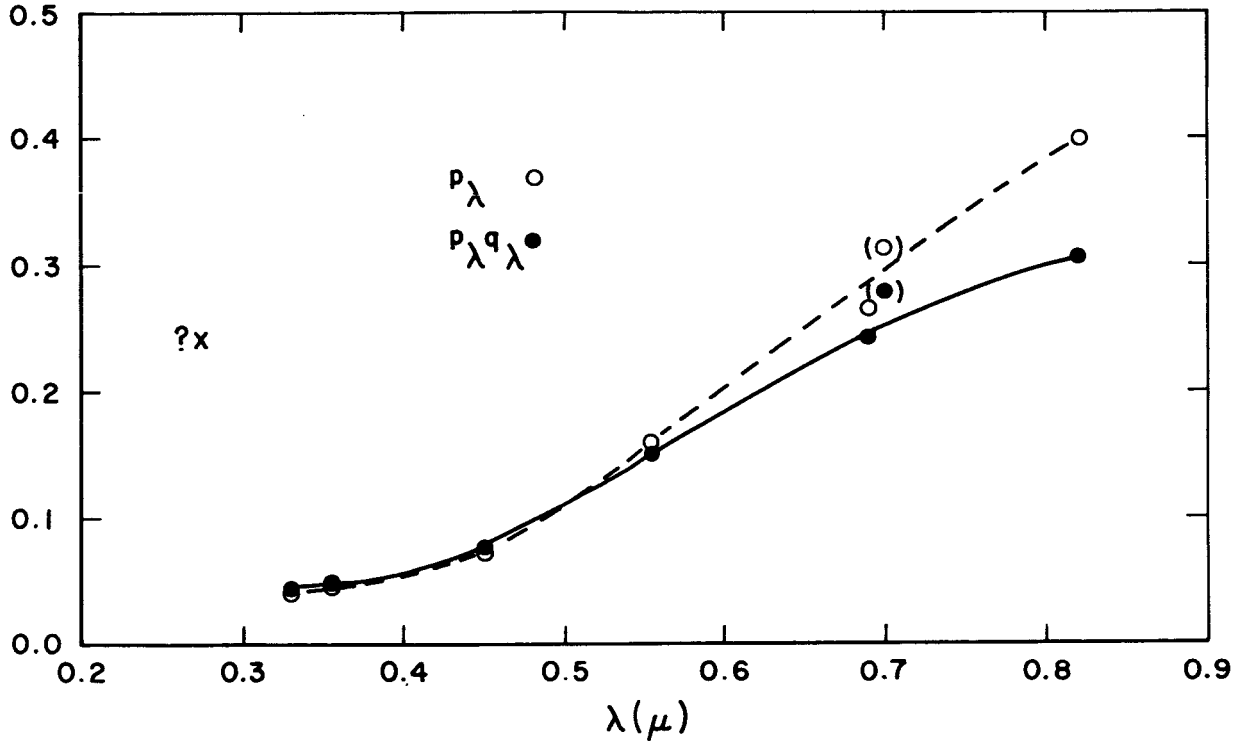

Fig. 26 Monochromatic albedos of Mars

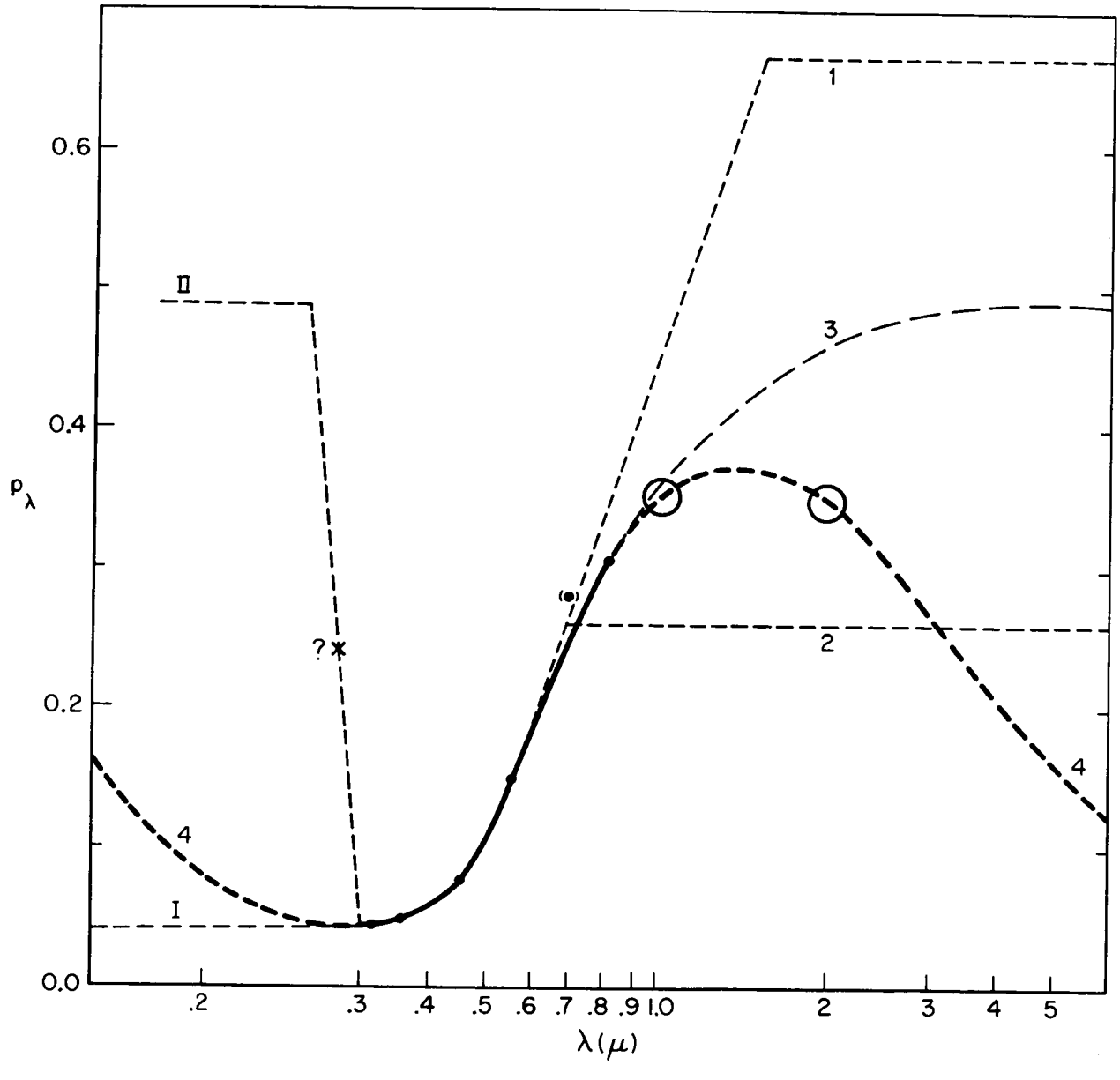

Fig. 27 Spectral reflectivity curve of Mars

12.3. Radiometric albedo

Because of the special interest in Mars for testing theoretical models of the general circulation of a planetary atmosphere (Mintz, 1961), an attempt was made to estimate lower and upper limits and the most probable value of the radiometric albedo A* given by Eq. (4.29) in spite of our incomplete knowledge of the spectral reflectivity curve. As was noted in Section 4, the visual value A_v often used in the past is not a good approximation in the case of Mars because of the strong dependence of p on λ and because (Section 3) over half the solar energy is emitted in the infrared where $p \gg p_v$.

Figure 27 shows the adopted spectral albedo $p\lambda$; the continuous curve in the interval $0.32 \leq \lambda \leq 0.82$ is observed; the dashed curves represent several tentative extrapolations. In the ultraviolet curve I, assuming that $p_\lambda \to 0.04$ for $\lambda < 0.32\mu$, is a plausible lower limit; curve II, probably an upper limit is based on the doubtful rocket observation $p = 0.24$ at $\lambda = 0.274\mu$. Curve 4 is a more plausible extrapolation. The uncertainty on p_λ in the ultraviolet has little effect on p*, because the source function $E_s(\lambda)$ has small values in this range (Fig. 3).

In the infrared, curve 1 is certainly an upper limit; it levels off at $p = 0.67$ beyond 1.5μ, because q is unlikely to exceed the Lambert value $q_0 = 1.5$ and obviously pq_0 cannot exceed unity. Curve 2, assuming that p_λ does not exceed its value at 0.7μ probably gives a lower limit for p* since the observed value at 0.82μ is already greater. Curve 3 allows for a further increase of p_λ beyond 0.8μ without reaching the implausibly high values of curve 1; it levels off at 0.49 and probably leads to an upper limit of p* because, as noted

earlier, p_λ must eventually decrease to a low value in the far infrared (beyond 5μ) since most natural minerals are known to have a low reflectivity (high emissivity) in the 10μ region. This is confirmed by direct measurements of the emissivity of the Sahara desert in the 8 to 12μ band from the Tiros III satellite (Buettner and Kern, 1963), indicating a vertical emissivity between 0.7 and 0.9 (reflectivity: 0.2 ± 0.1). Curve 4 is a tentative estimate of the probable run of $p(\lambda)$ allowing for this expected decrease beyond 2μ. The flat maximum in the 1 to 2μ region is in agreement with Kuiper's observation that the albedo is about the same at 1μ and 2μ (see above).

The integrals in Eqs. (4.27) and (4.28) can be written symbolically $S = S_u + S_0 + S_i$ where S_u, S_0, S_i represent respectively the contributions of the ultraviolet ($0.20 < \lambda \leq 0.32\mu$), of the well observed visible range ($0.32 \leq \lambda \leq 0.70\mu$) and of the infrared ($0.70 \leq \lambda \leq 5.0\mu$). The values of S are listed in Table 20a in such units that $S\,[E_s(\lambda)\, d\,\lambda] = 1.40$ erg cm^{-2} sec^{-1} = 2.00 cal cm^{-2} min^{-1}; the corresponding values of p* are given in Table 20b. The range is from 0.197 for case (I,2) to 0.313 for case (II,1), or in the mean $p^* \leq 0.255 \pm 0.058$. The more plausible lower and upper limits (II,2) and (I,3) give $0.198 < p^* < 0.244$, or in the mean $p^* = 0.221$; the "most probable" value (4,4) is $p^* = 0.233$. The adopted value is

$$p^* = 0.235 \quad ,$$

with an estimated probable error of 0.015.

The computation of q* follows similar lines. Figure 28 shows the adopted curve in the observed range $0.36 \leq \lambda \leq 0.64\mu$ and three possible extrapolations in the infrared. Case A assumes that q = 1.3;

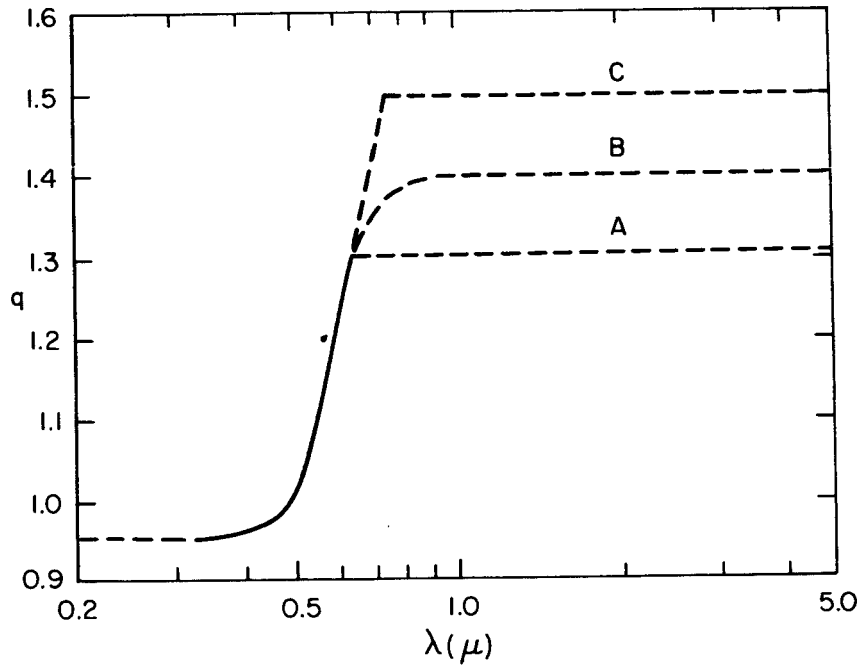

Fig. 28 Spectral dependence of phase integral of Mars

the value reached at $\lambda = 0.65\mu$ is characteristic of the surface and does not increase further beyond 0.65μ. This assumption probably leads to a lower limit for q*. Case C assumes that q increases beyond 0.65μ up to the value $q_0 = 1.50$ characteristic of a smooth (Lambert) sphere and remains at this constant value at longer wavelengths; this assumption probably leads to an upper limit for q*. Case B is a plausible intermediate assumption for which $q = 1.4$ beyond 1μ. The corresponding values of q* are listed in Table 20a; the lower and upper limits are 1.17 and 1.30 (mean 1.235); the more probable value is 1.25. The adopted value is

$$q^* = 1.24 \quad ,$$

with an estimated probable error of 0.02.

The products of the lower and upper limits of p* and q* give $0.23 < A^* \leq 0.41$, or $A^* \leq 0.32$. The product of the more probable values $p^* = 0.233$, $q^* = 1.251$ gives $A^* = 0.292$, whereas a direct integration of the product $p_\lambda q_\lambda$ for case (4,B) gives $A^* = 0.297$. The adopted value is

$$A^* = 0.295 \quad ,$$

with an estimated probable error of 0.02.

The average solar-flux density absorbed by Mars at the mean distance R = 1.524 A.U. corresponding to this value of A* by Eq. (4.30) is

$$\frac{F^*}{\pi r^2} = \frac{E_s^*}{R^2}(1 - A^*) = 0.61 \text{ cal cm}^{-2} \text{ min}^{-1}$$
$$= 0.43 \times 10^6 \text{ erg cm}^{-2} \text{ sec}^{-1} \quad .$$

This is about half the corresponding quantity for Earth and almost double the amount that would have been estimated by incorrectly using A_v instead of A*.

Table 1

EFFECTIVE WAVELENGTHS OF MAGNITUDE SYSTEMS

FOR SOLAR RADIATION

Symbols	U'	U	B	V	R	I
$\lambda(\mu)$	0.33	0.37	0.445	0.555	0.69	0.82
$\lambda^{-1}(\mu^{-1})$	3.03	2.70	2.23	1.80	1.45	1.22

Table 2

NORMALIZED SPECTRAL ENERGY DISTRIBUTION OF SOLAR RADIATION*

$\lambda(\mu)$	$E_s(\lambda)$	$\Sigma E_s(\lambda)\delta\lambda$	$k_s(\lambda)$	$\lambda(\mu)$	$E_s(\lambda)$	$\Sigma E_s(\lambda)\delta\lambda$	$k_s(\lambda)$
0.20	0	0	0	1.00	73	1.004	0.7162
.22	0	0	0	1.10	60	1.069	.7631
.24	4	0.0003	0.0002	1.20	49	1.123	.8019
.26	14	.0021	.0015	1.30	40	1.169	.8341
.28	25	.0058	.0042	1.40	33	1.205	.8598
.30	56	.0135	.0097	1.50	27	1.234	.8810
.32	76	.0268	.0191	1.60	22	1.258	.8978
.34	91	.0435	.0310	1.70	18	1.277	.9118
.36	107	.0633	.0452	1.80	15	1.294	.9235
.38	121	.0861	.0614	1.90	12	1.307	.9330
.40	148	.1117	.0797	2.00	11.1	1.318	.9410
.42	187	.1454	.1038	2.5	5.0	1.358	.9696
.44	207	.1848	.1319	3.0	2.7	1.378	.9832
.46	222	.2279	.1626	3.5	1.6	1.388	.9908
.48	223	.2725	.1945	4.0	0.9	1.395	.9956
.50	215	.3164	.2259	4.5	0.6	1.398	.9982
.52	209	.3588	.2561	5.0	0.4	1.402	1.0000
.54	203	.3999	.2854				
.56	198	.4402	.3141				
.58	194	.4793	.3421				
.60	190	.5177	.3695				
.62	182	.5549	.3960				
.64	172	.5903	.4213				
.66	164	.6239	.4453				
.68	157	.6559	.4681				
.70	150	.6865	.4895				
.75	132	.7568	.5401				
.80	117	.8183	.5841				
.85	104	.8732	.6232				
.90	91	.9220	.6580				
.95	81	.9656	.6891				
1.00	73	1.004	.7162				

* $E_s(\lambda)$ after Allen (1955) normalized to solar constant
= 2.00 cal cm^{-2} min^{-1} = 1.40 x 10^5 erg cm^{-2} sec^{-1} per Angström
(smoothed over 100 A bandwidth).

$\Sigma E_s(\lambda)\delta\lambda$ = integrated radiation from 0 to λ in erg cm^{-2} sec^{-1}.

$k_s(\lambda)$ = fraction of total radiation emitted between 0 and λ.

Table 3

APPARENT DIAMETER OF MERCURY AT UNIT DISTANCE

Year	Author	Instrument	$2\sigma_1$	Source
	1. Filar micrometer in daytime			
1882	De Ball	11" refr., Bothkamp	(7".456)	1
1898--1900	Barnard	40" refr. (15" dia.), Yerkes	6.591	2
1901	See	26" refr., Washington	(5.899)	3
1903--1909	Wirtz	20" refr., Strasbourg	6.431	4
1914	Rabe	8" refr., Breslau	6.62	5
	2. Heliometer or birefringent micrometer in daytime			
1865	Kaiser	7" refr., Leiden	6.606	6
1890	Ambronn	6½" helio., Göttingen	6.597	7
1890--1899	Hartwig	7" helio., Bamberg	6.78	8
1910	Ernst	12" refr., Heidelberg	6.56	9
1931--1951	Müller	6" refr., Strasbourg	6.42	10
	3. Filar micrometer in transits			
1894	Campbell	36" refr. (8" dia.), Lick	(5.726)	11
1891	Barnard	12" refr. (4" dia.), Lick	(6.042)	12
1894	Barnard	12" refr. (5--6" dia.), Lick	6.21	12
1914	Rabe	8" refr., Breslau	6.32	5
1914	Jonckheere, et al.	28" refr.(15--20"dia.),Greenwich	6.43	13
1914	Storey, et al.	15" refr.(6--10"dia.), Edinburgh	6.42	14
1960	Engle and Kraus	6" refl., Edinburg (Texas)	6.83	15
	4. Timing of contacts during transits			
1907	Stroobant	1 transit	(6.16)	16
1891--1924	Innes	5 transits	(6.16)	17
1799--1927	Williams	16 transits	6.30	18
1940	Clemence and Whittaker	1 transit, many observ.	6.41	19
1960	de Vaucouleurs	1 transit, 9" refr., Austin	6.73	20

Table 3 (Continued)

Year	Author	Instrument	$2\sigma_1$	Source
		5. Heliometer or birefringent micrometer in transits		
	Schur	6½" helio., Göttingen	6".38	21
	Hartwig	7" helio., Bamberg	6.72	8
1953	Dollfus	6" refr., Paris	6.45	22
1960	Dollfus	? , Mt Wilson	6.54	23
1960	Camichel	8½" refr., Pic du Midi	6.56	24
1960	Kuiper	? , Tucson	6.68	24
		6. Photoelectric photometry in transits		
1960	Camichel and Rosch	15" refr., Pic du Midi	6.75	24
1960	Leroy	? , Meudon	6.69	23

Sources

1. A.N., 2458.
2. A.N., 157, 3760, 264, 1901.
3. A.N., 156, 257, 1901.
4. Ann. Strasbourg, IV, Part 2, 245, 1912.
5. A.N., 234, 153, 1928.
6. Leiden Ann., III, 209, 1872. (Not included in 19th century compilation.)
7. A.N., 127, 157, 1891.
8. Naturforsch. Gesell., Bamberg, Bericht XXI, 1911.
9. Veröff. Heidelberg, 8, No. 1.
10. Bull. Astr., Paris, 14, 215, 1949; L'Astronomie, 69, 82, 1955.
11. A.J., 14, 148, 1894.
12. A.J., 14, 177, 1895.
13. M.N., 75, 31, 1914.
14. M.N., 75, 35, 1914.
15. Sky and Telescope, 21, 19, 1961.
16. A.N., 180, 339, 1909; Ann. Astr. Belg., 12, Fasc. 1, 1908.
17. Union Obs. Circ., 65, 307, 1925.

Table 3 (Continued)

18. Publ. Kirkwood Obs., No. 1, Suppl., 1940.
19. Publ. U.S. Naval Obs., 15, Part 2, 1942; $2\sigma_1$ computed from observed duration of egress (105 s.).
20. A.J., 66, 36, 1961; $2\sigma_1$ computed by Ashbrook from observed duration of egress ($118^{s}.7 \pm 0.9$ p.e.).
21. A.N., 3038.
22. L'Astronomie, 68, 337, 1954.
23. Trans. I.A.U., XI B, 242, 1962.
24. Compt. Rend. Acad. Sci., Paris, 255, 53, 1962.

Table 4

OPTICAL DIAMETER OF VENUS AT UNIT DISTANCE DERIVED

FROM MICROMETER OBSERVATIONS IN THE DAYTIME

Year	Observer	Instrument	Method	Superior conj.			Quadrature			Inferior conj.			Source
				$2\sigma_1$	(n)	d	$2\sigma_1$	(n)	d	$2\sigma_1$	(n)	d	
1862	Kaiser	8", Leiden	D	(16".20)	10	10".5	(17".12)	6	28"--35"	(17".07)	...	50"--52"	1
1865	Kaiser	8", Leiden	D	(16.31)	11	13.5	...	...	...	...	...	...	1
1898	Drew	24", Flagstaff	F	16.59	10	10.5	17.07	10	26.--34.	16.95	4	54.--61.	2
1900	See	26", Washington	F	...	...	...	16.72	13	29.--38.	16.88	5	51.--58.	3
1903	Wirtz	20", Strasbourg	F	16.79	8	11.5	16.97	2	35.--36.	...	...	...	4
1905	Wirtz	20", Strasbourg	F	...	...	...	(17.27)	4	34.--38.	(17.07)	3	54.--58.	4
1912--14	Rabe	8", Breslau	F	16.61	8	11.	(17.18)	17	25.--40.	(17.36)	18	50.--61.	5
1921	Graff	24", Bergedorf	F	...	...	...	...	...	...	(17.22)	8	56.--62.	6
1924	Danjon	20", Strasbourg	F	...	...	...	16.96	6	29.--31.	16.69	12	52.--57.	7
1938	Edson	24", Flagstaff	P	...	...	...	...	...	...	16.90	(?)	60.	8
1939	Muller	6", Strasbourg	D	16.64	21	10.5	...	...	...	...	...	...	9
1940	Richter	26", Berlin	F	...	...	...	...	...	...	(17.17)	8	55.--58.	10
1962	Smith	12", Las Cruces	P	...	...	...	...	...	...	16.97	5	...	11
Mean all values p.e. (N)				16".52 ".07		11". (6)	17".04 ".05		33". (7)	17".03 ".05		56". (10)	
Mean of selected val. p.e. (N)				16".66 ".03		(d_1>16".5) (4)	16".88 ".06		(d_1<17".0) (3)	16".88 ".03		(d_1<17".0) (5)	
Mean of refjected val p.e. (N)				... ...		... ...	17".16 ".03		(d_1>17".0) (4)	17".18 ".04		(d_1>17".0) (5)	

Adopted mean from daytime observations: $2\sigma_1$ = 16".88 ± ".03

Method -- D: double-image micrometer; F: filar micrometer; P: photographs.

(n): number of days. (N): number of values.

Sources

1. Ann. Leiden, 3, 209, 1872.
2. A. J., 22, 13, 1901.
3. A. N., 154, 81, 1900.
4. Ann. Strasbourg, 4, Part 2, 245, 1912.
5. A. N., 234, 153, 1928.
6. Mitt. Hamburg-Bergedorf, 5, No. 15, 29, 1922.
7. Ann. Strasbourg, 1, 307, 1926.
8. Lunar and Planetary Exploration Colloquium, 1, No. 5, 22, 1960.
9. Bull. Astron., Paris, 14, 215, 1949.
10. A. N., 274, 119, 1943.
11. A. J., 68, 544, 1963.

Table 5

OPTICAL DIAMETER OF VENUS AT UNIT DISTANCE
DERIVED FROM TRANSIT OBSERVATIONS

Transit	Author	Source	Method	$2\sigma_1$	w
1761	Wurm	1	22 sets of micrometer meas.	16".954	½
...	Encke	2	Timings of contacts	16.611	½
1769	Wurm	1	8 sets of micrometer meas.	16.810	½
...	Ferrer	3	Timing of contacts, 15 stations	16.676	½
1761--69	Powalky	4	General discussion	16.918	1
Mean of 18th century transits:				16".815	3
1874	Tenant	5	Double-image micrometer meas.	16".903	½
1874--82	Auwers	6	Timing of contacts (17 observ.)	16.85	1
...	Auwers	6	Heliometer, corrected (9 observ.)	16.820	1
Mean of 19th century transits				16".849	2½
Mean of all transits				16".830 ±.030	

Sources

1. Berliner Astr. Jahrbuch, 167, 1807.
2. Die Entfernung der Sonne, Gotha, 1824.
3. Mem. R.A.S., 5, 281, 1833.
4. A.N., Nr. 1841, 1871.
5. A.N., 35, 347, 1875.
6. A.N., Nr. 3068, 1891; 3214, 1894.

Table 6

APPARENT POLAR DIAMETER OF MARS AT UNIT DISTANCE FROM HELIOMETER AND DOUBLE-IMAGE MICROMETER MEASUREMENTS CORRECTED FOR ASSUMED CONSTANT ERROR

Years	Author	Method	d_1''	p.e.	c	p.e.
1813	Arago (Hartwig)	Rochon's microm., Paris	9".167	".049	+0".157	".094
1811--47	Arago (Hartwig)	Rochon's microm., Paris (60n)	9.311	...	...	...
1830--37	Bessel (Oudemans)	Heliom., Königsberg	9.342*	.019	-0.043	.070
1862--65	Kaiser (Hartwig)	Airy's microm., 7" Leiden	9.375	.013	+0.063	.021
1862--63	Main (Hartwig)	Heliom., Oxford	9.404	.036	-0.544	.070
1877--78	Hartwig (1879)	3" heliom., Strasbourg (34n)	9.300	.022	-0.107	.050
1879--80	Hartwig (1899)	3" heliom., Strasbourg (28n)	9.511	.063	-0.306	.099
1890--1909	Hartwig (1911)	Heliom., Bamberg (15n)	9.318	.028	0.	...
Unweighted mean			9".34	".02		
Interpolated for c = 0			9".305	".02		

* Mean diameter, 9".328, c = -0".027 ± 0".035

Sources: A.J., 15, 145, 1895; A.N., 234, 162, 1928.

Table 7

APPARENT POLAR DIAMETER OF DISK OF MARS AT UNIT DISTANCE

Year	Author	Instrument	d	d_1''	p.e.	c	p.e.	Rem.	Source
		1. Filar micrometer (night)							
1906--09	Wirtz	19", Strasbourg	4".--25".	9".634	".022	+0".117	".038	1	1
1914--16	Rabe	8", Breslau (bright field)	6.--14.	9.439	.128	+0.504	.132	1	2
1926--27	Rabe	8", Breslau (dark field)	4.5--21.	9.433	.038	+0.212	.051	2	2
		2. Heliometer and double-image micrometer (night)							
1896--99	Schur	6½",hel.,Göttingen	14.--17.	9.35	.02	...	...	...	3
1890--1909	Hartwig	Helio.,Bamberg	11.--23.	9.318	.019	...	...	...	4
1948	Muller	6", Strasbourg	13.--14.	9.29	.04	...	...	...	5
1954--58	Dollfus	24",Pic du Midi (near oppos. only)	19.--25.	9.31	(.03)	...	...	3	6
		3. Micrometer measures on photographs (yellow light)							
1924	Wright	36" refl., Lick	23.--25.	9.17	...	...	...	4	7
1924	Trumpler	36" refr., Lick	16.--25.	9.28	.06	+0.10	.16	5	8
1924	Trumpler	36" refr., Lick	21.--25.	9.32	.02	...	...	6	8
1924	Van de Kamp	26"refr.,McCormick	21.--25.	(9.26)	...	...	...	2,7	9
1924--27	Van de Kamp	26" refr., "	6.--25.	9.48	.06	-0.328	.108	2	10
1934--39	Reuyl	26" refr., "	4.5--24.	9.44	.07	-0.26	.13	1	11
		4. Microphotometer measures on photographs (yellow light)							
1941--50	Camichel	15".24" Pic du Midi (near oppos. only)	14.--22.	9.22	.01	...	...	...	12, 13

Remarks

1. Cusps diameter, d_1'' about 0".01 smaller for $f^{-1} = 100$.
2. Cusps diameter, d_1'' about 0".02 smaller for $f^{-1} = 100$.
3. Blue and red filters in agreement.
4. Two nights nearest opposition give 9".26; settings near maximum contrast contour.
5. $d_1' = 9''.37$ corrected for $f^{-1} = 105$.

6. Preferred solution.

7. Preliminary; range from 9".19 (13 underexposed images) to 9".31 (9 overexposed images); superseded by source 9.

Sources

1. Ann., Strasbourg, IV, Part 2, 250, 1912.

2. A. N., 234, Nr. 5600-01, 162, 1928.

3. M. N., 59, 330, 1899.

4. Naturforsch. Gesell., Bamberg, XXI, 1911.

5. L'Astronomie, 62, 201, 1948.

6. Compt. Rend. Acad. Sci., Paris, 255, 2229, 1962.

7. Lick Obs. Bull., 12, Nr. 366, 54, 1925.

8. Lick Obs. Bull., 13, Nr. 387, 27, 1927.

9. Pub. A. S. P., 37, 261, 1925.

10. A. J., 38, Nr. 894, 61, 1928.

11. A. J., 49, Nr. 1136, 125, 1941.

12. Bull. Astr., Paris, 18, 83, 1954.

13. Bull. Astr., Paris, 20, 131, 1956.

Table 8a

BEST DETERMINATIONS OF APPARENT POLAR DIAMETER OF MARS

Author	Time Period	(n)	$2\sigma_1''$	p.e.	w
Muller	1948	(4n)	9".29	±".04	½
Schur	1896--99	(7n)	9.35	.02	½
Hartwig	1890--1909	(15n)	9.32	.02	1
Dollfus	1954--58	(6n)	9.31	.03	1
Double image (c = 0)			9".305	".02	2
Photographic (c = 0)			9.32	.02	2
Weighted mean			9".315	".010	

Table 8b

BEST DETERMINATIONS OF APPARENT EQUATORIAL DIAMETER OF MARS

Author	Time Period	(n)	$2\sigma_1'$	p.e.	w
Douglass	1894	(10n)	9".42	...	½
Hartwig	1879	(12n)	9.445	...	½
Hartwig	1890--1909	(15n)	9.41	...	1
Muller	1948	(4n)	9.43	...	½
Trumpler	1924	(14n)	9.41	...	1
Camichel	1941--50	(7n)	9.33	...	½
Dollfus	1954--58	(6n)	9.435	...	1
Weighted mean			9".415	±".02	

Table 9

APPARENT OPTICAL FLATTENING OF DISK OF MARS

FROM MEASUREMENTS MADE NEAR OPPOSITION

Year	Author	Instrument	n*	d	d_1'	f	p.e.	Rem.	Source
			1. Filar micrometer						
1892	Campbell	36" refr., Lick	9	25"..	9".638	(0.0016)	.0018	1	1
1894	Barnard	36" refr., Lick	8	19.--22.	9.701	0.0087	.0022	1,2	2
1894	Douglass	24" refr., Flagstaff	10	21.--22	9.419	0.0066	.0015	1,3	3
1894	Young	23" refr., Princeton	...	...	(9.765)	(0.0017)	...	...	4
1903--09	Wirtz	19" refr., Strasbourg	27	15.--25.	9.674	0.0095	.0020	4	5
			2. Heliometer						
1879	Hartwig	3" hel., Strasbourg	12	17.--20.	9.445	0.0086	.0015	...	6
1890--1909	Hartwig	3" hel., Bamberg	15	...	9.41	0.0096	...	...	7
1896	Schur	6 1/2" hel., Göttingen	4	16.--17.	9.524	(0.0215)	.0017	...	8
1899	Schur	6 1/2" hel., Göttingen	3	14.--15.	9.563	(0.0187)	.0015	...	9
			3. Double-image micrometer						
1948	Muller	6" refr., Strasbourg	4	13.--14.	9.43	0.015	.003	...	10
1954	Dollfus	24" refr., Pic du Midi	2	22.	9.395	0.0118	...	...	11
1956	Dollfus	24" refr., Pic du Midi	2	25.	9.47	0.0117	...	...	11
1958	Dollfus	24" refr., Pic du Midi	2	19.	9.43	0.0116	...	...	11
			4. Micrometer on photographs (yellow)						
1924	Trumpler	36" refr., Lick	14	21.--25.	9.41	0.0094	.0007	40pl.	12
			5. Microphotometer on photographs (yellow)						
1941	Camichel	15" refr., Pic du Midi	1	22.5	9.48	0.016	.0027	3pl.	13
1943	Camichel	15" refr., Pic du Midi	2	17.	9.35	0.012	.0006	2pl.	13
1946	Camichel	24" refr., Pic du Midi	2	15.	9.30	0.013	.0028	2pl.	13
1948	Camichel	24" refr., Pic du Midi	1	14.	9.24	0.004	.0025	1pl.	13
1950	Camichel	24" refr., Pic du Midi	1	14.	9.29	0.012	.0047	1pl.	13

*n = number of nights

Remarks

1. Recomputed from published diameters.
2. Barnard's value f = 0.0091.
3. For period closest to opposition (Oct. 1894, mean phase angle i = 4°); corrected for 0".125 irradiation on d; Lowell's value f = 0.0052 involves doubtful corrections for phase effect attributed to "twilight arc".
4. Phase defect < 0".30.

Sources

1. A. J., 12, Nr. 282, 139, 1892.
2. A. J., 17, Nr. 403, 145, 1897.
3. Pop. Astron., 3, 287, 1896; Ann. Lowell Obs., I, 59, 1898.
4. Astronomy and Astrophysics, 1, 675, 1894.
5. Ann. Strasbourg, IV, Part 2, 252, 1912.
6. A. N., 150, Nr. 3494, 320, 1899.
7. Naturforsch. Gesell., Bamberg, XXI, 1911.
8. M. N., 67, 150, 1897; A.N., Nr. 3405.
9. M. N., 69, 330, 1899.
10. L'Astronomie, 62, 201, 1948.
11. Compt. Rend. Acad. Sci., Paris, 255, 2229, 1962.
12. Lick Obs. Bull., 13, Nr. 387, 26, 1927.
13. Bull. Astr., Paris, 18, 83, 1954.

Table 10

APPARENT EQUATORIAL AND POLAR DIAMETERS

OF GLOBE OF MARS AT UNIT DISTANCE

Year	Author	Instrument	d	d_1'	d_1''		Rem.	Source
		1. Filar micrometer (daytime)				c		
1894--95	Campbell	36" refr. (15"), Lick 106 meas., 31 d.	4".4--20".2	...	9".254 ±.018	+0".054	1	1
1901	See	26" refr., Washington 69 meas., 8 d.	6.	...	9.22 ±.013	...	2	2
		2. Double-image micrometer (daytime)						
1937--38	Muller	6" refr., Strasbourg 15 meas.	4.--6.5	...	9.00 ±.10	...	w=½	3
		3. Photographs (red light)				f		
1924	Trumpler	36" refr., Lick 40 im., 19 pl., 13 n.	21.--25.	9".33 ±.02	9.24 ±.02	.0098 ±.0011	3	4
		4. Surface markings						
1909	Wirtz	20" refr., Strasbourg (vis.) 3+2 meas., 2 spots	21.--25.	9.122 ±.071	...	...	4 w=½	5
1924	Trumpler	36" refr., Lick (photo.) 1409 obs., 192 points	16.--25.	9.178 ±.014	9.074	.0113 ±.0048	...	4
1941	Camichel	15" refr., Pic du Midi (photo.) 20 meas., 1 spot	22.5	9.48 ±.026	...	...	5	6
1943	Camichel	15" refr., Pic du Midi 3 meas., 1 spot	17.	9.40 ±.042	...	...	5	6
1946	Camichel	15" 24" refr., Pic du Midi 13 meas., 1 spot	15.	9.20 ±.061	...	...	5	6
1948	Camichel	24" refr., Pic du Midi 11 meas., 2 spots	14.	9.26 ±.028	...	...	5	6
1950	Camichel	24" refr., Pic du Midi 11 + 9 meas., 2 spots	14.	9.23 ±.063	9.30 ±.016	...	6	6
1954	Camichel	24" refr., Pic du Midi 19 + 16 meas., 2 spots	21.	9.466 ±.028	...	...	7	7
Unweighted mean (n)				9".275 (8)	9".182			
Weighted mean (w)				9".285 (7½)	9".198 (5½)			

Remarks

1. d_1'' derived from cusps' diameters with f^{-1} = 219.
2. d_1'' derived from cusps' diameters with f^{-1} = 200.
3. λ = 6000 A, limb settings.
4. Syrtis Major and Sinus Meridiani.
5. d_1' by path of Juventae Fons.
6. d_1' by paths of Oxia Palus and Ismenius Lacus; d_1'' by North Polar Cap.
7. d_1' by paths of Oxia Palus and Juventae Fons; not included in means.

Sources

1. A. J., 15, Nr. 354, 145, 1895.
2. A. N., 157, Nr. 3750, 97, 1901.
3. Bull. Astr., Paris, 14, 215, 1949.
4. Lick Obs. Bull., 13, Nr. 387, 27, 1927.
5. Ann. Strasbourg, IV, Part 2, 250, 1912.
6. Bull. Astr., Paris, 18, 83, 1954.
7. Bull. Astr., Paris, 20, 131, 1956.

Table 11

VISUAL PHASE FUNCTIONS OF MERCURY (AFTER DANJON)
AND THE MOON (AFTER ROUGIER)

	Mercury				Moon			
i	Δm	Φ(i)	Φ(i)sin i	$\Phi(i)/\Phi_0(i)$	Δm	Φ(i)	Φ(i)sin i	$\Phi(i)/\Phi_0(i)$
0°	0.00	1.000	0.000	1.000	0.00	1.000	1.000	1.000
10	0.35	0.721	0.125	0.733	0.30	0.773	0.135	0.785
20	0.67	0.541	0.185	0.573	0.56	0.595	0.204	0.630
30	0.95	0.417	0.209	0.473	0.85	0.459	0.230	0.521
40	1.21	0.328	0.211	0.410	1.13	0.353	0.227	0.441
50	1.47	0.258	0.198	0.364	1.40	0.274	0.210	0.387
60	1.73	0.204	0.177	0.333	1.69	0.211	0.183	0.346
70	2.01	0.157	0.148	0.309	2.00	0.158	0.149	0.312
80	2.32	0.118	0.116	0.289	2.35	0.115	0.113	0.282
90	2.67	0.0858	0.0858	0.269	2.74	0.080	0.080	0.252
100	3.07	0.0592	0.0583	0.251	3.11	0.057	0.0561	0.242
110	3.51	0.0394	0.0370	0.236	3.52	0.039	0.0367	0.235
120	4.09	0.0232	0.0201	0.215	3.98	0.0255	0.0221	0.234
130	4.72	0.0129	0.0099	0.198	4.52	0.0155	0.0119	0.238
140	5.46	0.00656	0.0041	0.193	5.11	0.009	0.0058	0.265
150	6.31	0.00300	0.0015	0.200	5.89	0.0044	0.0022	0.293
160	(7.28)	(0.00123)	0.0004	(0.273)	(7.16)	(0.0014)	0.0005	(0.3)
170	(8.40)	(0.00044)	0.0001	(0.674)	(8.80)	(0.0003)	0.0001	(0.3)
q			0.560				0.584	
$2.20\Phi(50^\circ)$			0.568				0.603	

Table 12

VISUAL ALBEDOS OF TERRESTRIAL PLANETS FOR $m_s = -26.81$

	Mercury	Venus	Mars
σ_1	3".365	8".44	4".682
ρ''/σ_1	61,297	24,439	44,055
$2 \log \rho''/\sigma_1$	9.575	8.776	9.288
m_0	-0.42	-4.40	-1.52
$m_0 - m_s$	26.39	22.41	25.29
$0.4(m_0 - m_s)$	10.556	8.964	10.116
log p	-0.981	-0.188	-0.828
p(V)	0.104	0.650	0.149
q(V)	0.560	1.087	1.07
$A_v = pq$	0.058	0.705	0.159

Table 13

SPECTRAL REFLECTIVITY OF MERCURY

Band	U	B	V	R	I
$\Delta m(\mathbb{\u263F})$	...	+0.97	.00	-0.85	-1.37
$E(\mathbb{\u263F} - \odot)$	(0.72?)	+0.34	.00	-0.40	-0.63
$E(\mathbb{C} - \odot)$	+0.61	+0.29	.00	-0.35	-0.52
p_λ	0.053?	0.076	0.104	0.150	0.186

Table 14

REDUCED VISUAL MAGNITUDES* OF VENUS AT PHASE ANGLES 0° AND 50°

Author	Year	$V_1(0)$	$V_1(50)$	q
Muller	1893	-4.16	-3.44	(1.194)
Muller	1926	...	...	1.078
King	1919	...	-3.50	...
Danjon	1949	-4.27	-3.71	1.296
Knuckles, et al.	1961	-4.76	-3.69	0.888
Adopted		-4.40	-3.58	1.087

* $R\Delta = 1$.

Table 15

ADOPTED VISUAL PHASE FUNCTION OF VENUS

i	Δm	log I_0/I	Φ(i)	Φ(i)sin i	Φ/Φ_0
0^o	0.00	0.000	1.000	1.000	1.000
10	0.14	0.056	0.880	0.153	0.894
20	0.29	0.116	0.765	0.262	0.810
30	0.45	0.180	0.660	0.330	0.750
40	0.63	0.252	0.560	0.360	0.700
50	0.82	0.328	0.470	0.360	0.664
60	1.03	0.412	0.387	0.335	0.635
70	1.25	0.500	0.316	0.297	0.620
80	1.48	0.592	0.256	0.252	0.626
90	1.72	0.688	0.205	0.205	0.645
100	1.97	0.788	0.163	0.160	0.690
110	2.22	0.888	0.129	0.121	0.780
120	2.48	0.992	0.102	0.088	0.935
130	2.77	1.108	0.078	0.060	1.20
140	3.06	1.224	0.060	0.039	1.77
150	3.39	1.356	0.044	0.022	2.94
160	3.72	1.488	0.032_5	0.011	7.2
170	4.11	1.644	0.022_5	0.004	34.6
180	4.50	1.80	0.016	0.000	...
q			1.087		
$2.20\Phi(50^o)$			1.035		

Table 16

REDUCED VISUAL MAGNITUDES OF MARS ($i = 0^{\circ}$, $R\Delta = 1$); AFTER HARRIS, 1961*

Year	Source	$V_1(0)$	Ref.	Year	Source	$V_1(0)$	Ref.
1864--65	Zöllner (vis.)	-1.59	1	1916	King (Pv)	-1.52	3
1877--78	Müller (vis.)	-1.44	2	1918	"	-1.51	3
1879--80	"	-1.48	2	1920--21	"	-1.45	3
1881--82	"	-1.57	2	1922	"	-1.56	3
1883--84	"	-1.55	2	1952	McDonald Obs. (Pe)	-1.56	4
1886	"	-1.51	2	1954	Lowell Obs. (Pe)	-1.51	5
1888--89	"	-1.52	2	1958	Lowell Obs. (Pe)	-1.56	6

* Except last entry.

References

1. Zöllner, 1865.
2. Müller, 1893.
3. King, 1917, 1919, 1923.
4. Kuiper and Harris, 1961.
5. Johnson and Gardiner, 1955, give -1.49.
6. de Vaucouleurs, 1960.

Table 17

ADOPTED VISUAL FUNCTIONS OF MARS AND THE EARTH*

	Mars				Earth
i	Δm	$\Phi(i)$	$\Phi(i)\sin i$	Φ/Φ_0	$\Phi(i)$
0°	0.00	1.000	1.000	1.000	1.000
10	0.15	0.871	0.152	0.884	0.885
20	0.30	0.758	0.259	0.804	0.779
30	0.45	0.661	0.330	0.750	0.679
40	0.60	0.576	0.370	0.720	0.586
50	(0.79)	(0.482)	(0.369)	(0.680)	0.497
60	(0.99)	(0.403)	(0.349)	(0.682)	0.416
70	(1.20)	(0.332)	(0.312)	(0.653)	0.342
80	(1.43)	(0.268)	(0.264)	(0.654)	0.274
90	(1.70)	(0.208)	(0.208)	(0.655)	0.214
100	(2.01)	(0.158)	(0.156)	(0.670)	0.163
110	(2.34)	(0.116)	(0.109)	(0.700)	0.120
120	(2.69)	(0.084)	(0.073)	(0.766)	0.086
130	(3.09)	(0.058)	(0.044)	(0.885)	0.059
140	(3.55)	(0.038)	(0.024)	(1.13)	0.040
150	(4.05)	(0.024)	(0.012)	(1.62)	0.025
160	(4.56)	(0.015)	(0.005)	(3.32)	0.015
170	(5.1)	(0.009)	(0.002)	(13.4)	0.009
q		1.076			1.100
$2.20\Phi(50^\circ)$		1.060			1.091

* After Danjon.

Table 18

MONOCHROMATIC MAGNITUDES $m_1(0)$ OF MARS*

$\lambda_e(\mu)$	Mount Stromlo			Flagstaff			McDonald	$1/\lambda$
	1952	1954	Mean	1954	1958	Mean	1952--54	
0.33 (U')	...	...	...	...	+0.39	...	...	3.03
0.37 (U)	...	...	...	+0.41	+0.495	+0.45	+0.42	2.70
0.405	+0.53	+0.24	+0.40	...	...	...	...	2.47
0.425	+0.29	+0.08	+0.19	...	...	...	...	2.35
0.450 (B)	...	...	...	-0.17	-0.235	-0.20	-0.16	2.22
0.455	-0.32	-0.53	-0.42	...	...	...	...	2.20
0.495	-0.72	-1.04	-0.88	...	...	...	...	2.02
0.543	-1.24	-1.50	-1.37	...	...	...	...	1.84
0.555 (V)	...	...	...	-1.49	-1.56	-1.53	-1.52	1.80
0.598	-1.86	-1.88	-1.87	...	...	...	...	1.67
0.636	-2.10	-2.21	-2.15	...	...	...	...	1.57
0.69 (R')	...	...	...	...	-2.505	...	...	1.45
0.70 (R)	...	...	...	...	...	...	-2.64	1.43
0.82 (I)	...	...	...	...	...	...	-3.02	1.22

* Mt. Stromlo data (Woolley, et al., 1953, 1955), with zero point correction +0.10.

Flagstaff data, 1954: Johnson and Gardiner (1955)

1958: de Vaucouleurs (1960).

McDonald data, mean of 1952, 1954 after Harris and Hardie (1961); the solar λ_e of B, V, R filters (Table 1) were corrected to allow for the gradient of Mars.

Table 19

SPECTRAL ALBEDOS OF MARS

Band	U'	U	B	V	R'	R	I
λ_e	0.33	0.355	0.450	0.555	0.69	0.70	0.82
m_0	+0.39	+0.44	-0.19	-1.52	-2.50	-2.64	-3.02
m_s	-26.18	-26.04	-26.18	-26.81	-27.33	-27.26	-27.55
$m_0 - m_s$	26.57	26.48	25.99	25.29	24.83	24.62	24.53
σ_1	4"70?	4"70	4"70	4"68	4"65	4"65	4"62?
p	0.045	0.049	0.077	0.149	0.238	0.279	0.306
a	0.018?	0.018	0.018	0.015	0.012	0.012	0.012?
q	0.94?	0.94	0.94	1.07	1.30	1.30	1.30?
A	0.042?	0.046	0.072	0.159	0.308	0.363	0.398?

Table 20a

COMPONENTS OF RADIOMETRIC ALBEDO OF MARS

S_u	Case	S_0	Case	S_i	Case	q*
0.0013	I	...	1	0.349	A	1.169
			2	0.187	...	...
0.0026	II	...				
			3	0.262	B	1.251
0.0015	4	0.087	4	0.2375	C	1.303

Table 20b

LIMITS AND PROBABLE VALUE OF RADIOMETRIC ALBEDO p* OF MARS

S_i		Case			
		1	2	3	4
S_u	I	0.312	0.197	0.244	0.233
	4	...	...	...	0.233
	II	0.313	0.198	0.245	0.234

REFERENCES

Allen, C. W., 1955, Astrophysical Quantities, Athlone Press, London, 140.

-----, 1958, Quart. J. R. Met. Soc., 84, 307; also Comm. Univ. London Obs., No. 35.

Ambronn, L., 1891, A. N., 127, No. 3034, 157.

-----, 1900, A. N., 152, No. 3646, 351.

Barnard, E. E., 1895, A. J., 14, No. 335, 177.

-----, 1897, Ap. J., 5, 299.

-----, 1897, A. J., No. 403, 145.

-----, 1902, A. N., 157, No. 3760, 261.

Bogess, A., and L. Dunkelman, 1959, Ap. J., 129, 236.

Buettner, K. J. K., and C. D. Kern, 1963, Science, 142, 671.

Camichel, H., 1954, Bull. Astron., Paris, 18, 83.

-----, 1956, Bull. Astron., Paris, 20, 131.

-----, 1958, Ann. d' Ap., 21, 217.

Camichel, H., and J. Rösch, 1962, Compt. Rend. Acad. Sci., Paris, 255, 53.

Campbell, W. W., 1892, A. J., 12, No. 282, 137.

-----, 1894, A. J., 14, No. 331, 148.

-----, 1895, A. J., 15, No. 337, 1; No. 354, 145.

Clemence, G. M., and G. C. Whittaker, 1942, Publ. U. S. Naval Obs., 15, Part 2.

Danjon, A., 1936, Ann. Obs. Strasbourg, 3, Fasc. 3, 139.

-----, 1949, Bull. Astron., Paris, 14, 315.

-----, 1950, Bull. Astron., Paris, 15, 105.

-----, 1954, in The Earth as a Planet, G. P. Kuiper, ed., University of Chicago Press, Chicago, 726.

Danjon, A., 1959, Astronomie Generale, 2nd ed., Sennac, Paris, 158.

Darwin, G. H., 1876, M. N., 37, 77.

Dollfus, A., 1962, Compt. Rend. Acad. Sci., Paris, 255, 2229.

Evershed, J., 1919, M. N., 80, 7.

Fabry, C., 1924, "Leçons de Photométrie," Revue d'Optique, Paris, p. 120.

Goody, R. M., 1949, Proc. Roy. Soc., London, 197, 487.

Guérin, P., 1962, Ann. d' Ap., 25, 43, 429.

Guthnick, P., and R. Prager, 1914, Veroff. K. Sternw. Berlin-Babelsberg, I, Heft 1, 53.

-----, 1918, Veroff. K. Sternw. Berlin-Babelsberg, II, Heft 3, 117.

Harris, D. L., 1961, in Planets and Satellites, G. P. Kuiper, ed., University of Chicago Press, Chicago, 272.

Hartwig, E., 1879, Publ. der Astron. Gesell., 15, 77.

-----, 1899, A. N., 150, No. 3594, 316; M. N., 59, 488.

-----, 1911, Naturf. Gesell., Bamberg, Bericht XXI.

Horak, H. G., 1950, Ap. J., 112, 445.

Innes, R. T. A., 1925, Union Obs. Circ., 65, 307.

Johnson, H. L., 1954, Ap. J., 120, 196.

Johnson, H. L., and A. J. Gardiner, 1955, Publ. Astron. Soc. Pacific, 67, 74; also see correction, A. Young, Publ. Astron. Soc. Pacific, 69, 568.

Jonckheere, R., 1914, M. N., 75, 31.

Kaiser, F., 1872, Ann. Sternw. Leiden, III, 209.

Kellogg, W. W., and C. Sagan, 1961, The Atmospheres of Mars and Venus, NAS--NRC, Publ. 944, Washington, D. C.

King, E. S., 1919, Ann. Harvard Obs., 81, 201.

-----, 1923, Ann. Harvard Obs., 85, 63.

Knuckles, C. F., M. K. Sinton, and W. M. Sinton, 1961, Lowell Obs. Bull., 115, (5, No. 10), 153.

Kozyrev, N. A., 1954, Publ. Crimean Astrophys. Obs., 12, 177.

Lamar, D. L., 1962, Optical Ellipticity and Internal Structure of Mars, The RAND Corporation, RM-3127-JPL; also Icarus, 1, 258.

Lau, H. E., 1914, L'Astronomie, 28, 421.

Link, F., and L. Neuzil, 1956, Bull. Astr. Inst. Czechoslovakia, 8, No. 2, 23.

Livländer, R., 1933, Publ. Obs. Astr. Univ. Tartu, 27, No. 6.

Lowell, P., 1895, Ap. J., 2, 136.

-----, 1896, Pop. Astron., 3, 287.

-----, 1898, Ann. Lowell Obs., I, 59.

Menzel, D. H., and G. de Vaucouleurs, 1961, Final Report on the Occultation of Regulus by Venus, July 7, 1959, AF Cambridge Res. Lab., Report 227.

Mintz, Y., 1961, "The General Circulation of Planetary Atmospheres," in The Atmospheres of Mars and Venus, NAS--NRC, Publ. 944, Washington, D. C.

Muhleman, D. O., et al., 1962, A. J., 67, 191.

Muller, G., 1893, Publ. Potsdam Astrophys. Obs., 8, No. 4, 326.

-----, 1926, A. N., 227, 71.

Muller, P., 1948, L'Astronomie, 62, 201.

-----, 1949, Bull. Astron., Paris, 14, 215.

-----, 1955, L'Astronomie, 69, 82.

Pettengill, G. H., et al., 1962, A. J., 67, 181.

Polozhenzeva, T., 1962, Astr. Zirk. Ak. Nauk USSR, No. 232, 4.

Rabe, W., 1928, A. N., 234, Nr. 5600-01, 153.

Radlova, L. N., 1940, Astron. J. USSR, 17, 30.

Reuyl, D., 1941, A. J., 49, No. 1136, 125.

Rougier, G., 1933, Ann. Obs. Strasbourg, 2, Part 3, 319.

Russell, H. N., 1916, Ap. J., 43, 173.

Schur, W., 1896, M. N., 57, 150.

-----, 1899, A. N., 149, Nr. 3569, 295; M. N., 59, 330.

See, T. J. J., 1900, A. N., 154, No. 3676, 81.

-----, 1901, A. N., 156, No. 3737, 257.

-----, 1901, A. N., 157, No. 3750, 97.

Sharonov, W. W., 1936, Publ. Astr. Obs. Univ. Leningrad, 7, 33.

Taylor, G. E., 1963, Roy. Obs. Bull. (Greenwich), No. 72.

Trumpler, R. J., 1927, Lick Obs. Bull. 13, No. 387, 19.

Van de Kamp, P., 1925, Publ. Astron. Soc. Pacific, 37, 261.

-----, 1928, A. J., 38, No. 894, 61.

de Vaucouleurs, G., 1942, Ann. Obs. Houga, I, Fasc. 1.

-----, 1954, Physics of the Planet Mars, Faber and Faber, London.

-----, 1960, J. Planet. Space Sci., 2, 26.

-----, 1964, The Physical Ephemeris of Mars, The RAND Corporation, RM-3999-NASA.

de Vaucouleurs, G., and D. H. Menzel, 1960, Nature, 188, No. 4744, 28.

Williams, K. P., 1939, Publ. Kirkwood Obs. Indiana Univ., No. 1 (with suppl. 1940).

Wilson, D. (comp.), 1962, Notes of Working Symposium on Solar System Constants, The RAND Corporation, RM-3425.

Wirtz, C., 1912, Ann. d. K. Univ. Sternw. Strasbourg, IV, Part 2, 245.

Woollard, E. W., 1944, A. J., 51, 33.

Woolley, R. v. d. R., et al., 1953, M. N., 113, 521.

-----, 1955, M. N., 115, 57.

Wright, W. H., 1925, Lick Obs. Bull., 12, No. 366, 48.

Young, C. A., 1894, Astron. and Astrophys., 1, 675.

Zöllner, J. C. F., 1865, Photometrische Untersuchungen, W. Engelmann, Leipzig.